UNIVERSITÉ DE SHERBROOKE
Faculté de génie
Département de génie civil

COMPRESSION LAP SPLICES OF GFRP BARS IN REINFORCED CONCRETE COLUMNS

ÉTUDE SUR LE RECOUVREMENT (OU LE CHEVAUCHEMENT) DE BARRES LONGITUDINALES EN PRFV DANS DES COLONNES EN BÉTON SOUS CHARGE AXIALE

Thèse de doctorat
Spécialité : génie civil

Amirhomayoon Tabatabaei Kashani

Sherbrooke (Québec) Canada

March 2019

MEMBRES DU JURY

Prof. Brahim Benmokrane
Directeur de recherche (PhD Thesis Supervisor)

Prof. Omar Chaallal
Évaluateur

Prof. Adel Elsafty
Évaluateur

Prof. Sébastien Langlois
Rapporteur

ABSTRACT

Corrosion of concrete structures reinforced with steel bars is a concern in regions where weather condition is harsh. Fiber-reinforced-polymers (FRP) reinforcement has proven its feasibility through different civil structural elements as an alternative reinforcement to overcome corrosion. Recent advances in the applicability of GFRP reinforcement in axially loaded members has lightened the need for further investigation into detailing of GFRP bars under compression. Due to the lack of experiments, present guidelines for FRP structures have not yet addressed this issue. This research takes charge of providing experimental database as well as extensive analyses and design recommendations to estimate the required splice length of GFRP reinforcement under compression for concrete columns. A total of thirty large scale circular RC specimens were fabricated and tested experimentally under concentric axial load. The 300 mm diameter columns with total height of 1600 mm were designed according to CAN/CSA S806-12 (2012) code requirements. The specimens were divided into four series; series I contained three columns reinforced with steel bars and one plain concrete column. Series II contained seven specimens internally reinforced with GFRP bars, while series III included nine specimens with different amount of transverse reinforcement. Series IV is comprised of ten columns reinforced with different longitudinal reinforcement ratio. The test variables were bar type (steel and GFRP), spacing of transverse reinforcement (40 mm, 80 mm, 800 mm), bar diameter (#5, #6, #8) and splice length as a factor of bar diameter (0, 4, 8, 12, 24, 36). The experimental results were reported in terms of failure modes, load displacement behavior and the components of splice strength. Based on the findings of experimental investigation, the splice length of GFRP bars is much less than that of steel bars. It was found that the specimens reinforced with spliced bar at a specific splice length can behave the same as those reinforced with continues longitudinal bar. The use of condensed GFRP spirals (spacing at 40 mm) provided sufficient restraint against the buckling of the spliced GFRP bars up to the limit of concrete crushing in the post peak stages. The well confined specimens were also able to achieve the second peak load at a specific splice length.

The results revealed the splice strength is comprise of end bearing and bond stress. Both components were evaluated precisely, and effect of variables on these components were determined. Despite spliced steel bars, end bearing stress has a prominent role in the strength of spliced GFRP bars. An analytical model capable of predicting the required splice length, was developed and verified with the experimental results. Moreover, a simplified design equation was presented including the effect of bar diameter, transverse reinforcement, elasticity modules of GFRP reinforcement and compressive strength of concrete. This equation accurately and simply predicts the required splice length.

Keywords: GFRP bars, reinforced concrete column, splice length, analytical model, end bearing, bond, failure mode, compression, axial load, circular section.

RÉSUMÉ

La corrosion des ouvrages en béton armé d'acier constitue une préoccupation dans les régions aux conditions climatiques difficiles. Les armatures en matériaux composites de polymère renforcé de fibres (PRF) ont fait leurs preuves à travers différents éléments structuraux en béton comme armature alternative pour résoudre le problème de la corrosion. Les récents progrès réalisés dans l'utilisation des barres d'armature de polymère renforcé de fibres de verre (PRFV) dans les éléments structuraux sous sollicitations axiales ont montré la nécessité de réaliser davantage d'études sur les détails relatifs aux barres de PRFV en compression. En raison du manque de données expérimentales, les guides de conception actuels pour les structures armées d'armatures de PRF n'ont pas encore traité cette question. Ce projet de recherche a pour but de fournir une base de données expérimentales ainsi que de réaliser des analyses approfondies et de fournir des recommandations de calcul pour déterminer la longueur de chevauchement (recouvrement) requise des barres d'armature de PRFV dans les poteaux en béton armé soumis à des charges axiales. Trente (30) poteaux pleine grandeur en béton armé de section circulaire ont été fabriqués et testés sous une charge axiale concentrique. Les poteaux de diamètre 300 mm et de hauteur totale de 1600 mm ont été calculés conformément aux exigences de la norme CAN/CSA S806-12 (2012). Les poteaux ont été répartis en quatre séries. La série I comprenait trois (3) poteaux en béton armé de barres d'acier et un poteau en béton non armé. La série II comprenait sept (7) poteaux en béton armé de PRFV, tandis que la série III comprenait neuf (9) poteaux avec différents taux d'armature transversale. La série IV était composée de dix (10) poteaux avec différents taux d'armature longitudinale. Les paramètres d'essais comprenaient ;1) le type de barre (acier et PRFV), 2) l'espacement des armatures transversales (40 mm, 80 mm, 800 mm), 3) le diamètre de la barre (n° 5, n° 6, n° 8) et 4) la longueur de recouvrement définie en fonction du diamètre des barres (0, 4, 8, 12, 24, 36). Les résultats expérimentaux ont été présentés selon les modes de rupture, le comportement charge-déplacement et les composantes de la résistance du recouvrement. D'après les résultats expérimentaux, la longueur de recouvrement des barres en PRFV est inférieure à celle des barres d'acier. Il a

été établi que les poteaux armés de barres d'armature ayant des jonctions de longueur de recouvrement donnée pouvaient se comporter de la même manière que ceux armés avec des barres longitudinales continues. L'utilisation de spirales en PRFV rapprochées (espacement de 40 mm) permettait de limiter suffisamment le flambement des barres de PRFV ayant des jonctions par recouvrement, jusqu'à la rupture par écrasement du béton dans les phases post-pic. Le confinement adéquat des poteaux a permis également l'atteinte d'une seconde charge de pointe correspondante à une longueur de recouvrement donnée.

Les résultats ont montré que la résistance de la jonction par recouvrement est fonction des contraintes d'appui bout à bout et des contraintes d'adhérence des barres chevauchées. Les deux composantes ont été évaluées et chacune d'elle a été déterminée en fonction d'une variable effective. Contrairement aux jonctions par recouvrement dans le cas des barres en acier, la contrainte sur les appuis bout à bout joue un rôle important dans la résistance des barres de PRFV ayant une jonction par recouvrement. Un modèle analytique permettant de prédire la longueur de recouvrement requise a été développé et vérifié à l'aide des résultats expérimentaux. En outre, une équation de calcul simplifiée prenant en compte le diamètre des barres, les armatures transversales, et le module d'élasticité des barres de PRFV, ainsi que la résistance en compression du béton a été développée. Cette équation permet de prédire avec précision la longueur de recouvrement requise des barres en PRFV sous charge de compression.

Mots-clés: Barres de PRFV, poteau en béton armé, longueur de recouvrement, modèle analytique, appui bout à bout, adhérence, mode de rupture, compression, charge axiale, section circulaire.

ACKNOWLEDGMENTS

I wish to express my deep gratitude to everyone who made this research possible. The author is greatly indebted to my supervisor Professor Brahim Benmokrane for giving me the opportunity to conduct such research and providing me with the necessary technical support at times when it was most needed.

Special thanks should be extended to Dr. Hamdy Mohamed and Dr. Abolfazl Eslami for their valuable advices, constant cooperation, continues encouragement and assistance with experimental work, testing and analysis.

I must also thank Natural Sciences and Engineering Research Council of Canada (NSERC), the Fonds de la recherche du Quebec en nature et technologies (FRQ-NT) and the Quebec Ministry of Transportation for their financial support and Pultrall Inc for donating the GFRP reinforcement.

Sincere words of thanks must also go to Jérôme Lacroix, technician, for his valuable contributions to testing and Alireza Asadian, PhD student, for his help during fabrication of the specimens.

I would like to convey my love to my father, my sister, and my brother and my uncle for their patience, prayers, extensive support, encouragement and endless love. I wish I could express my great respect to my mother's soul for all the life which I have and to be always beside me when I need her. This journey started three years ago because of her.

I view this document as not necessarily an individual accomplishment but done with the collective contributions of those listed above and many more. Thank you!

TABLE OF CONTENTS

LIST OF TABLES

LIST OF FIGURES

CHAPTER 1 INTRODUCTION

1.1. **GENERAL BACKGROUND**

Many structures are constructed from reinforced concrete such as bridges, parking garages, pavements, and buildings. Traditionally, ribbed steel bars are used as main reinforcement in concrete structures. However, conventional steel bars are vulnerable to electro-chemical corrosion. This problem can be exacerbated by factors such as de-icing salt, moisture, temperature variation, wet and dry cycles, and freeze and thaw conditions (Zaman et al. 2013). In North America, corrosion of steel reinforcing bars is considered as the main source of deterioration in concrete infrastructure leading to a huge loss of money. In fact, repairing, rehabilitating or reconstructing of an infrastructure costs an enormous amount of investment (Boyle and Karbhari 1994). For instance, in Ohio, the state annually spends 200 million dollars to replace or rehabilitate its nearly 4300 bridges owing to corrosion (Singhvi and Mirmiran 2002). In 2013, the American Society of Civil Engineers (ASCE 2013) estimated that civil infrastructure needs 3.6 $trillion to alleviate the hazardous devastation by 2020. Several techniques such as galvanized coating, electro static spray, epoxy coating, polymer impregnated concrete and high compressive strength concrete have been implemented to address the corrosion issue whereas none of them were effectively successful (ACI 440.1R 2015; Nkurunziza et al. 2005). Consequently, a new kind of fibre-reinforced polymer (FRP) composite material, with corrosive-resistant characteristics, has been developed in the last decades as an alternative to steel reinforcement for concrete structures. Many investigations have been directed to assess durability and the structural behavior of concrete members reinforced with FRP bars (ACI 440.1R 2015). Among different types of FRP composites, glass FRP (GFRP) is considered to have a cost nearly similar to conventional/specialized steel reinforcing bars. Therefore, it is deemed as a good alternative to steel bars (Mohamed and Benmokrane 2012). Due to its inherent properties such as corrosion resistance, light

weight, and high tensile strength, GFRP reinforcement has been considered by many research councils and companies worldwide (Hamilton et al. 2009).

Growing application of GFRP bars as a replacement for steel reinforcement in concrete members has led to publish several design guidelines and codes for bridges and buildings such as ACI 440.1R-15; CAN/CSA S6-14 and CAN/CSA S806-12.

Despite many research conducted on the use of GFRP bars in concrete structures as main reinforcement, some issues have not been precisely scrutinized yet. Lap splicing of bars which is inevitable in reinforced concrete (RC) construction, can be considered as one of these unsolved issues. While numerous scientific endeavors have attempted to elaborate on lap splicing of FRP bars under tension, no study has been found on compression lap splicing of FRP bars. In addition, the provisions stipulated by design guidelines and codes for lap spliced GFRP bars under tension are very limited and mainly adopted from those suggested for steel bars. However, fundamental inherent differences of GFRP and steel bars such as brittle fracture, relatively low modulus of elasticity, high ultimate load, linear stress-strain response, and external surface configurations would probably lead to different performance. Particularly, the surface configuration, playing an important role in the mechanical interlock, friction and bond strength in lap-spliced bars, can be even different from one brand to another. Therefore, using the same models for both types of reinforcement may be neither efficient nor rational.

Thus, the proposed research study is pertaining to investigate the structural behavior of lap-spliced GFRP bars under compression. The outcomes can not only propose a reliable length for lap splicing of bars in compression, but also can result in a more efficient use of GFRP reinforcement. This would reassure engineers to implement GFRP bars with more confidence.

1.2. **OBJECTIVES AND SCOPE**

In the past decade, FRP bars have been extensively accepted as an alternative for conventional steel reinforcement in harsh and corrosive environments. However, the

development length of compression lap-spliced GFRP bars has not been fully explored yet. The present study aims to establish technical information replenishing distinct lack of provisions in design guidelines for compression spliced bars.

Briefly, the specific objectives of this research study are:

- To assess the compression strength of full-scale circular concrete columns reinforced with spliced GFRP bars.
- To assess the strength and compression capacity of spliced GFRP bars considering their bond and end-bearing strength components.
- To investigate the effect of compression splice length of GFRP bars and confinement on the ultimate capacity, strain in the GFRP bars, and failure mechanisms.
- To develop design equations to predict the required splice length of GFRP bars in compression to avoid sliding and premature failure.

1.3. RESEARCH METHODOLOGY

In order to achieve the aforementioned objectives of this study, an experimental program and analytical investigation research is being conducted at department of civil and building engineering, Universite de Sherbrooke. The experimental phase comprised 30 reinforced concrete columns reinforcing with GFRP and steel bars. The columns were tested under monotonically increasing static concentric load. Each column specimen has 300 mm in diameter and 1600 mm in height. The test variables included: 1) the bar type (steel and GFRP), 2) the splice length, 3) the confinement using spirals, and 4) the bar diameter. The 30 specimens were divided into four series:

- Series 1 includes four columns to investigate the effect of bar type on the manner of the spliced bars. Three columns were reinforced with steel bars with different splice length. One of the columns was made from just plain concrete to assess the effect of reinforcement on the ultimate strength of the columns.
- Series 2 comprises seven columns reinforced with GFRP bars. The splice length of bars is diverse in each specimen. One column was reinforced with continuous bars.

- Series 3 includes nine columns to assess the confinement effect; the pitch of GFRP spirals is 40 mm for 5 specimens and rest of the columns were just reinforced longitudinally.
- Series 4 consists of 10 columns: 5 specimens were reinforced with longitudinal GFRP bars of No. 6 (20 mm-diameter), and 5 specimens were reinforced with GFRP bars of No. 8 (25 mm-diameter).

The analytical study will focus on assessing the factors affecting the bond and the end bearing strength of GFRP spliced bars under compression and proposing an expression to predict the minimum splice length required for compression lap-spliced GFRP bars. The accuracy and efficiency of the expression will be verified against the experimental results. Towards this, the experimental results include the axial load, displacement and strain for the tested specimens. Normalized curves in terms of each parameter will be drawn. The effects of the variables on the components of the spliced bars strength will be assessed using regression analysis as well as comparison between the curves. Also, the test results of each column will be compared to the values predicted by design codes as well as recently published equations in the literature. Finally, an equation will be derived based on effective variables and a simplified design equation to calculate the length of the spliced bar under compression will be developed.

1.4. ORGANIZATION OF THE DISSERTATION

- Chapter 1 provides an outline of the thesis with brief description of the contents of each chapter
- Chapter 2 provides background concepts including end bearing and bond strength of FRP bars under compression, and structural behavior of FRP or steel RC columns. Specifications of design codes related to lap splicing are also described in this section.
- Chapter 3 describes the experimental part of this study including the construction and testing of 30 full-scale columns reinforced with GFRP or steel bars. The geometry, reinforcement details, and instrumentation of the specimens as well as the material properties and test set-up are presented in this chapter.

- Chapter 4 presents analysis of the experimental test results including the overall performance of each specimen in terms of cracking patterns, stress strain behavior, displacement. Effect of bar type on the load displacement of the columns are also evaluated.
- Chapter 5 introduces effect of confinement on the columns reinforced with spliced GFRP bars. The results are presented in terms of strength, load-strain response and displacement. Moreover, the splice strength is formulated regarding the confinement index and splice length.
- Chapter 6 presents the theoretical investigation of this dissertation. Based on the experimental data obtained in this study, a new proposed model for the required splice length of GFRP bars under compression are presented in this chapter. The results are also compared with the available models.
- Chapter 7 summarized and concludes the finding of the experimental and theoretical studies. Recommendations for future work are also presented.

CHAPTER 2 LITERATURE REVIEW

Columns are compression elements in a structure that transmit the load from the upper level to the lower one and finally to the foundation. Thus, they play a prominent role in stability of the structure so that failure of one column in a critical zone would cause progressive collapse and entire destruction of the structure. The behavior of FRP reinforced concrete columns have been extensively investigated by researchers. However, lap splicing of longitudinal FRP bars under compression has not been studied so far. Even, a few researches can be found in literature which focused on compression lap-spliced steel reinforcement. Compressive lap splicing was explored enough neither for FRP bars nor for conventional steel ones whereas numerous investigations were devoted to performance of tension lap splicing.

Despite many studies were conducted on tension lap-spliced FRP bars and parameters affecting on bond between FRP bars and concrete, no study can be found specifically on compression lap-spliced FRP bars. In order to explore the current state of art, this chapter comprehensively reviews the past knowledge on lap-spliced bars and evaluate parameters that might influence on the performance of lap-spliced GFRP bars in columns.

2.1. **FRP COMPOSITE MATERIALS**

The general idea of composite materials is that two or more components work together to provide a new material with certain specification. Fiber reinforcement polymer (FRP) composite material consists of fibers and a matrix as shown in Figure 2-1. The fibers embedded in the matrix with distinct boundary resist against forces and have a main roll in structural behavior of FRPs. The matrix conveys the forces to the fibers through interface shear resistance and keeps them in the desired shape and situation (Mallick 2007). Different kinds of fibers are used in composite materials such as aramid (AFRP), carbon (CFRP) and glass (GFRP). GFRP is the most common kind of FRP composite in civil engineering on

account of lower price in comparison to the others (Nkurunziza et al. 2005). The matrix or a resin utilized to impregnate fibers can be thermosetting or thermoplastic. Thermosetting resins are more thermal stable and have more chemical resistance. Thermoplastic resins provide more fracture resistance and shelf life. Todays, thermosetting resins such as epoxy and vinyl esters are used widely in construction industry (Hamilton et al. 2009). An engineering material is evaluated by its mechanical properties which are mainly based on fibers properties in FRP composites. In the following, properties of FRP bars and explicitly those affecting on the spliced GFRP bars are discussed:

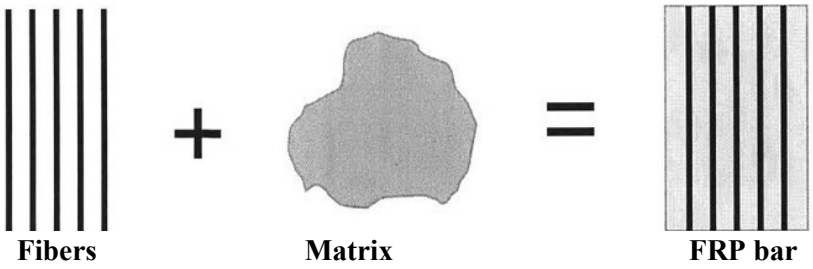

Figure 2-1. Components of FRP bars.

2.2. MECHANICAL PROPERTIES OF FRP BARS

2.2.1. Tensile properties

Unlike the stress-strain behavior of steel reinforcement, FRP bars exhibit a linear stress-strain behavior up to failure so that it breaks without any yield area or large deflection. Strain-stress curves for different kinds of FRP and steel bar are compared in Figure 2-2 by Zhishen et al. (2012). Tensile capacity of FRP bars depends on the fibers volume fraction, rate of curing and manufacturing process. Design guidelines such as ASTM D7205M-06 (2011), CAN/CSA-S806-12 (2012) and ACI440.3R (2004) proposed well-defined procedures to determine tensile properties of FRP bars.

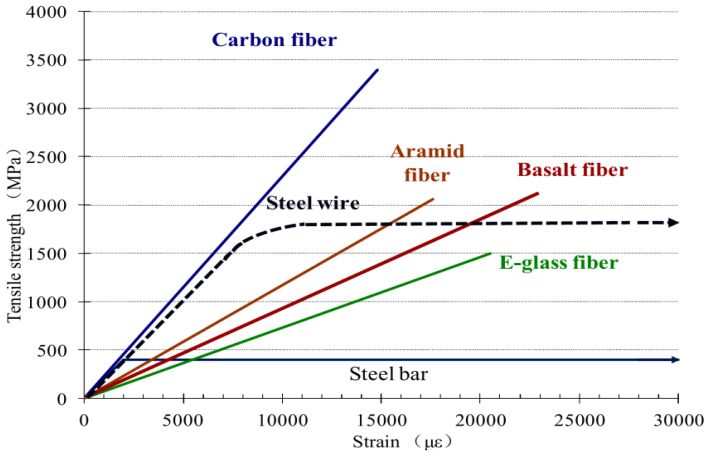

Figure 2-2. Stress strain curve for diverse materials (Zhishen et al. 2012).

2.2.2. Compressive properties

Ehsani (1993) reviewed the mechanical properties of FRP materials. Based on his research, compressive strength of GFRP bars are generally less than their tensile strength. Different experimental results showed that compressive modulus is about 77% of tensile one which relies heavily on the size, surface, type, bar diameter, ratio of diameter to length of the bars and manufacturing process.

Kobayashi and Fujisaki (1995) evaluated compressive behavior of FRP bars covered by concrete. Specimens were conducted under concentric monotonic and cyclic loadings. Fiber types were aramid, carbon and glass fibers. Their experimental measurements showed the compressive strengths of AFRP, CFRP and GFRP equal to 10%, 30% and 30% of their corresponding tensile strength, respectively. Regarding to the results, values of the tensile and compressive stiffness were almost the same for different types of FRP bars. The failure strain of concrete is almost 0.003 which was around 20-50% of the tensile strain of FRP bars. Hence, ultimate compression strain of FRP bars is not able to go higher than 0.003 since concrete fails at this limit. Therefore, difference in strain of tension and compression probably led to difference in strength of FRP bars under tension and compression.

Due to the absence of a specific standard test for FRP bars under compression, Deitz et al. (2003) designed an apparatus to evaluate the compressive strength of FRP bars. This equipment is illustrated in Figure 2-3. The holes in threaded rods were slightly larger than

the diameter of the bar. In this way, the effect of the end cut in specimens can be eliminated. Axial loading produces eccentric load and corresponding moment unless end cut of bars is flat and perpendicular to the longitudinal axis. The experimental program was comprised of 45 bars, 15 mm in diameter, and different length varying between 50 mm to 380 mm. Experimental results substantiated that free distance between threaded rods is nearly equal to unbraced length of bars. Regarding different unbraced lengths, three kinds of failure modes including crushing, buckling and combination of both crushing and buckling were recognized as shown in Figure 2-4. Crushing failure mode probably occurs when FRP bars are completely confined in concrete. According to the results of compression tests, which were presented in Figure 2-5, Deitz et al. (2003) derived a conservative relation for compression strength of #15 GFRP bars. This expression was based on the unbraced length of GFRP bars. Crushing failure would happen if the free length of a GFRP bar was less than 100 mm. In this case, compression strength is half of that in tension. However, the modulus of elasticity under compression was the same as that under tension. If the unbraced length of FRP was more than 200 mm, buckling failure mode would occur and the compression strength was calculated on the base of Euler buckling curve. For the specimens, the radius of gyration was calculated as 3.6 while the effective length was determined to be 0.67. The compressive strength of GFRP bars with a free length between 100 mm and 200 mm was presented by a linear interpolation and their failure mode was a combination of crushing and buckling.

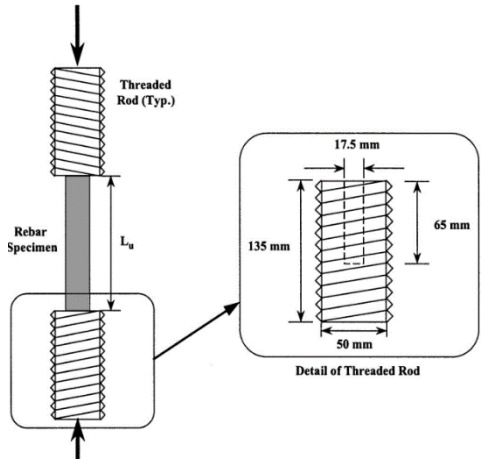

Figure 2-3. Scheme of equipment used in compression tests (Deitz et al. 2003).

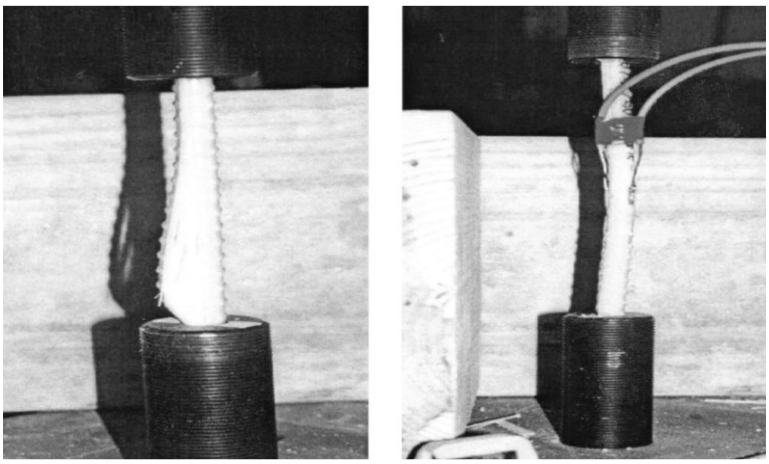

Figure 2-4. Crushing and buckling of GFRP bars for different free lengths (Deitz et al. 2003).

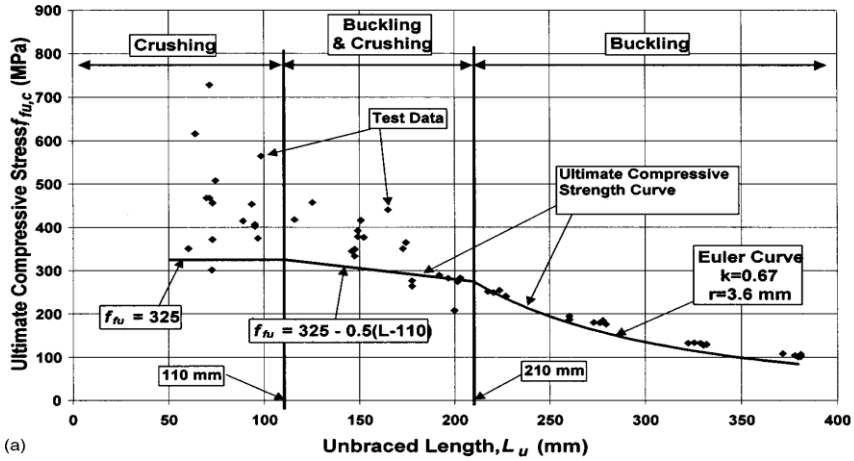

Figure 2-5.Compressive strength of FRP for diverse lengths and published provision by (Deitz et al. 2003).

Afifi et al. (2014a) stated compression test for FRP bars is complicated because of fiber micro buckling. Therefore, a standard test for FRP bars under compression has not been introduced and guidelines often neglect the contribution of FRP strength in compression zone.

ACI440.1R-15 (2015) states that further research is needed to determine behavior of FRP bars under compression. It also noted the reduction in the compression strength of FRP bars is due largely to the premature failure resulting from either end brooming or fiber micro buckling.

Tavassoli et al. (2015) carried out compression tests on FRP bars to clarify behavior of FRP bars used in columns. The nominal axial load capacity of the columns can be predicted by

$$P_0 = 0.85f_c'(A_G - A_{GFRP}) + \varepsilon_C' E_{GFRP} A_{GFRP} \quad (2\text{-}1)$$

where A_G is the gross area of column section, A_{GFRP} is the total cross section of FRP, ε_C' is the concrete strain at peak strength and E_{GFRP} is the elastic modulus of FRP reinforcement. They concluded that the compressive strength of the FRP bars varied between 10-50 percent of their tensile strength if $L/D < 6$ where L and D are the free length and diameter of FRP bars, respectively. The amount of this change is based on the fiber content, resin type and manufacturing process. Regarding to the spiral pitch used in their columns, Tavassoli et al. (2015) tested 25 mm GFRP bars with the free lengths of 50, 160 and 275mm. Figure 2-6 shows the failure modes of FRP bars under compression. According to their results, modulus of elasticity in compression is identical to that in tension. However, considering the difference between compressive and tensile strains, compressive strength of GFRP bars is approximately half of that in tension if $L/D < 6$.

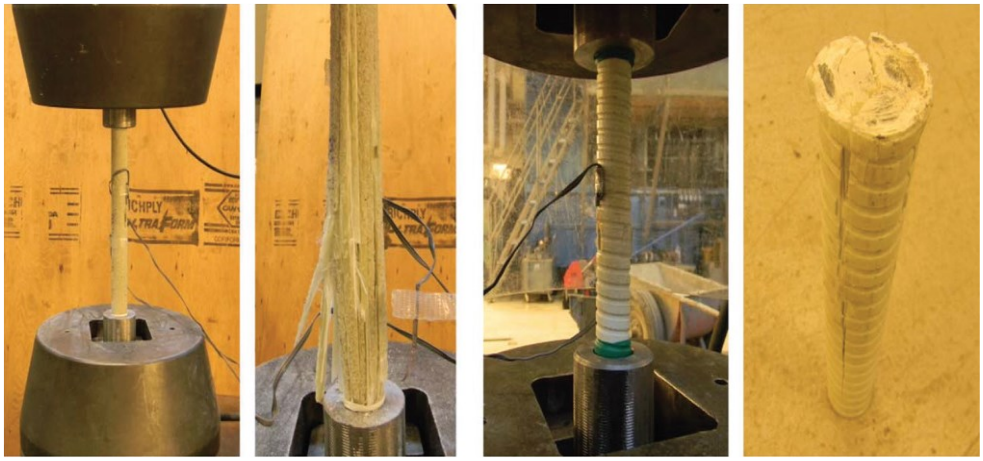

Figure 2-6. Failure modes of GFRP bars in compression (Tavassoli et al. 2015).

Khan et al. (2015) conducted compression and tension tests on CFRP and GFRP bars to evaluate their strength properties. Tension tests as per ASTM D7205M-06 (2011) on 6 FRP bars and compression tests were conducted according to modified ASTM D695-15 (2015). The ultimate strength, modulus of elasticity and ultimate compression strain of FRP bars were assessed. The surface of CFRP bars was smooth although that of GFRP bars was sand coated. The length of the tensile specimens was 1555 mm whereas two lengths of 60 mm and 80 mm were considered for the compression specimens. With regard to the test observations, the tensile bars failed due to the fiber rupture. However, failure mode of the

compressive bars was in the form of fiber separation rather than buckling of fibers probably ensuing from weakness of resin. Failure modes of the bars are shown in Figure 2-7. Due to the slippage of the tensile specimens, ultimate strain of bars was calculated based on the ultimate strength and modulus of elasticity. Modulus was also the gradient of stress strain curve in the range of 0.1% to 0.3% strain. Results showed that GFRP bars tolerate more strength and strain by contrast to CFRP bars. Ultimate compressive strength of GFRP bars and its corresponding strain were 1.4 and 1.65 times higher than those of CFRP bars, respectively. Compression and tensile modulus of elasticity for CFRP bars were 1.17 and 1.6 times higher than the ones for GFRP bars. The ultimate tensile strength of GFRP and CFRP bars were 65% and 94% greater than their compressive strength, respectively. Also, the tensile modulus of elasticity for GFRP and CFRP bars were, respectively, 33% and 98% greater than their values of compressive elasticity modulus.

Figure 2-7. Failure modes of GFRP and CFRP bars in tension and compression tests (Khan et al. 2015).

2.3. BEHAVIOR OF CONCRETE COLUMNS IN COMPRESSION

An extensive research is being done in Universite de Sherbrooke into application of GFRP bars as longitudinal reinforcement in concrete columns (Afifi et al. 2014d; b; c, 2015, Ali et al. 2016, 2017, Hadhood et al. 2016, 2017a, e; b; c, 2018; M. Guérin B. Benmokrane, C. K. Shield, and A. Nanni n.d.; Mohamed et al. 2014, 2017; Mohamed and Benmokrane 2014; Mohammed and Ali n.d.; Tabatabaei et al. 2018). The review of the researches conducted on the concrete members under axial load is presented here. At first, behavior of plain concrete column is described and then the influence of FRP bars on it is presented.

2.3.1. Plain concrete

The ultimate axial load of a column is the sum of the load carried with net concrete and the load capacity of vertical reinforcement as defined in (2-2). The effect of each element at diverse steps of strain was presented in Figure 2-8. It is manifest that the contribution of the concrete is more than steel reinforcement. However, steel reinforcement is able to make the columns ductile.

$$P_0 = kf_c'(A_G - A_{steel}) + f_y A_{steel} \quad (2\text{-}2)$$

The load capacity of the plain concrete is based on the compressive strength of the standard cylinder. Nevertheless, compression strength of a concrete columns is less than that of the standard cylinder. Park and Paulay (1975) mentioned it may be because that quality of concrete in vertical columns is rather less than that in cylinders following from sedimentation and air bubble and water gain at the top part of the columns. Experimental results conducted by Richart and Brown (1934) substantiated that k in Eq. (2-2) should be considered a value of 0.85. Their experimental works were summarized in Figure 2-9. Ultimate strength of concrete and the strength of cylinder were illustrated on vertical and horizontal axis, respectively. It is obvious that the slope of trend line for plain concrete is almost 0.85. It is noted by ACI318M-14 (2014) that reduction in compressive strength of concrete is on account of accidental eccentricity in a pure compression section.

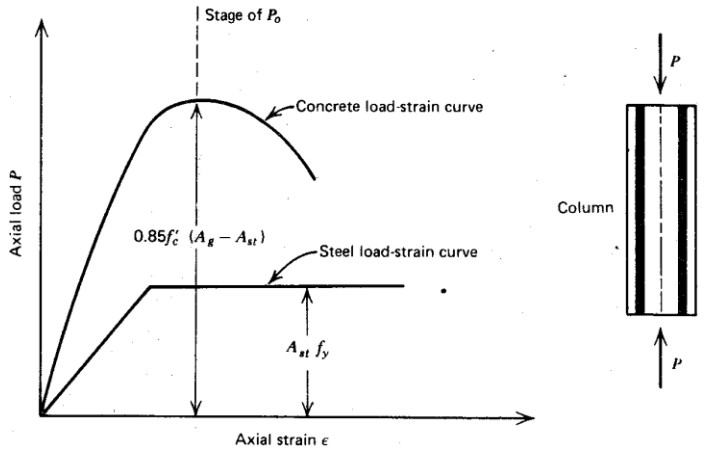

Figure 2-8. Strength components a reinforced concrete column vs strain (Park and Paulay 1974).

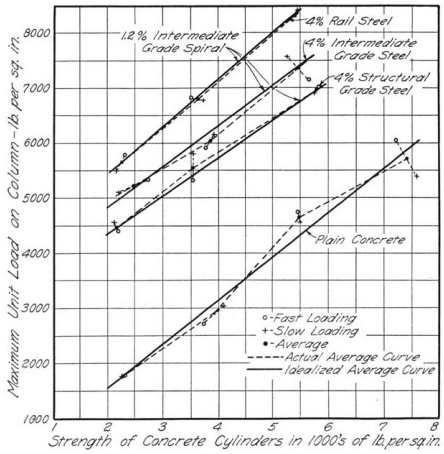

Figure 2-9. Ultimate stress of columns vs the compressive strength of standard cylinder (Richart and Brown 1934).

2.3.2. Concrete columns reinforced with FRP bars

The compressive performance of FRP bars has not been widely clarified by guidelines. There is not any standards defining the compressive strength of FRP bars. This may be because of the micro buckling of fibers or heterogeneous condition of FRP. Hence, CAN/CSA-S806-12 (2012) neglected the compressive contribution of FRP bars. Some studies related to the concrete columns reinforced with FRP are presented in the following.

Results of an experimental study on the behavior of short RC columns were scrutinized by Lotfy (2010). Eight columns with 250×250 mm cross section were carried out under concentric compression axial load. The variables were vertical and transverse reinforcement

ratio, bar type and compressive strength of concrete. Based on the observations, steel RC columns were more ductile than GFRP RC columns. The columns reinforced with steel bars withstood at least 17 percent more carrying load and displacement in comparison with those reinforced with GFRP ones. However, increase in the amount of longitudinal GFRP reinforcement had considerable consequence to the columns' behavior. So that, increment in the reinforcement ratio from 0.723% to 1.08% enhanced the ultimate load, strain and initial cracking load. Nonetheless, adding more bars slightly affected structural parameters as seen in Figure 2-10. With respect to the results, Lotfy (2010) stated that the more transverse ties, the more ultimate and initial cracking load. The columns made of higher compressive strength concrete endured more ultimate load as seen in Figure 2-11.

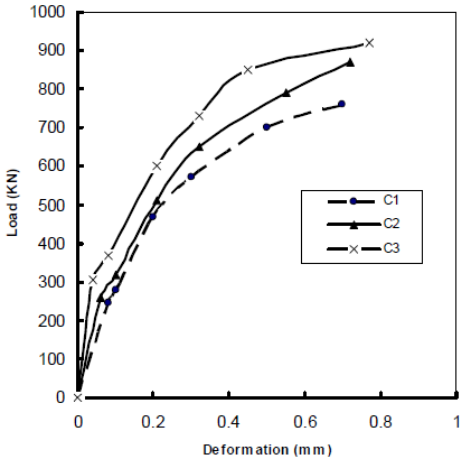

Figure 2-10. Load vs deflection for the columns with different longitudinal reinforcement ratio. C1: $\rho_l = 0.723$, C2: $\rho_l = 1.08$, C3: $\rho_l = 1.45$ (Lotfy 2010).

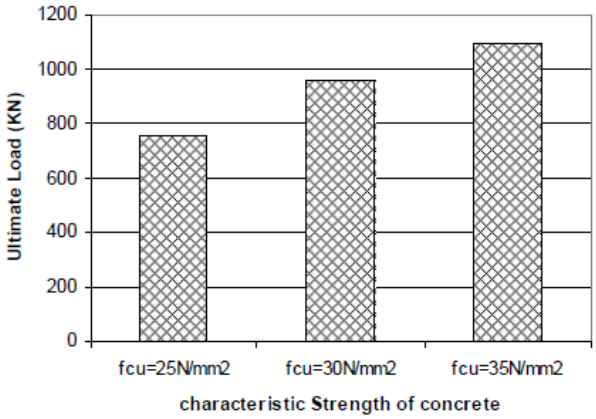

Figure 2-11. Impact of compressive strength of concrete on the ultimate load (Lotfy 2010).

Luca et al. (2010) investigated the contribution of GFRP bars and ties on the ultimate load of RC columns. Five concrete columns with 610×610 mm cross section were conducted. In terms of experiments, three kinds of failure modes were observed. In the case of large space of ties, buckling of GFRP or steel bars dominated the failure mode. However, the columns with small spacing decayed with rupture of GFRP ties and buckling of bars as illustrated in Figure 2-12. The closed spacing ties didn't contribute to improve the peak load. Nevertheless, they influenced strongly on the failure mode by postponing the buckling of bars and generation of unstable cracks. In other words, small spacing ties provided the lateral constraint on development of the cracks and decreased the free length of the bars which sequentially caused to delay in collapse of the columns. Luca et al. (2010) asserted that no considerable difference was observed between GFRP RC columns and conventional steel RC columns except that contribution of GFRP bars in the ultimate load was 5 percent whereas that of the steel bars was almost 12 percent. This diversity in the contribution may be attributed to difference in the modules of elasticity.

Figure 2-12. Failure modes in the columns (Luca et al. 2010).

Tobbi et al. (2012) conducted an experimental study on behavior of concrete columns reinforced with GFRP. They evaluated parameters such as longitudinal type (steel and GFRP), tie configuration, its spacing and cover spalling on eight 350×350 columns.

Different tie configuration used in the specimens were exhibited in Figure 2-13. Experimental results showed that axial strength of GFRP RC columns was the same as steel ones or just a bit more. Typical crack appeared on the specimens in three loading steps were depicted in Figure 2-14. Sudden concrete crushing with buckling of longitudinal bars was the main failure mode of low confined columns. However, progressive crack development and more axial deflection were observed in well confined specimens. In other word, effective tie configuration and closed ties delayed final collapse so that it would lead to the second peak load. Axial stress vs axial strain for the specimens were presented in Figure 2-15. The second peak load was monitored in well confined specimens. The cross section of confined columns after concrete cover spalling decreases. Then, load-displacements were calculated in terms of real cross section of columns and presented in Figure 2-16. Concerning confinement effectiveness, defined as the ratio of peak strength of confined concrete to that of unconfined one, tie configuration would improve the confinement effectiveness from 20 to 70 percent. In terms of enhancement in ductility, defined as the ratio between ultimate strains of unconfined columns to confined ones, ductility upgraded up to 4 times for some columns. Strain of transverse reinforcement vs axial strain was also presented in Figure 2-17. Strain in the ties experienced 10 percent of GFRP bars' ultimate strain till cover spalling. After that, it sharply raised to 70 percent of their ultimate strain for poorly confined columns and gradually increased to 50 percent of it for well confined column. Based on the stress-strain of specimens illustrated in Figure 2-18, the volumetric strain response was calculated in Figure 2-19. It is clear that in the specimen, consisting of the best tie configuration and small spacing between ties, cracked concrete core was restricted laterally and led to gradual crack progression. Therefore, its load displacement behavior was in the elastic area for longer time by contrast to other columns. Tobbi et al. (2012) also predicted GFRP bars withstand up to 35% of their ultimate tensile strength under compression which complemented with experimental results. Therefore, GFRP bars contributed up to 10% of axial load of the tested columns which is fairly equivalent to the contribution of the steel bars.

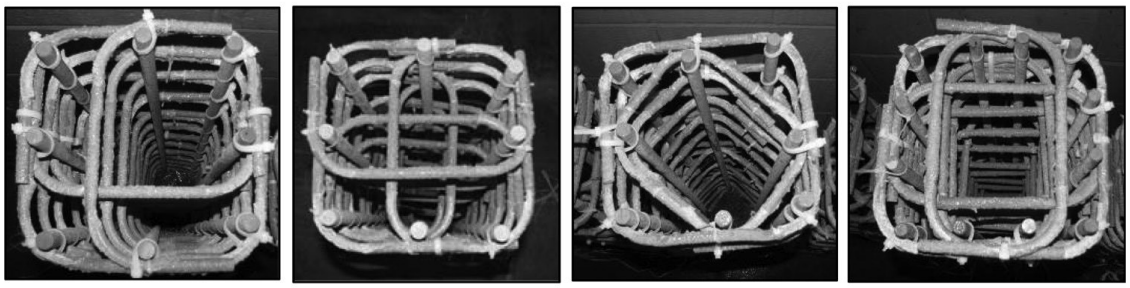

Figure 2-13. Diverse tie configurations used in the specimens (Tobbi et al. 2012).

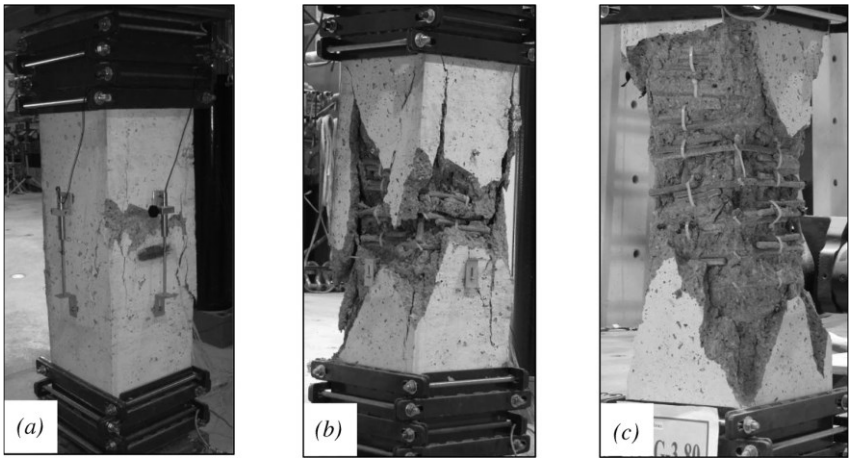

Figure 2-14. Typical crack pattern during loading: appearance of the cracks, cover spalling, collapse of the column (Tobbi et al. 2012).

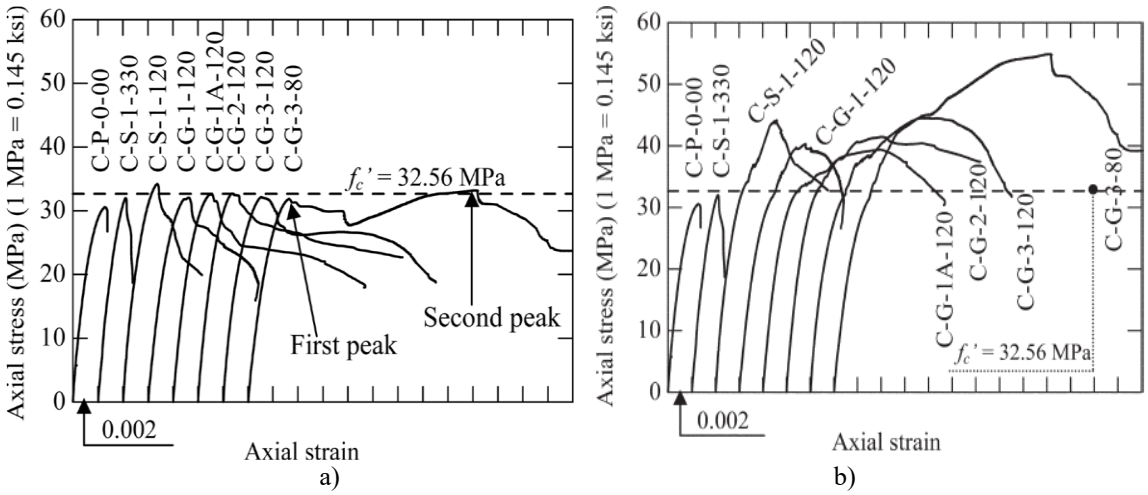

Figure 2-15. Axial stress vs axial strain after spalling off for: a) gross, b) net cross section (Tobbi et al. 2012).

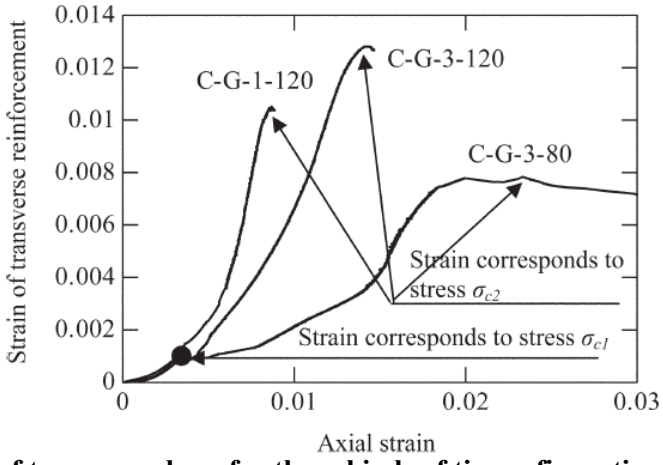

Figure 2-16. Strain of transverse bars for three kinds of tie configurations (Tobbi et al. 2012).

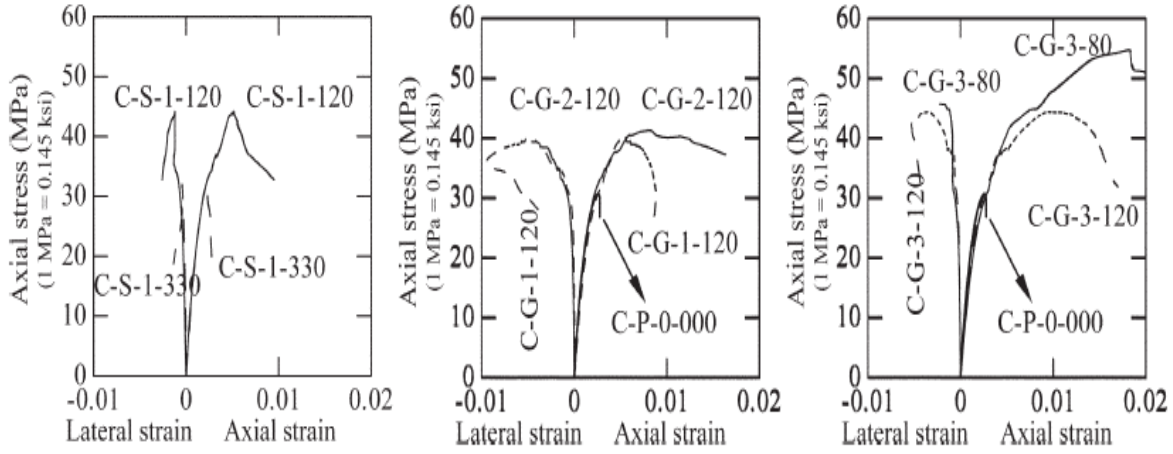

Figure 2-17. Strain and its volumetric response for three tie configurations (Tobbi et al. 2012).

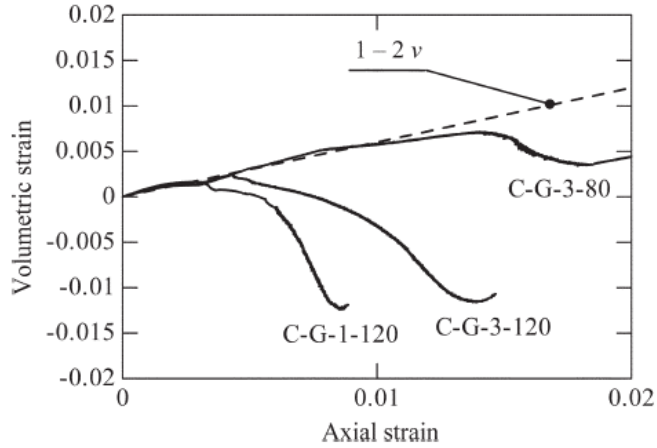

Figure 2-18. volumetric response for specimens with three tie configurations (Tobbi et al. 2012).

In another study, to achieve the precise effect of transverse reinforcement, configuration, spacing, longitudinal reinforcement ratio and confinement on axial members, Tobbi et al. (2014) conducted twenty concrete columns with 350×350 cross section under concentric compressive load. Failure mode of the specimens depended on the bar diameter and configuration of transverse bars as well as on the longitudinal bar type. Failure mode of the specimen, reinforced exclusively by FRP bars, initiated with concrete crushing and buckling of bars and ended up with rupture of transverse bars. Failure modes were depicted in Figure 2-20. Results showed that the ultimate axial load of the columns reinforced with GFRP was almost 30 percent less than those reinforced with steel. However, longitudinal FRP bars withstood high compression load in well confined specimens. Therefore, the contribution of FRP bars in compression should be considered in the design process. As shown in Figure 2-21, the efficiency of closed stirrups is much more than the C-shaped ones. In case of low transverse volumetric ratio with large space between stirrups, CFRP transverse bars confined better than GFRP ones. Even though, GFRP transverse reinforcement more effectively confined the concrete core as spacing is small. Tobbi et al. (2014) stated that a combined reinforcement of steel longitudinal bars and GFRP transverse ones in concrete columns leads to high compressive axial load capacity and ductile behavior.

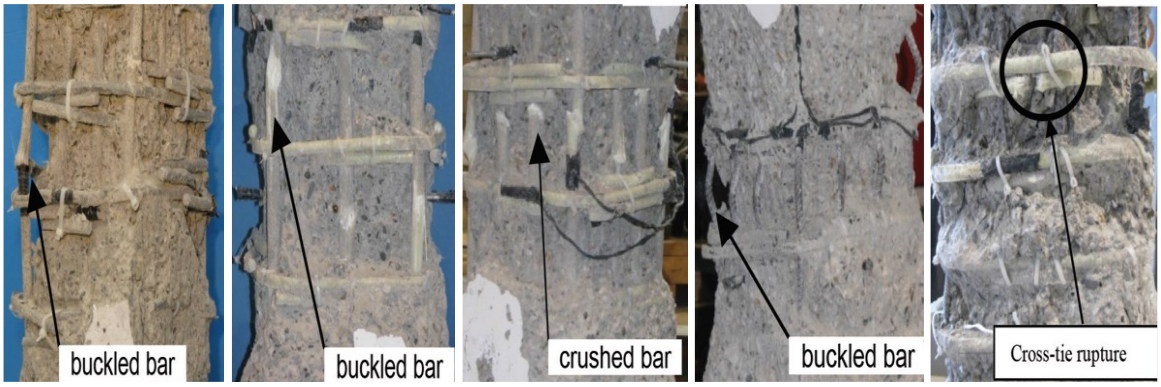

Figure 2-19. Possible failure modes in the specimens (Tobbi et al. 2014a)**.**

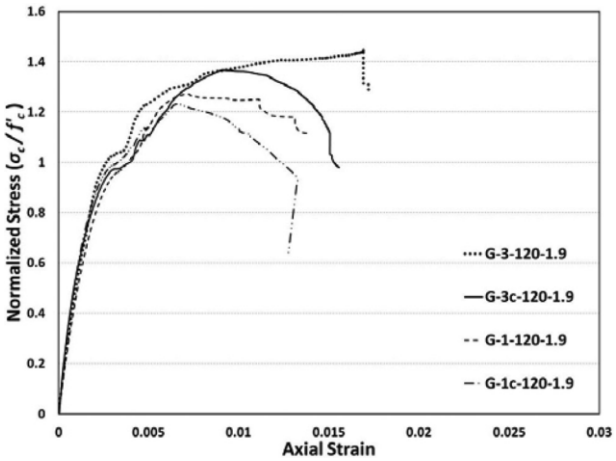

Figure 2-20. Normalized stress-strain for the columns with different tie configuration (Tobbi et al. 2014a)**.**

Afifi et al. (2014b) investigated the effect of GFRP bars on axial capacity of columns. In order to achieve that, they carried out 12 circular GFRP reinforced columns under concentric load. Afifi et al. (2014b) explored the effect of reinforcement type, longitudinal bar ratio, diameter and spacing of spirals. The behavior of the columns reinforced with GFRP bars were generally the same as those reinforced with steel bars even though the GFRP ones withstood almost 7 percent less load as shown in Figure 2-21. GFRP bars carried 5 to 10 percent of axial load whereas steel bars tolerated approximately 16 percent of it. Failure modes of the columns were displayed in Figure 2-22. The red line showed the shear rupture plan in concrete. Spirals spacing strongly influenced the failure mode. When the spiral hooks were very close to each other, failure mode was rupture of GFRP spirals. However, the columns with less confinement failed by buckling of longitudinal bars. Hence, smaller transverse bar diameter and spacing were suggested to increase ductility of the columns. With respect to the experimental results, if transverse volumetric ratio is less than 1.5 percent or space of spirals is more than 80 mm, specimens will be exploded in a brittle manner. It was also clear that increase in the number of GFRP bars in the section of the columns significantly led to more ductile behavior. Afifi et al. (2014b) urged an equation to estimate the axial capacity of the columns and suggested that compression contribution of a GFRP bar should be considered as 0.35 of its tensile strength. Therefore, neglecting the GFRP bars in compressive section is too conservative. Comparison between CAN/CSA-S806-12 (2012) provision and suggested equation were shown in Figure 2-24.

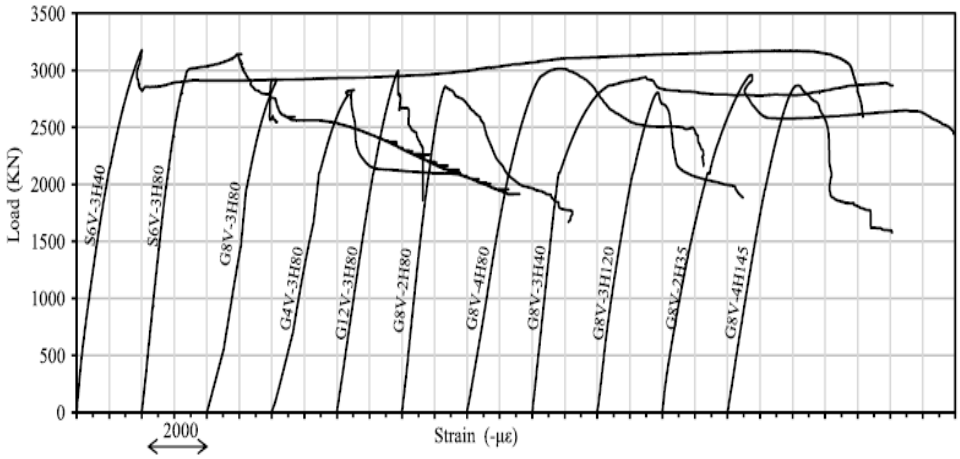

Figure 2-21. Load vs axial displacement for diverse columns (Afifi et al. 2014b)**.**

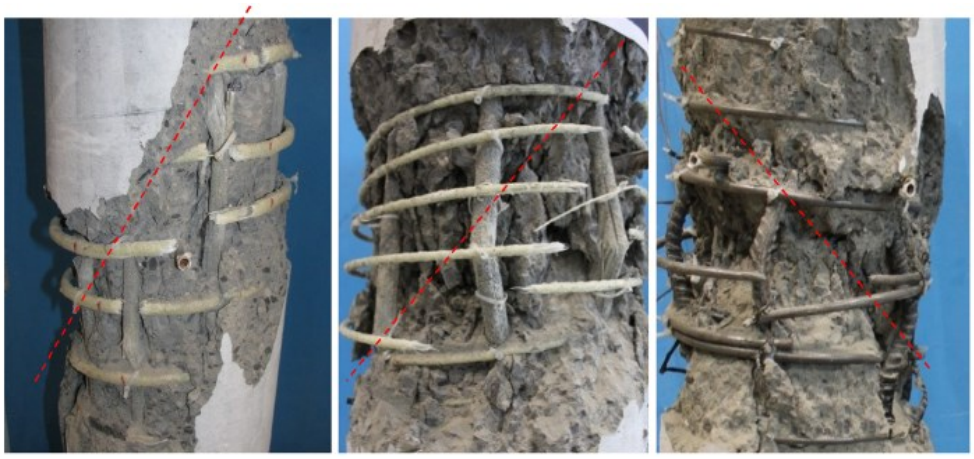

a) **b)** **c)**

Figure 2-22. Different failure mode of the columns: a) rupture of GFRP spirals, b) rupture of GFRP spirals accompanied with buckling of GFRP bars and crushing of concrete core, c) rupture of steel spirals and buckling of steel bars (Afifi et al. 2014b)**.**

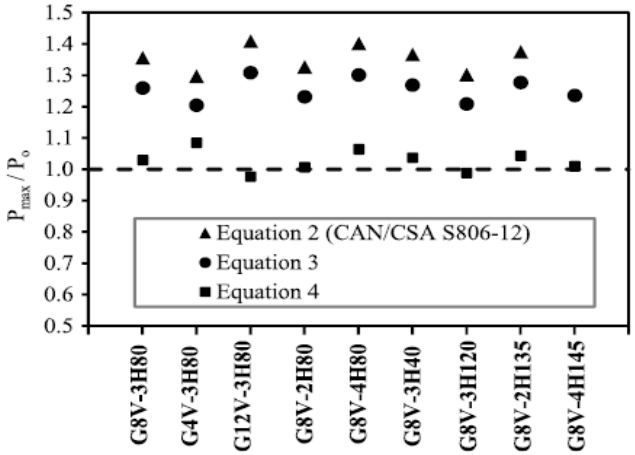

Figure 2-23. Comparison between Canadian guideline and proposed equation (Afifi et al. 2014b)**.**

In another similar study, Afifi et al. (2014c) scrutinized usage of CFRP bars as reinforcements in circular columns and investigated structural parameters such as longitudinal bars ratio, space and size of spirals. They conducted eleven columns 300 mm in diameter. Generally, CFRP RC columns behaved the same as those reinforced with steel bars. CFRP bars were effective even after concrete crushing and developed 75 percent of their tensile strain. They approximately improved the axial compressive strength of columns up to 13 percent but it was just 3 percent less than the effect of steel bars in the columns. Stress strain curves of columns were presented in Figure 2-25. Experimental results showed that failure of well-confined columns controlled with concrete core crushing and rupture of spirals. They exhibited more ductile manner and piecemeal failure after peak load as well. However, failure mode of the rest of the columns accompanied with diagonal shear plan in the middle of the columns. Failure modes of all specimens were demonstrated in Figure 2-26. Despite provided provision in CAN/CSA-S806-12 (2012) that belittles compression strength of CFRP bars in the columns, Afifi et al. (2014c) proposed to take into account 25 percent of tensile strength of concrete as contribution of CFRP bars in compression. Figure 2-26 revealed that their prediction was in good agreement with measured loads.

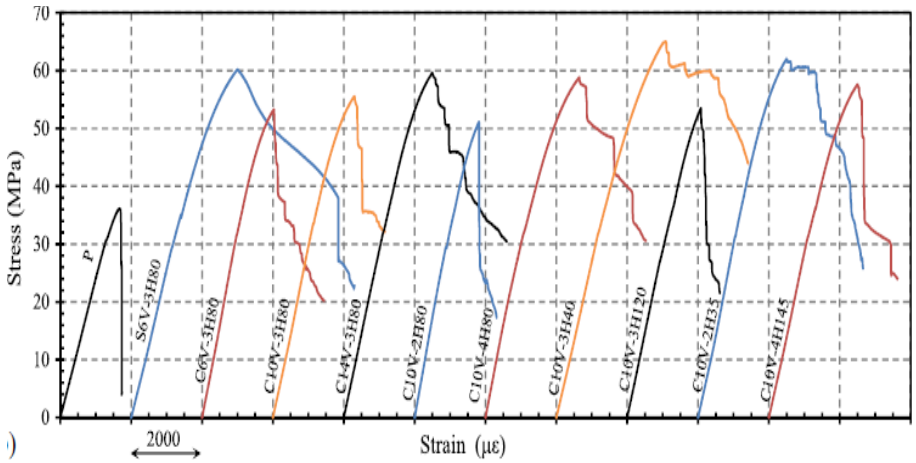

Figure 2-24. Axial stress vs strain for the specimens (Afifi et al. 2014c)**.**

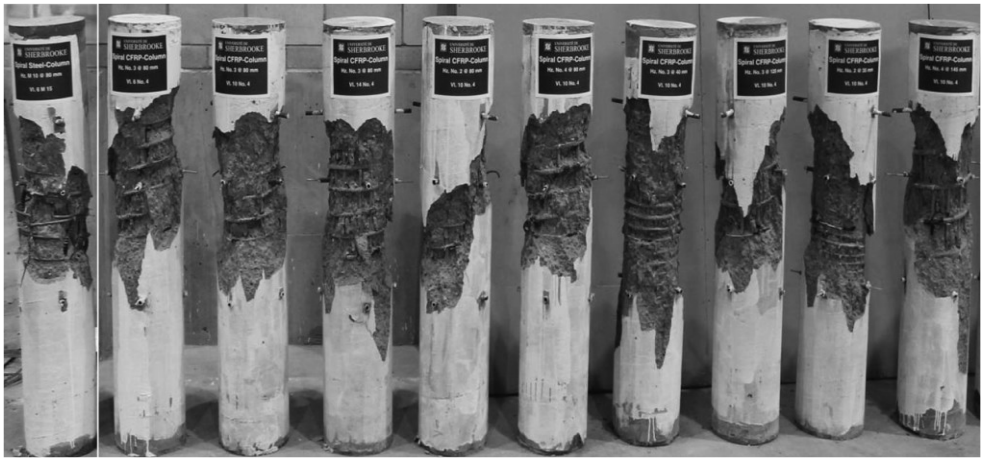

Figure 2-25. The appearance of the specimens after failure (Afifi et al. 2014c)**.**

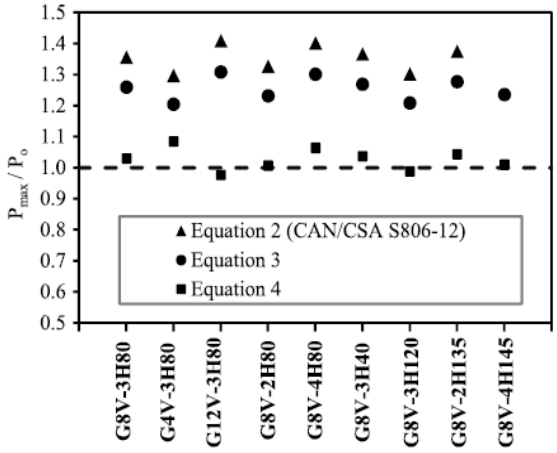

Figure 2-26. Comparison between different equations (Afifi et al. 2014c)**.**

2.4. CONCEPTS OF BOND STRENGTH

2.4.1. Basics

The transfer of stress between bars and their surrounding concrete is called bond between concrete and bars. Bond force is transferred by friction, adhesion and mechanical interlock. In other words, the force conveys through shear stress parallel to a bar at interface between concrete and the bar. Then, bond stress equals to the changes of axial force per unit perimeter of the bar.

The strength of lap-spliced bars under tension is just comprised of one component that is bond strength. The main difference between lap-spliced bars under tension and compression is that end bearing also contributes to transmission of forces in spliced bars under

compression. It should be emphasized that compression force in a concrete element prevents cracks from developing whereas too much compression force results in concrete crushing. Crushing of concrete at the end of bars is a possible failure mode particularly in a large size bar. However, end bearing effect in a small size bar is less important. In case of long term loading, end bearing is insignificant owing to creep in concrete (Park and Paulay 1974). A typical failure mode of end bearing was shown in Figure 2-27.

Figure 2-27. End bearing failure mode (Park and Paulay 1974).

2.4.2. Lap splicing of reinforcing bars under compression

To study the performance of steel reinforcing bars in columns, Pfister and Mattock (1963) tested 16 specimens under concentric load. Their specimens were comprised of circular and rectangular columns with or without splices. The splice length ranged from 0 to 30 times reinforcement bar diameter. They measured the strains in longitudinal bars at different places to evaluate the force conveying through end bearing and bond interface between steel bars and the surrounding concrete. Measured strains showed that contribution of end bearing in spliced bars is significant to transfer compressive force. Monitoring circular specimens with continuous bars revealed that vertical cracks appeared on the surface of the columns at strain of 0.002 and cover splitting occurred at a strain of 0.0026. Meanwhile the columns sustained large deflection. Failure of these columns was accompanied by buckling of longitudinal bars, spiral reinforcements rupture and crushing and disintegrating of concrete core. Failure mode of circular columns with spliced bars was slipping of longitudinal bars and concrete crushing as indicated in Figure 2-28. The load vs. displacement graphs and behavior of rectangular

columns were almost identical to the circular specimens. However, rectangular columns failed suddenly by slipping of spliced bars followed by splitting and crushing of concrete. Spirally reinforced columns also tolerated more load than tied columns. Regarding differences in strains between gages mounted on bars and concrete, Pfister and Mattock (1963) declared that bar slipping occurred before concrete crushing. Compared to the load deflection of the column with continuous bars, they found out that the load in the columns reinforced by spliced bars could not rise when strain initiated to increase rapidly as shown in Figure 2-29 for columns. Pfister and Mattock (1963) stated that the ultimate stress can be developed in a spliced bar is the sum of the end bearing and bond components as shown in Figure 2-30. According to the trend lines for experimental results, it is clear that stress in bars is comprised of a constant value and a linear value. The constant value at the splice length of zero presents the end bearing strength and the inconstant value, being linearly proportional to the splice length, presents the bond strength. It should be considered that constant values for circular columns and rectangular ones are different. Additionally, the end bearing stresses showed that the compressive strength at the end of bars could rise up to 5 times the normal compressive strength of concrete owing to the confinement provided by the surrounding concrete and lateral reinforcement. It is worth mentioning that, at zero lap length, indicating end bearing exclusively, the maximum stresses in reinforcements for circular columns equal to 40 ksi. However, the compressive strength of concrete was almost 4 ksi.

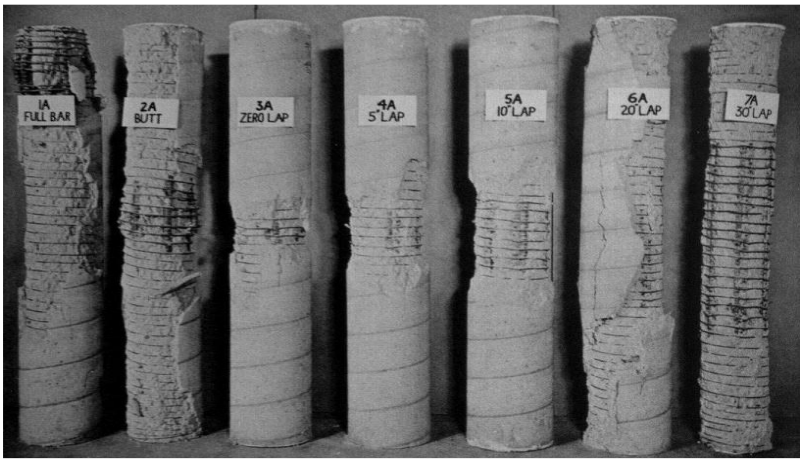

Figure 2-28. Failure mode of circular columns (Pfister and Mattock 1963).

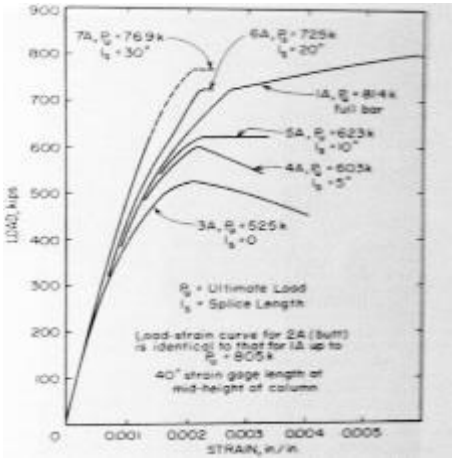

Figure 2-29. Load displacement of specimens (Pfister and Mattock 1963).

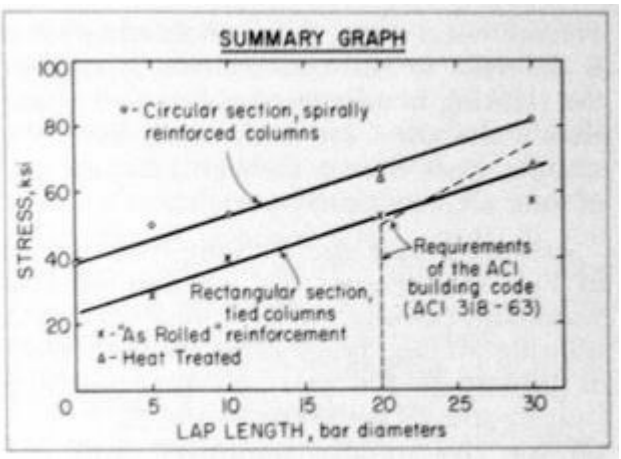

Figure 2-30. Stress in longitudinal bars versus length of spliced bars (Pfister and Mattock 1963).

Cairns and Arthur (1979) conducted an experimental program comprised of 51 full scale columns to assess variables affecting compressive splicing of steel reinforcement. Their experimental objectives were to evaluate the influence of the end bearing, length of spliced bars, compressive concrete strength and position of transverse bars on the splice strength. To distinguish the net contribution of the end bearing and bond in splice strength, they implemented some modification on bars. Some columns were made from bars which their end had been coated with long polystyrene cylinders to eliminate end bearing contribution to splice strength. Furthermore, to prevent bonding in some columns, they were made from smooth and polished bars in splice region and the rest of these bars were wrapped by thick layer of polystyrene and P.V.C tape. Experimental observations revealed that in the latter columns, cracks propagated to the outside of the splice region whereas in the former group,

cracks developed at the center of the splice region. On the other hand, in columns with continuous bars, cracks developed toward each end of the bars. Cairns and Arthur (1979) investigated the rebar and concrete after failure. Shape of concrete remained on the ribs of reinforcement bars at spliced region showed bond failure occurs when inclined concrete surfaces beyond the ribs slid on the surrounding concrete. The concrete cons at the end of spliced bars and the remained concrete on the bars ribs were identical in shape. This similarity confirmed that both bonding and end bearing failure modes naturally work in the same way. In other words, inclined concrete surfaces slide on each other in both failure modes. Experimental results also showed that transverse bars located at the end of the splice were more effective since the measured strains were four times higher than the strain in ties located at the middle of the splice. Moreover, confinement ensuing from stirrups improved spliced bars performance up to a certain degree. After that, adding more stirrups along the splice length have no effect on the strength of splice. Regarding the bond stress measured by strain gages as shown in Figure 2-31, Cairns and Arthur (1979) concluded that the distribution of bond stress along the splice length was not uniform. This was due to increase in the rigidity of splice zone. In other words, the ratio between steel reinforcement to concrete in the splice region was more than outside of it. Then contribution of concrete will be reduced in the middle of splice region inducing increase in the bar stresses. Consequently, toward the end of the bars, the bond stress increased, and the compressive force transferred between steel bars and concrete to a large extent at the end of the bars. Cairns and Arthur (1979) also found out that roughness of bars raises the strength of compressive splice bars up to 13 percent for ribbed bars, and compressive strength of concrete was exclusively effective in short spliced bars where bond force is limited. This fact confirms the significant contribution of the end bearing component.

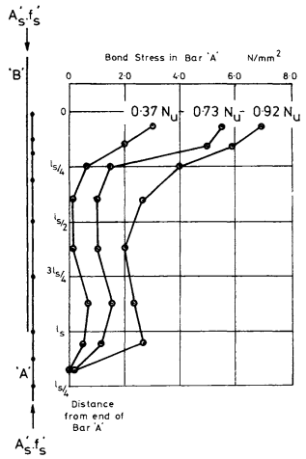

Figure 2-31. Stress distribution along the splice region (Cairns and Arthur 1979).

In another study, Cairns (1985) performed a numerical study on the strength of compressive spliced bars. He used data of 23 rectangular columns conducted in his previous study (Cairns and Arthur 1979) and data of 6 columns gathered from literature (Pfister and Mattock 1963). Regarding the data analysis, Cairns (1985) modified Eq. (2-3), initially developed by Orangun et al. (1977) for estimating the strength of spliced bars under tension, to reflect the effects of concrete strength, bar diameter, splice strength and transverse reinforcement on the spliced bars under compression. Cairns (1985) proposed Eq. (2-4) to predict the required length for spliced bars under compression.

$$f_{st} = \left[\left(0.4 + 1.08\frac{c}{d_b}\right)\frac{L_s}{d_b} + 17.6 + 0.1\frac{L_s A_{tr} f_{yt}}{s_{tr} d_b^2}\right]\sqrt{f_c'} \quad (2\text{-}3)$$

$$f_{sc} = \left[1.4\frac{L_s}{d_b} + 29.4 + 0.32\frac{L_s A_{tr} f_{yt}}{s_{tr} d_b^2}\right]\sqrt{f_c'} \quad (2\text{-}4)$$

where c is the minimum concrete cover to spliced bars or half of the clear spacing between bars in mm; d_b is the bar diameter in mm; L_s is the length splice in mm; A_{tr} is the area of transverse reinforcement perpendicular to splitting plane in mm^2; f_{yt} is the yield strength of transverse reinforcement in N/mm^2; s_{tr} is the spacing of transverse reinforcement in mm; f_c' is the cylinder compressive strength of concrete in N/mm^2; f_{st} is the tensile stress of bar in N/mm^2; f_{sc} is the compressive stress of bar in N/mm^2. Experimental results showed that the transverse bars have a prominent role in compressive spliced bars so that specimens failed when those bars yielded. Cairns (1985) propose a modification to the upper limit for transverse reinforcement above which bond stress would not improve. He proposed Eq. (2-5)

for the upper value while this limit which had been proposed for tension splices is given in Eq. (2-6).

$$\frac{A_{tr}f_{yt}}{sd_b} = 6\ N/mm^2 \quad (2\text{-}5)$$

$$\frac{A_{tr}f_{yt}}{sd_b} = 10.35\ N/mm^2 \quad (2\text{-}6)$$

Furthermore, they noticed that tied bars can affect the splice strength if they are located at the end of the splice region. Analysis showed that stirrup influence on compressive provision can be up to three times greater than its effect on tensile splices. Effect of concrete strength in compressive equation was the same as that in tensile equation and it is proportional to the square root of compressive strength of concrete. Cairns (1985) stated that the bond strength in spliced bars under compression is smaller than that of under tension. This is because compressive force conveying through bars (compression force parallel to bars) reduces the tensile strength in perpendicular direction. Drop in tensile force causes decrease in the confinement force. In the same way, contribution of concrete cover is also negligible.

In the latest studies conducted on compression behavior of lap-spliced steel bars, Chun et al. (2010) carried out some tests including 44 specimens to assess the strength and sufficient length for compressive lap-spliced steel bars in unconfined columns. Their compressive strength of concrete varied from 40 MPa to 60 MPa. The test parameters were comprised of compressive strength of concrete, clear space between bars, concrete cover and bar diameters. Strain gages were applied at the end and along the spliced bars in order to measure the contribution of end bearing and bond strength components in compression splices of reinforcing bars. Based on the results of their tests, they asserted that the strength of spliced bars is proportional to the square root of compressive strength of concrete as mentioned in ACI 318-08 (2008) provision. That strength was also proportional to the square root of ratio between length of splice and bar diameter. Using the regression analysis of their data, they have developed a relation to calculate the strength of compression splices in unconfined columns as defined by

$$f_{sc,p} = \left(11.1 \times \sqrt{{l_s}/{d_b}} + 16.4\right)\sqrt{f_c'} \quad (2\text{-}7)$$

where $f_{sc,p}$ is the strength of compression splice in N/mm^2. The predictions of the proposed equation were in a good agreement with their experimental results. A constant value indicating end bearing effect was added to the formula provided by Chun et al. (2010) because measured strain at the end of the bars remained constant irrespective of other properties of the bars. Observation data showed that the strain measured by gages was irrelevant to the clear spacing between bars, so the proposed provision ignore the clear spacing effect.

In addition, Chun et al. (2010) evaluated the relation provided by ACI 318-08 (2008) for compressive lap splicing. They found out that strength of compression splices is comprised of two components including bond and end bearing. Despite the significant contribution of the latter component, it is not considered in ACI provision resulting in a conservative prediction of the required length for spliced bars in compression. ACI estimations also become even more conservative for the concrete strengths higher than 45 MPa.

The advantage of transverse confinement on compressive strength of lap-spliced steel bars was investigated by Chun et al. (2010b). Their experimental program consisted of 24 columns loaded concentrically to put spliced bars in the same severe pressure and preclude strain gradient in the section of columns. Effect of confinement ratio, compressive strength of concrete and ratio between cover concrete and bar diameter were evaluated in their experimentation. Contribution of bond strength and end bearing are measured by strain gages. Situation of transverse bars were also examined. Failure mode of specimens all accompanied by sudden cover splitting. However, cover splitting in the specimens reinforced with transverse reinforcements along the splice length was less than those reinforced just at the end of the splice. Similar to the unconfined specimens, the experimental results confirmed the negligible effect of the clear spacing between longitudinal bars in splice strength. Transverse bars would influence on splice strength unless the splice length had been enough for bars to reach the yield stress. Similarly, confinement of splice bars improves the end bearing performance if the transverse bars are located at the end of lap-

spliced bars. Transverse bars upgraded the bond contribution in the splice strength up to a specific amount. Chun et al. (2010b) declared that the transverse bars prevent the crack propagation into the splice region inducing an improvement of the both splice performance and its strength. Furthermore, comparing different expressions predicting compressive strength of steel spliced bars, as presented in Figure 2-32 and Figure 2-33, they found out that ACI 318-08 (2008) estimates the strength of splice too conservative. Eq. (2-8) is offered in ACI 318-08 (2008) to predict the strength of lap-spliced bars under compression.

$$f_{sc,p} = 0.071 f_y d_b if\ f_y \leq 420\ MPa$$
$$f_{sc,p} = \left(0.13 f_y - 24\right) d_b\ if f_y > 420\ MPa \quad (2\text{-}8)$$

The conservative prediction of ACI provision can be attributed to ignoring the influence of the concrete strength and the transverse bars. Eq. (2-3) suggested by Orangun et al. (1977) also wouldn't take into account the end bearing effect. On the other hand, Cairn's provision, which was already defined as Eq. (2-4), underestimated the strength. Consequently, with respect to Eq. (2-7) derived for splice strength in unconfined columns, Chun et al. (2010b) offered Eq. (2-9) which is based on regression analysis of experimental results. This equation was developed for confined columns consisting of transverse reinforcement effect on both end bearing and bond strength. To reflect the influence of transverse reinforcement on end bearing contribution δ was added to Eq. (2-7). It equals one if a transverse bar is placed at the end of spliced bars otherwise δ is zero. Bond contribution also enhances with transverse bars. This increment, presenting by Eq. (2-9), is proportional to the amount of transverse bars.

$$f_{sc,p} = \left[\left(11.1 + 1.5\frac{K_{tr}}{d_b}\right)\sqrt{\frac{l_s}{d_b}} + 16.4 + 1.8\delta\right]\sqrt{f_c'} \quad (2\text{-}9)$$

$$K_{tr} = \frac{40 A_{tr}}{s_{tr} n} \quad (2\text{-}10)$$

In the above equations, K_{tr} is the transverse reinforcement index as defined in ACI 318M-14 (2014).

Figure 2-32. Splice strength calculated by different equations (Chun et al. 2010c)**.**

Figure 2-33. Bond strength calculated from different equations (Chun et al. 2010c)**.**

In another study Chun et al. (2012) investigated the influence of high compressive strength of concrete varying from 80 MPa to 100 MPa on lap splice strength under compression. To achieve this goal, 72 columns, made from high concrete strength, were loaded under concentrically compressive axial load. Moreover, results of 22 specimens were gathered from literature (Chun et al. 2010c). Similar to the results obtained from specimens with normal concrete strength, experimental results for columns with high concrete strength showed that the confinement improves the bond strength and end bearing as illustrated in Figure 2-34. Transverse bars located at the end of lap-splicing also enhances the end bearing strength. Based on the analysis of results, Chun et al. (2012) stated that strength of the spliced steel bars is proportional to a power of f_c'. Even though, this power changed between 0.37 and 0.76, in order to simplify, they suggested the strength of spliced should be considered proportional to the square root of compressive strength of concrete. In addition, they derived

Eq. (2-11) and Eq. (2-12), on base of $\sqrt{\frac{l_s}{d_b}}$ and $\frac{l_s}{d_b}$ respectively, for the strength of the spliced bars in high strength concrete. Experimental results of 94 specimens were gathered to verify the accuracy of equations. The COV (coefficient of variation) for ratio of predicted splice strength to experimental strength in both equations was 9.8%.

$$f_{scp} = \left[\left(11.1 + 1.7\frac{k_{tr}}{d_b}\right)\sqrt{f_c'} + 16.5 + 1.7\delta\right]\sqrt{f_c'} \quad (2\text{-}11)$$

$$f_{scp} = \left(1 + 0.11\frac{k_{tr}}{d_b}\right)\left(1.59\frac{l_s}{d_b} + 34.5\right)\sqrt{f_c'} \quad (2\text{-}12)$$

Both equations predicted the splice strength with a reliable accuracy at spliced length larger than zero. However, the latter equation presents neither the end bearing precisely nor the splice strength at zero length as shown in Figure 2-35. The non-continuous trend line in Figure 2-35 for end bearing contribution is constant and equals to 16.5. This amount is the same as the constant value shows in Eq. (2-11).

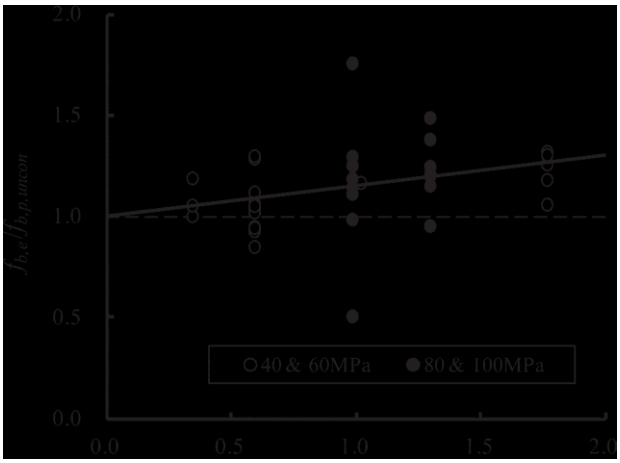

Figure 2-34. Effect of confinement on the bond strength (Chun et al. 2012).

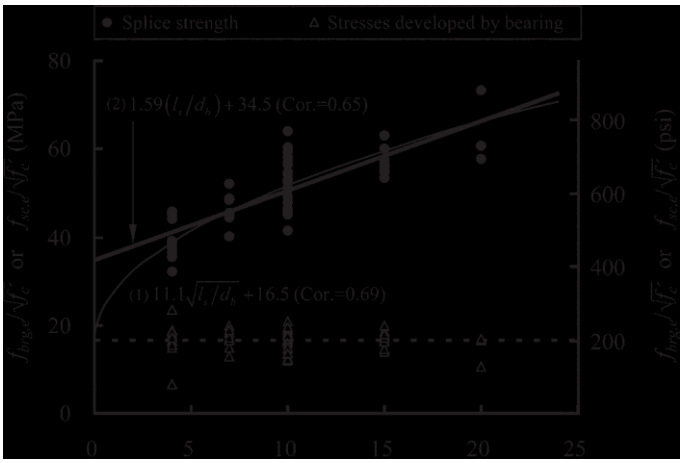

Figure 2-35. Two different trend lines to predict splice strength (Chun et al. 2012).

2.5. CODE PROVISIONS FOR LAP-SPLICED REINFORCEMENT

This section has aimed at providing a brief description of the provisions stipulated in the design codes for lap-splicing bars. No formula can be find in design codes for GFRP bars to estimate splice length under compression. Then, the code provisions specified for steel bars are presented in lieu of an explicit code expression to estimate the required splice length of GFRP bars under compression.

2.5.1. ACI 318M-14 (2014)

Lap splices shall satisfy the requirements for all load combinations which are comprised of wind, earth quack and gravity forces. If the critical combination loads cause compressive force in a bar, that bar has to be designed in compression. However, the provisions for compressive lap splices have been formulated to provide at least $0.25f_y$ resistance to tension stress. According to Clause 10.7.5.2.1, a reduction factor which is 0.83 for tied columns should be applied on the splice length if transverse reinforcements throughout the splice region have an effective area at least $0.0015\ hs$ in each direction where h is perpendicular leg of stirrup to that direction. The splice length is also permitted to decrease to 0.75 for spiral columns if clear space between turns is greater than 25 mm and $4/3d_{agg}$ and less than 75mm. However, the deducted length shall be more than 300 mm. Owing to the lack of

experimental results on spliced bars of No. 43 and No. 57, Clause 25.5.1.1 declares that lap splice for these bars is prohibited except where they are spliced to No. 36 and smaller bars. In this case, Clause 25.5.5.4 states that the splice length of two different bar size shall be greater than the development length of larger bar in compression and the splice length of smaller bar in compression. Regarding Clause 25.5.5.1, the length of compression lap splice for No. 36 or smaller bars is $0.071 f_y d_b$ if $f_y \leq 420 Mpa$ or this length equals to $(0.13 f_y - 24) d_b$ if $f_y > 420 MPa$. The splice length also increased by 33 percent if $f_c' < 21 MPa$. Clasue 25.5.1.2 points out that clear space between spliced bars or adjacent bars shall be greater than 25 mm, d_b and $4/3 d_{agg}$. Regarding to R10.7.6.1.5, longitudinal reinforcement in compression shall be enclosed in transverse bars. So it is necessary to put a set of ties at each end of lap-spliced bars in tied columns and one turn of spiral reinforcement per specified spacing is necessary in circular columns.

As specified in Clause 10.7.5.1.1, end bearing splices, called butt joint by Pfister and Mattock (1963b), is permitted if the bar stressed in compression. The splices shall be staggered or additional bar provided at splice location so that in each face of columns, the tensile capacity of continuous bars are $0.25 f_y$. Regarding to R 10.7.6.1.5, a set of ties should be provided at below and above end bearing splices, and Clause 25.5.6.2 states end bearing is just permitted in members with closed stirrups, ties, spirals or hoops to ensure minimum shear resistance in section. Clause 25.5.6.1 also points out that ends of the bars shall be hold in concentric contact by a suitable device particularly for inclined bars. Clause 25.5.6.3 declares “bars ends shall terminate at surface within 1.5 degrees of right angle to axis of the bars and between 3 degrees of full bearing after assembly”.

2.5.2. S6-14 CAN/CSA-S6-14 (2014)

The Clause 8.15.9.1 states that bars greater than 35M shall not be spliced by over lapping. The transverse space between bars spliced in flexural members shall be smaller than 0.2 times the required splice length and 150 mm. According to Clause 8.15.9.4 the splice length for bars in compression is $(0.133 f_y - 24) d_b$. This clause also offers reduction factors similar to those suggested in Clause 7.5.2.1 of ACI318M-14 (2014).

2.5.3. CAN/CSA-A23.3-14 (2014)

Regarding to the Clause 12.14.2.1, bars greater than 35M shall not spliced unless these bars are spliced to 35M bars or smaller ones. In this case, the splice length is greater than both the development length of larger bar and the splice length of smaller one. Clause 12.14.2.3 is the same as Clause 8.15.9.1 in CAN/CSA-S6-14 (2014). Clause 12.16.1 states the minimum lap splice length for bars with yield strength less than 400 MPa equals $0.073f_y d_b$ or $(0.133f_y - 24)d_b$ if yield strength of steel bars is greater than 400 MPa. However, the splice length shall not be less than 300 mm. Clauses 12.17.3.4 and 12.17.3.5 presents reduction factors for the splice length the same as those mentioned in Clause 7.5.2.1 of ACI318M-14 (2014) for both tied columns and spiral ones.

According to Clause 12.16.4.3, end bearing splices is allowed just for members containing closed ties, stirrups and spirals. Clause 12.17.2 states the ratio between reinforcement and gross area of the section shall not exceed 0.04. If this restriction is not respected, the splice locations should be spaced at least 750 mm apart.

2.6. CONCLUSIONS

The critical literature review presented in this chapter was aimed at identifying the existing gaps in the current knowledge of lap-spliced FRP bars under compression in reinforced concrete columns. All the investigations conducted on splicing of FRP bars were dedicated to spliced bars under tension. Even for steel, a few experimental attempts have performed on compression lap splicing. The code provisions for lap-splicing of steel bars under compression remained the same since 1963 which raises some questions regarding their accuracy as they have not considered the effect of compressive strength of concrete in lap-spliced length. Therefore, a research study should be conducted to fill the existing gap to develop a new design expression for accurate calculation of lap splice length of GFRP bars under compression.

CHAPTER 3 EXPERIMENTAL RESEARCH

3.1. **GENERAL**

Lack of experimental data on lap splicing of GFRP bars under compression has led to the scarcity of design provisions in most of international codes and guidelines. In order to broaden our knowledge in this area, the current study has conducted to elaborate the behavior of lap-spliced GFRP bars under compression. For the purpose of developing an appropriate relation between parameters affecting the strength of spliced bars, the research was divided in two phases: 1) An experimental work to evaluate the effective parameters, 2) An analytical work to develop an expression to calculate the required length of spliced GFRP under compression. The latter work will be validated by results obtained from the experimental tests. In the following sections, the steps which are carried out to satisfy the objectives of this research consisting of experimental work and parametric study are described in detail.

3.2. **MATERIALS**

3.2.1. Concrete

The test specimens were casted using a mix normal weight concrete with a target compressive strength 40 MPa after 28 days. To simulate real conditions of field applications, the columns were casted vertically by a pump in three layers and compacted by an electrical vibrator to remove air bubbles as illustrated in Figure 3-1.

16 standard cylinders (200×100 mm) were prepared in accordance to ASTM C192/C192M (2016) to determine the actual compressive strength of concrete after, 7 days, 28 days and at the time of testing. Table 3-1 summarized the results obtained through compressive tests on cylinder specimens. Three and four cylinder tests were carried out after 7 and 28 days, respectively, while the rest were conducted on the first and the last day of testing period to determine the mean compressive strength of concrete at the time of testing. The workability

of concrete was also measured to be about 100 mm according to ASTM C143/C143M (2015) as seen in Figure 3-2.

Figure 3-1. Casting the specimens.

Figure 3-2. Slump test.

After the slump test, super plasticizer was added to improve the workability of concrete. The columns and cylinders were unmolded one day after casting and cured for at least 7 days with wet burlaps at similar environmental conditions.

Table 3-1. Concrete test results summary.

Mean compressive strength (MPa)			Slump (mm)
7 days	**28 days**	**Testing day**	**Casting day**
30	40.5	49.3	100

3.2.2. Steel

Two kinds of steel reinforcements were used to construct the steel RC columns, #15 as longitudinal bars and #10 as spiral stirrups. To facilitate the construction process, the steel cages were produced by a contractor; and mechanical properties of this batch of steel, provided by the manufacturer, were presented in Table 3-2. However, the GFRP cages were assembled in the laboratory of the Université de Sherbrooke.

Table 3-2. Mechanical properties of steel.

Bar number	Diameter (mm)	Area (mm^2)	Modulus of elasticity (GPa)	Yield strength (MPa)	Ultimate tensile strength (MPa)	Tensile strength (%)
M10	10	71	200	460	660	0.2
M15	16	200	200	460	660	0.2

3.2.3. Glass fiber reinforcement polymer (GFRP) reinforcement

Sand coated standard modulus GFRP bars (Grade 2 in accordance with CAN/CSA S807-10) was used in this study as shown in Figure 3-3. The mechanical properties of this type of bar are given in Table 3-3.

Figure 3-3. Sand coated GFRP bars used in the study.

Table 3-3. Mechanical properties of GFRP materials.

Bar size	Diameter (mm)	Area (mm2)	Modulus of elasticity (GPa)	Tensile strength (MPa)	Tensile strain (%)

Standard modulus sand coated GFRP bars (V-ROD, Pultrall Inc)					
#5	15.9	209	51.2	1374	2.7
#6	19.1	299	51.3	1318	2.6
#8	25.4	541	50.3	1269	2.5
Sand coated spiral stirrups (V-ROD, Pultrall Inc.)					
#3	9.5	83	54.1[1]	819	2.2[1]

[1] Based on the results of straight portion bars.

3.3. SPECIMENS DETAILS AND TEST MATRIX

The test specimens considered in the study were designed to evaluate the effects of four variables including: 1) bar type, 2) bar diameter, 3) splice length, and 4) spacing of transverse reinforcement on the strength of lap-spliced bar under compression. To achieve the objectives of the study, the proposed experimental program consisted of 30 full-scale circular reinforced concretes with 300 mm in diameter and 1600 mm in height. The geometric and reinforcement details of the test specimens are illustrated in Figure 3-4.

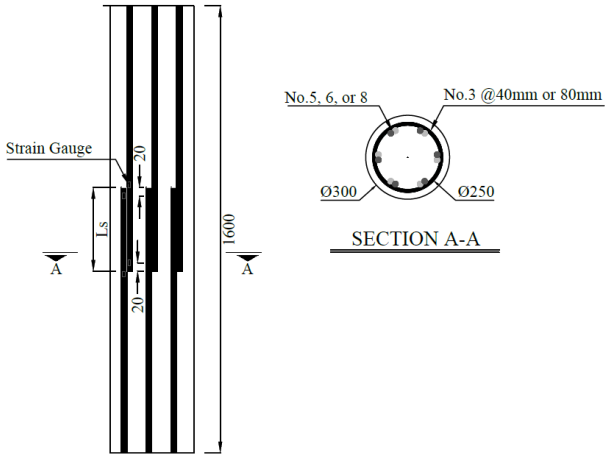

Figure 3-4. Geometry and reinforcement details of the test specimens.

All the columns have the same geometry, while they were reinforced with six longitudinal bars with different splice length and transverse reinforcement configuration. The specimens were transversely reinforced with #3 spiral stirrups made of steel or GFRP, such that the steel and GFRP stirrups were used in steel and GFRP RC columns, respectively. In addition, a clear concrete cover of 25 mm was considered from the surface of the spiral stirrups.

The specimens were divided into four groups as presented in Table 3-4. Each specimen is identified by five codes. The first letter "S" or "G" refers to steel or sand-coated GFRP bar, respectively. The following digit indicates the bar diameter of longitudinal bars. The second number after the letter "L" indicates the splice length as a coefficient of bar diameter whereas the word "C" is for specimens with continuous FRP bars. The last number corresponds to the spiral spacing (40 and 80 mm) whereas "UC" indicates unconfined specimens. To assess the contribution of plain concrete in the total strength of concrete, one specimen is cast without any longitudinal or transverse reinforcement and nominated as UR (Unreinforced).

Table 3-4. Details of test specimens.

Test series	Specimen designation	Rebar	Splice length, l_s (mm)		Spiral pitch	Bar type	Segment length (mm)
	UR	-	-	-	-	-	-
Series I	S5-L4-80	6 #5	4db	64	80	Steel	812
	S5-L8-80	6 #5	8db	128	80	Steel	844
	S5-LC-80	6 #5	CONTINUOUS		80	Steel	1560
Series II	G5-L0-80	6 #5	0	0	80	GFRP1	780
	G5-L4-80	6 #5	4db	64	80	GFRP1	812
	G5-L8-80	6 #5	8db	128	80	GFRP1	844
	G5-L12-80	6 #5	12db	192	80	GFRP1	875
	G5-L24-80	6 #5	24db	384	80	GFRP1	971
	G5-L36-80	6 #5	36db	576	80	GFRP1	1066
	G5-LC-80	6 #5	CONTINUOUS		80	GFRP1	1560
Series III	G5-L0-40	6 #5	0	0	40	GFRP1	780
	G5-L4-40	6 #5	4db	64	40	GFRP1	812
	G5-L8-40	6 #5	8db	128	40	GFRP1	844
	G5-L12-40	6 #5	12db	192	40	GFRP1	875
	G5-LC-40	6 #5	CONTINUOUS		40	GFRP1	1560
	G5-L4-UC	6 #5	4db	64	-	GFRP1	812
	G5-L8-UC	6 #5	8db	128	-	GFRP1	844
	G5-L12-UC	6 #5	12db	192	-	GFRP1	875
	G5-LC-UC	6 #5	CONTINUOUS		-	GFRP1	1560
Series IV	G6-L0-80	6 #6	0	0	80	GFRP1	780
	G6-L4-80	6 #6	4db	76	80	GFRP1	818

G6-L8-80	6 #6	8db	152	80	GFRP1	856
G6-L12-80	6 #6	12db	228	80	GFRP1	894
G6-LC-80	6 #6	CONTINUOUS		80	GFRP1	1560
G8-L0-80	6 #8	0	0	80	GFRP1	780
G8-L4-80	6 #8	4db	102	80	GFRP1	831
G8-L8-80	6 #8	8db	204	80	GFRP1	882
G8-L12-80	6 #8	12db	304	80	GFRP1	932
G8-LC-80	6 #8	CONTINUOUS		80	GFRP1	1560

In each series, one specimen was made with continuous longitudinal bars and was used as the reference column. Series I, containing four steel reinforced specimens, was proposed to investigate the effect of bar type and the splice length in comparison with rest of specimens. Three of the specimens in this series, were reinforced with steel bars to compare with others reinforced with GFRP bars. Another column was just made from plain concrete without any reinforcement to provide insight regarding the contribution of concrete to the ultimate strength of columns. Three columns were reinforced longitudinally with six M15 steel bars and transversely with M10 spiral stirrups with pitch length of 80 mm. Continuous steel bars were used in one column whereas two other columns were constructed by lap-spliced bars with $4d_b$ and $8d_b$ (64 mm and 128 mm) length. The results of this series would provide a basis to identify the fundamental differences between the bond strength of steel and GFRP bars. Steel cages were presented in Figure 3-5 .

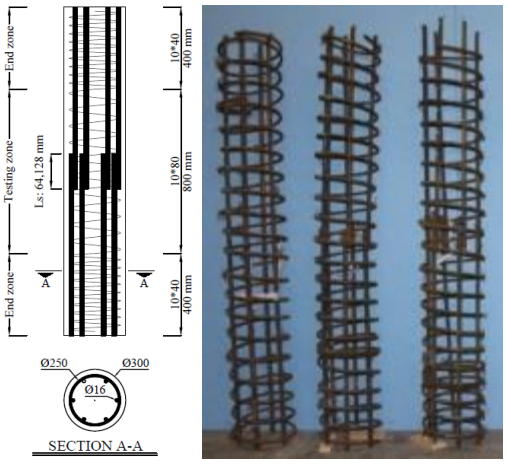

Figure 3-5. Steel cages of specimens in series I.

The second series includes seven columns with different lap splice length as presented in Figure 3-6. Based on the literature review, two components of the strength of spliced bars under compression consists of: end bearing and bond strength. The latter is strongly reliant on the splice length. Splice length, varying from zero to 32 times the bar diameter, were considered to explore the effect of embedded length on the bond strength whereas other parameters remained constant.

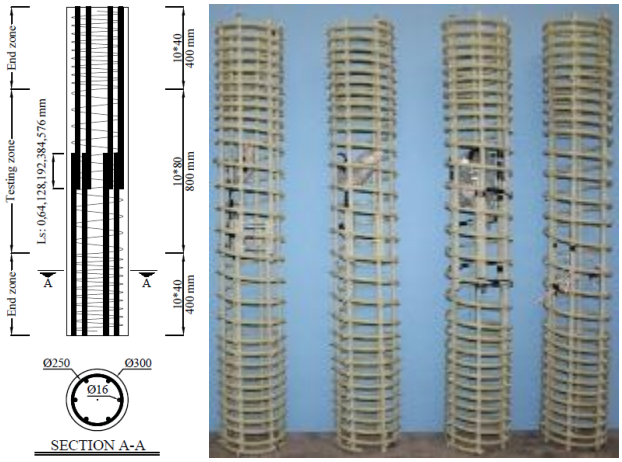

Figure 3-6. Details of columns in series II and fabricated cages.

Series III comprises nine columns with different ratio of transverse spiral reinforcement. Five columns were confined with pitch of 40 mm while the rest were unconfined. Moreover, in this series five columns of series 2 (G5-L0-80, G5-L4-80, G5-L8-80, G5-L12-80, G5-LC-80) would widen the database of series III and assess the effect of confinement on lap splicing strength more precisely. Details and some fabricated cages were displayed in Figure 3-7.

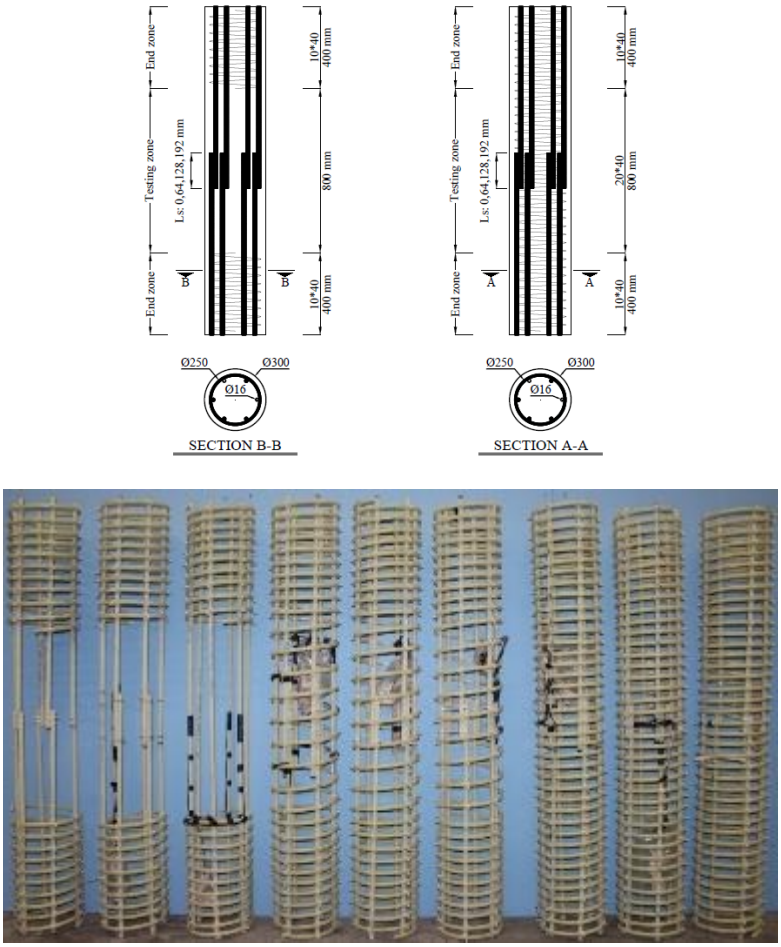

Figure 3-7. Configuration of specimens in series III.

The fourth series was composed of ten columns to investigate the effect of bar diameter on the strength of spliced GFRP bars under compression. Details of the specimens in this series are presented in Figure 3-8. They were reinforced with either #6 or #8 longitudinal bars. In cooperation with five columns from the series I (G5-L0-80, G5-L4-80, G5-L8-80, G5-L12-80, G5-LC-80), the effect of bar diameter will be examined on splice strength of compression bars.

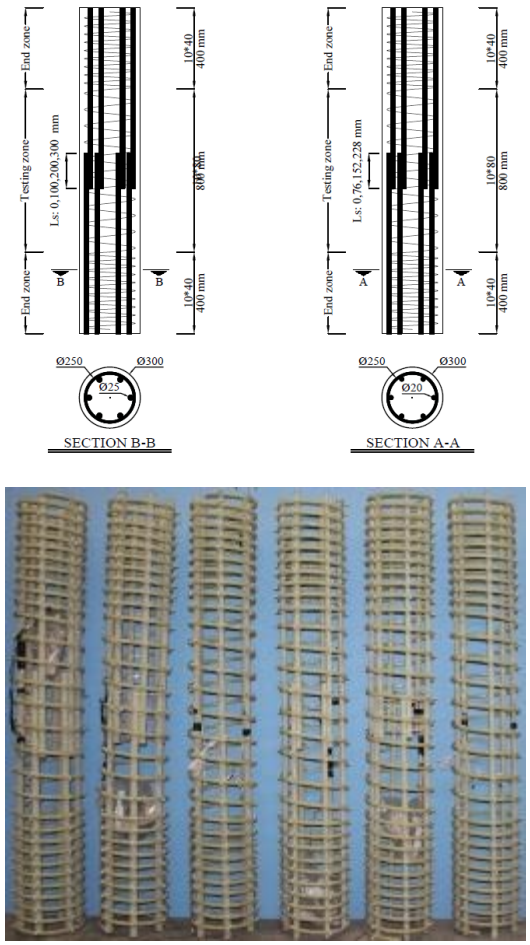

Figure 3-8. Details of specimens and cages in series IV.

It is worth mentioning that six columns, made from continuous bars, are deemed as a reference. Results obtained from these six columns could also enrich the available literature on behavior of columns reinforced with GFRP longitudinal bars under compression.

3.4. INSTRUMENTATION AND TEST SET-UP

The variation of strain in GFRP bars and concrete as well as deformation of specimens was measured by using a series of strain gages and linear variable differential transformers (LVDTs) during the tests. The testing process will be monitored and recorded through a data logger connected to a computer and control unit of hydraulic pump.

Before casting, electric resistance strain gages were carefully installed on the longitudinal bars and spirals to measure the strain distribution during the tests. A total of five strain gages

were installed in each column except for column G5-L24-80 which is equipped with 11 strain gages. One strain gage was mounted on spiral at the mid height of each column. Four strain gages were also installed on a pair of lap-spliced bars along the splice length as illustrated on Figure 3-9.

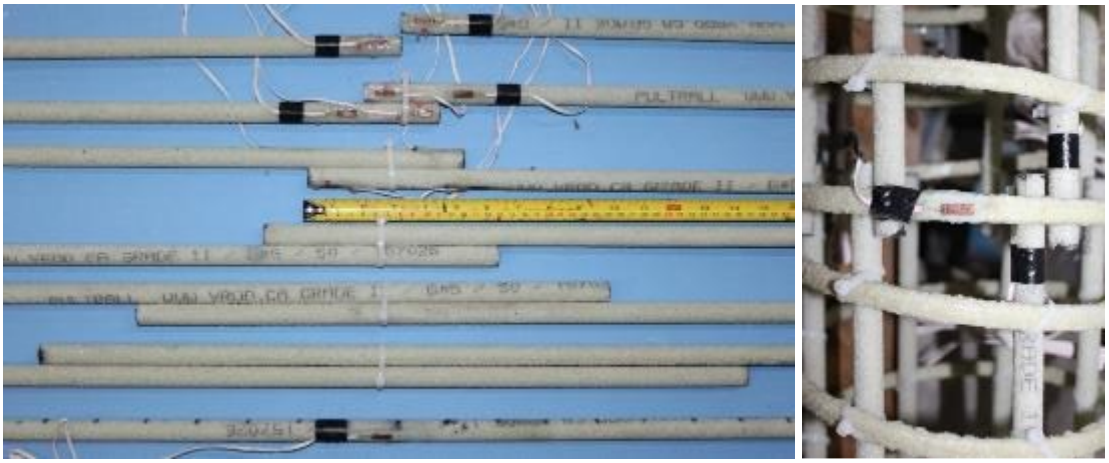

Figure 3-9. Location of strain gages on the reinforcements.

To clarify, just one pair of bars out of six longitudinal spliced bars were instrumented. Two strain gages were installed at the beginning of the splice length, and two other strain gages were also installed at a distance of 20 mm from the free end of the splice length. This space (20 mm) is considered to allow well development of strains in spliced bars. In the column G5-L24-80 three pairs of lap-spliced GFRP bars were instrumented by eight strain gages. It should be noted that in the columns with continuous bars, three strain gages were applied at the middle of three out of six longitudinal bars with an angle of 120°. For columns with zero splice length, three strain gages were just installed at a distance of 20 mm from the end of the bars. To measure strain of concrete, two strain gages were deliberately attached on the surface of specimens as depicted in Figure 3-10. Furthermore, four LVDTs were used to measure the axial deformation of the columns. The specimens were tested under a concentric load applied by Forney machine as shown in Figure 3-11.

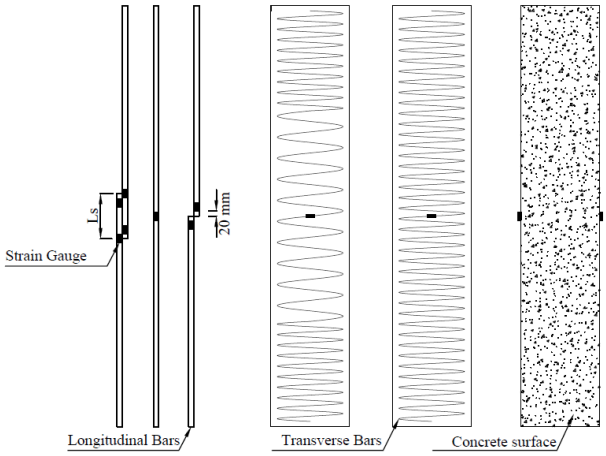

Figure 3-10. Outline of strain gages situation used in the study.

Figure 3-11. Test set-up and hydraulic machine used in tests.

Firstly, loading was carried out up to 1000 kN at the rate of 1 kN/s. Then, loading rate was decreased to 0.5 kN/s until the ultimate load of specimens. The test was continued until a 35 percent drop in the peak load. The internal load cell of Forney machine was used to monitor axial load. The test set up was demonstrated in Figure 3-11. To prevent any premature crack at the top or bottom of the specimens, two pairs of steel collars were used to keep the failure mode at the testing zone as shown in Figure 3-12.

Figure 3-12. Steel collar.

3.5. **FORMWORK CONSTRUCTION**

Six formworks containing five specimens have been constructed to cast thirty columns. Each formwork was made of four layers of plywood with 5 mm thickness. One plywood was screwed on some pieces of wood to provide a level base. Others were drilled to prepare six holes with 310 mm in diameter. Sonotubes, used to form circular columns, would be supported in the holes. One of the holed plywood was fixed on the base and others were situated in the middle and the top of the Sonotubes. Some vertical and diagonal wooden braces firmed the plates in their positions. Cages were fixed in the Sonotubes by plastic chairs to insure the desire concrete cover. Figure 3-13 displayed the details of the formwork.

Figure 3-13. Overview of formworks and cages in the Sonotube.

CHAPTER 4 STRENGTH OF COMPRESSION LAP-SPLICED GFRP BARS IN CONCRETE COLUMNS WITH DIFFERENT SPLICE LENGTHS

Foreword

Authors and affiliation:

- Amirhomayoon Tabatabaei, PhD candidate, Department of Civil Engineering, University of Sherbrooke, Quebec, Canada.
- Abolfazl Eslami, Postdoctoral Fellow, Department of Civil Engineering, University of Sherbrooke, Quebec, Canada.
- Hamdy M. Mohamed, Postdoctoral Fellow, Department of Civil Engineering, University of Sherbrooke, Quebec, Canada
- Brahim Benmokrane, Professor of Civil Engineering and Tier-1 Canada Research Chair in Advanced Composite Materials for Civil Structures and NSERC Chair in FRP Reinforcement for Concrete Structures, Department of Civil Engineering, University of Sherbrooke, Quebec, Canada.

Journal: Construction and Building Materials.

Status: Published, 2018.

4.1. ABSTRACT

Recent years have seen valuable research work on using glass-fiber-reinforced-polymer (GFRP) bars in reinforced-concrete (RC) members under compression. Nonetheless, lap splicing of GFRP bars under compression has not yet been explored with due consideration of its components. To address this knowledge gap, this paper comparatively demonstrates

the results of an experimental investigation pertaining to the effect of splice length on the compression lap splicing of GFRP bars in concrete columns. The experiment comprised 11 large-scale circular columns measuring 300 mm in diameter and 1600 mm in height: seven specimens reinforced with GFRP bars, three specimens with steel bars for comparison purposes, and one specimen without reinforcement (plain concrete). All columns were tested under a monotonically increasing concentric load. The test variables included the reinforcement type (GFRP versus steel) and splice length. The results were compared in terms of the stress–strain curves, ultimate loading, displacement capacity, and splice strength. The test results indicate that the required compression splice length for GFRP bars is less than that required for steel. As the strength of a compression splice consists of end-bearing and bond components, the contribution of each part was scrutinized in detail using measured strain values. The required splice length for GFRP bars was based on the end-bearing component. Based on the experimental results, a length of $8d_b$ can reliably be considered as the required splice length for No. 5 GFRP bars in compression.

Key words: GFRP bar, compression splices, concrete columns, bond strength, end-bearing contribution, splice length.

4.2. INTRODUCTION

Corrosion of steel reinforcing bars stands out as a significant factor limiting the life expectancy of reinforced-concrete infrastructure exposed to harsh environmental conditions. In the last decade, the use of fiber-reinforced polymer (FRP) as an alternative reinforcing material in reinforced-concrete (RC) structures has emerged as an innovative solution to the corrosion problem (ACI 440.1R 2015). Extensive research programs have been conducted to investigate the flexural and shear behavior of concrete members reinforced with FRP bars (Ali et al. 2016; Bentz et al. 2010; El-Gamal et al. 2005; El-Sayed et al. 2012; Farghaly and Benmokrane 2013; Guadagnini et al. 2006; Hassan et al. 2014; Razaqpur and Spadea 2015; Tottori and Wakui 1993; Zadeh and Nanni 2017). FRP design provisions for shear and flexure are now well established and included in codes and design standards.

Glass-FRP (GFRP) bars are becoming more attractive to the construction industry because they cost less than other types of FRP materials. GFRP bars have been used successfully as the main shear and flexural reinforcement in concrete bridges, parking garages, tunnels, and water tanks (ACI 440.1R 2015; Mohamed and Benmokrane 2014; Zadeh and Nanni 2013). Nevertheless, current guidelines do not cover the subject of FRP-reinforced concrete members subjected to axial compression loads. Using GFRP bars as the main reinforcement in compression members is still under consideration. This can be partly attributed to the insufficient recognition of certain parameters that influence the analysis and design of such members. These parameters may include, but are not limited to, reinforcement type, ratio of longitudinal FRP reinforcement, and volumetric ratio and configuration of transverse reinforcement. While the first two parameters influence the loading capacity of an FRP-reinforced concrete column, the displacement capacity and ductility are mainly affected by the confinement action provided by the transverse reinforcement. Lateral confinement can also prevent local and global buckling of longitudinal reinforcement. Recently, valuable research work has been conducted to investigate the effect of different parameters on the behavior of concrete members reinforced with GFRP bars subjected to compression axial loads or simultaneous flexural loads (Afifi et al. 2014a; d, Hadhood et al. 2017c; d; b; Hadi et al. 2016; Luca et al. 2010; Tobbi et al. 2014a). The outcomes of these experimental studies may ultimately provide a convincing case to allow the limited use of FRP bars in columns. Aside from the current study, almost no experimental work on concrete members reinforced with lap-spliced GFRP bars subjected to compression loads has been conducted.

The results of axially loaded concrete columns reinforced with GFRP bars could hardly be different than that of their steel-reinforced counterparts. Luca et al. (2010) tested rectangular concrete columns reinforced with GFRP and conventional steel bars. The reinforcement ratio of the longitudinal bars in all the columns was equal to 1% of the total cross-sectional area. Within this range of longitudinal reinforcement, the loading capacity of the columns reinforced with GFRP bars were similar to those reinforced with steel. In addition, the contribution of GFRP bars to the column capacity at peak load was about 5%, compared to approximately 12% for the steel reinforcement. Assuming a reduction factor of 0.35 for the contribution of GFRP reinforcement, Afifi et al. (2014b)reported an equal ultimate strength

for circular columns reinforced with GFRP and steel longitudinal reinforcement at ratios of 2.2% and 1.7%, respectively. Based on their results, the load carried by the GFRP-reinforced columns was 7%, on average, less than those reinforced with steel. The average load carried by the longitudinal GFRP bars, however, ranged between 5% and 10% of the peak load, compared to about 16% for the steel bars. In another study, Tobbi et al. (2014) tested rectangular GFRP-reinforced concrete columns with two longitudinal reinforcement ratios of 0.8% to 1.9%. Their results indicated a relatively close contribution of the GFRP and steel reinforcement to the column capacity (10% and 12% of the peak load for the GFRP and steel bars, respectively).

Research works conducted on eccentrically loaded GFRP-reinforced concrete columns have also demonstrated the efficiency of using GFRP bars in the tension and compression sides (Hadhood et al. 2017c; d; e; Hadi et al. 2016). The experimental results showed that the axial load and bending-moment capacity of the GFRP-reinforced concrete columns were comparable to those of the conventional steel-reinforced concrete columns with similar reinforcement ratio, concrete strength, and cross section (Hadi et al. 2016). Hadhood et al. (2017a) experimentally constructed the failure envelope for 10 large-scale circular GFRP-reinforced concrete columns. They concluded that compression failure due to concrete crushing controlled the ultimate capacity of the specimens tested under concentric and low eccentric loading. The experimentally predicted axial and flexural capacities of the GFRP-reinforced high-strength-concrete columns using ACI 440.1R 2015 and CAN/CSA S806-12 2012 assumptions and ignoring the compression contribution of the GFRP bars were reasonable but rather conservative relative to the experimental results (Hadhood et al. 2017d).

In addition to the experimental studies, valuable theoretical approaches have been developed by many researchers to better estimate the nominal axial force and bending moment of GFRP-reinforced concrete columns under static eccentric loading. Zadeh and Nanni (2013) developed axial load-bending moment interaction diagrams theoretically, assuming that longitudinal GFRP bars are only effective in tension. When subject to compression, they can be replaced with the equivalent area of concrete as if they were not present in the cross

section. Recently, Zadeh and Nanni (2017) proposed design equations to estimate the flexural stiffness of GFRP-reinforced concrete columns whether for structural analysis or for slenderness effects.

While numerous research endeavors have elaborated on the use of FRP bars as the main reinforcement in compression elements, lap splicing of FRP bars in compression has not been explored in detail. It should be noted that, due to considerations such as ease of storage and transportation, FRP bars are manufactured in certain lengths. Thus, splicing is inevitable in reinforced-concrete structures, although it should be minimized in field applications. In such cases, the resistance of a bar spliced along its length is mainly governed by the splice strength. Inadequate splicing can lead to undesirable failure of the member. The pioneering scrutiny of compression splicing dates back to over 50 years ago in which Pfister and Mattock (1963) examined the requisite length for spliced steel bars in compression. Based on their experimental findings, the strength of a spliced steel bar comprises two components: end bearing and bond as depicted in Figure 4-1. The provisions for splicing under compression in ACI 318M (2014) were mainly derived from this study. Chun et al. (2010a) later evaluated the relation in ACI 318M (2014) to determine the splice length of bars in compression. Comparing the experimental and predicted values underlined the necessity to modify the ACI relation. Due to the inherent differences between GFRP and steel reinforcement, the provisions recommended in design codes and guidelines for steel bars (ACI 318M 2014; CSA A23.3-14 2014) cannot be used for GFRP reinforcement. This knowledge gap was the main motivation behind the current experimental campaign aimed at describing the performance of compression lap-spliced GFRP bars in concrete columns with different splice lengths.

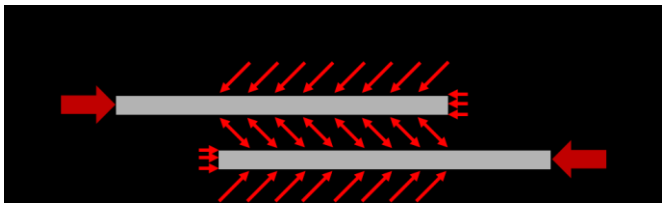

Figure 4-1. Components of compression lap spliced bars.

4.3. RESEARCH SIGNIFICANCE

Despite the recent investigations confirming the possibility of using FRP bars as longitudinal reinforcement in columns, no research has been conducted to investigate the lap splicing of FRP reinforcement bars in compression. The primary aim of this research was to yield a better understanding of the strength of lap-spliced FRP bars under compression. This was achieved by describing the strength components in compression splices and their contributions. In addition, the experimental results can be used to assess the load-carrying capacity and behavior of circular concrete columns reinforced with spliced GFRP bars under concentric axial compression.

4.4. EXPERIMENTAL PROGRAM

4.4.1. Material Properties

All of the specimens were cast on the same day with normal-weight, ready-mix concrete. The 28-day compressive strength of the concrete, determined by the average test results of five cylinder samples (100×200 mm), was about 40.5 MPa. On the testing date, the compressive strength of the concrete cylinders was around 49.3 MPa.

The GFRP-reinforced columns had No. 5 (15.9 mm diameter) sand-coated bars as longitudinal reinforcement and No. 3 (9.5 mm diameter) sand-coated spirals as transverse reinforcement. Figure 4-2 provides an illustration of the GFRP reinforcement. The tensile properties of the GFRP bars were determined according to the ASTM D7205 (2011) test method. The longitudinal and spiral reinforcement in the steel-reinforced columns consisted of grade 60 deformed M15 (16 mm diameter) and M10 (9.5 mm diameter) bars, respectively. The mechanical properties of the steel and GFRP bars are provided in Table 4-1 and Table 4-2, respectively.

Figure 4-2. Sand-coated GFRP spirals and straight reinforcement.

Table 4-1. Mechanical properties of steel reinforcement.

Bar number	Diameter (mm)	Area (mm^2)	Modulus of elasticity (GPa)	Yield strength (MPa)	Ultimate tensile strength (MPa)
M10	10	100	200	450	660
M15	16	200	200	460	660

Table 4-2. Mechanical properties of GFRP reinforcment.

Bar number	Diameter (mm)	Area (mm^2)	Modulus of elasticity (GPa)	Garanteed tensile strength (MPa)	Tensile strain (%)
#3	9.5	71	54.1	1206[1]	2.2
#5	15.9	198	51.2	1374	2.7

4.4.2. Test Specimens

The experimental program aimed at investigating the effects of bar type and splice length on the strength of lap-spliced bars under compression. To pursue this objective, 11 circular concrete columns were constructed and tested under monotonically increasing load. The columns specimens were reinforced with either GFRP or steel bars. Two columns were reinforced with continuous bars and used as reference specimens. One column was cast without any reinforcement, while all the other specimens were reinforced with spliced bars. All of the specimens measured 300 mm in diameter and 1600 mm in height. All of the columns had a clear concrete cover of 25 mm to the spiral reinforcement as well as a concrete

cover of 20 mm on both column bottom surfaces. The minimal ratio of concrete cover and half of the bar clear spacing over bar diameter was determined to be 2.2. The geometric and reinforcement details of the test specimens are illustrated in Figure 4-3. All of the GFRP-reinforced concrete columns were designed according to CAN/CSA S806-12 (2012), Clause (8.4.3.13) code requirements for longitudinal and transverse reinforcement. The steel-reinforced concrete columns were designed according to CSA A23.3-14 (2014) and ACI 318M (2014) code requirements. According to these codes, circular columns should have a minimum of six longitudinal bars. CAN/CSA S806-12 (2012), Clause (8.4.3.7), states that the area of longitudinal bars in compression members shall be not less than 1% of the gross area, A_g, of the section. In addition, the area of longitudinal bars for compression members, including regions containing lap splices, shall not exceed 8% of the gross area of the section (CAN/CSA S806-12 (2012), Clause (8.4.3.9)). Furthermore, the minimum FRP bar size for longitudinal FRP bars shall be not less than 15 mm in diameter (CAN/CSA S806-12 (2012), Clause (8.4.3.10)). In this study, the longitudinal reinforcement consisted of six No. 5 (15.9 mm diameter) sand-coated GFRP or M15 (16 mm diameter) steel bars evenly spaced circumferentially and providing reinforcement ratios (ρ_s) of 1.6%. No. 3 (9.5 mm diameter) sand-coated GFRP or M10 (9.5 mm diameter) steel spirals were used as transverse reinforcement in the GFRP- and steel-reinforced columns, respectively.

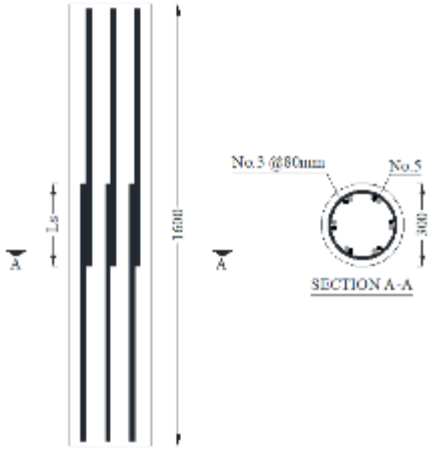

Figure 4-3. Geometric and reinforcement details of the test specimens (all dimensions are in mm).

The spiral reinforcement was designed considering the CAN/CSA S806-12 (2012) limitations for FRP spiral reinforcement (Clause 8.4.3.13) and CSA A23.3-14 (2014) and

ACI 318M (2014) specifications for steel spirals: (spiral reinforcement shall have a minimum diameter of 6 mm; the pitch or distance between turns of the spirals shall not exceed 1/6 of the core diameter; the clear spacing between successive turns of a spiral shall not exceed 75 mm nor be less than 25 mm). In this study, the spiral pitch at the central half of the columns was taken as 80 mm (center-to-center) using No. 3 GFRP spirals for the GFRP-reinforced concrete columns and 10M for the steel-reinforced concrete columns. The pitch was reduced to 40 mm at both ends to ensure failure in the spliced region. Plastic ties were used to fasten the spliced bars together and the spirals to the longitudinal reinforcement. In addition, the position of splices with zero lap length was secured with wooden sticks. The transverse reinforcement aimed at providing a moderate level of confinement for the spliced bars. Increasing the transverse reinforcement would indeed improve the strength of the spliced bars (Cairns 1985; Chun et al. 2010a; Park and Paulay 1974). Moreover, the clear spacing between spliced bars and concrete cover has a negligible effect on the splice strength of compression splices (Cairns 1985; Chun et al. 2010c; Quintana 2008). Therefore, concrete cover, transverse reinforcement, and bar clear spacing were excluded from the test parameters.

Table 4-3 provides the details of the test specimens. One specimen was cast without any reinforcement to assess the concrete's contribution in the columns' loading capacity. Moreover, three specimens were reinforced with steel bars and the remainder with GFRP bars. For comparison purposes, the test specimens were divided into two series. Series I contains the unreinforced and steel-reinforced specimens and Series II comprises all of the specimens reinforced with GFRP bars. For each reinforcement type, one specimen was reinforced with continuous bars and served as a control specimen. The loading capacity of the control specimens can be considered as a target that the other columns were supposed to reach. The test specimens are designated using mnemonic notations in terms of numbers and letters. The first letter indicates the bar type (S for steel, and G for GFRP), while the first digit (5 for No. 5 GFRP or M15 steel bars) refers to the diameter of the longitudinal bars. The second number after the letter L indicates the splice length in terms of bar diameter, whereas the letter C is for specimens with continuous FRP bars. The last number corresponds

to the spacing of the spiral reinforcement (80 mm). Moreover, UR stands for the unreinforced specimen.

All of the cages were made with special attention to the tolerance of approximately ±2 mm. The columns were cast vertically in cylindrical molds made of composite materials. Before casting, all of the molds were adjusted to ensure the verticality of the columns. Figure 4-4 shows the column fabrication process. The day after casting, all of the columns were unmolded and cured with wet burlap for seven days before storing them in the laboratory at ambient temperature.

a) **b)** **c)**

Figure 4-4. Preparation of the test specimens: (a) assembled cages, (b) GFRP and steel cages inside the formwork, and (c) wooden formwork and Sonotubes.

Table 4-3. Details of test specimens.

Test series	Specimen designation	Longitudinal Reinforcement	Splice length, l_s (mm)		Spiral pitch	Bar type
Series I	UR	-	-	-	-	-
	S5-L4-80	6 M15	$4d_b$	64	80	Steel
	S5-L8-80	6 M15	$8d_b$	128	80	

	S5-LC-80	6 M15	CONTINUOUS		80	
	G5-L0-80	6 #5	0	0	80	
	G5-L4-80	6 #5	$4d_b$	64	80	
	G5-L8-80	6 #5	$8d_b$	128	80	
Series II	G5-L12-80	6 #5	$12d_b$	192	80	GFRP
	G5-L24-80	6 #5	$24d_b$	384	80	
	G5-L36-80	6 #5	$36d_b$	576	80	
	G-5-LC-80	6 #5	CONTINUOUS		80	

4.4.3. Instrumentation and Test Setup

The experiment was carried out under a monotonically increasing concentric load with a rate of 0.5 kN/s. The testing was continued until the load dropped to a level of approximately 65% of the ultimate strength. Figure 4-5 shows the testing machine and a typical column under loading.

Figure 4-5. Testing machine and a column specimen under loading.

To help ensure the uniform distribution of load, both ends of the specimens were leveled with a thin layer of high-strength cementitious grout prior to testing. These parallel layers can also mitigate load eccentricity. Although the end portions of the specimens were reinforced with more dense spirals, they were additionally confined by steel collars during loading to prevent premature failure at the end regions.

During loading, the strain variations in the longitudinal bars, spiral reinforcement, and concrete were measured with a set of electrical strain gauges. Figure 4-6 shows the position

of these strain gauges. In all of the specimens, one strain gauge was attached to spiral stirrups at column mid-height. The contribution of end bearing and bond was distinguished by attaching gauges at the beginning and end of the splice region of a longitudinal bar. To allow for strain development in the bars, the gauges were mounted at a distance of 20 mm from the end of each spliced bar. For the columns with zero splice length, only two strain gauges were installed at the end of the spliced bars. Moreover, in the columns with continuous bars and control specimens, three strain gauges were mounted at the mid-length of three bars, 120° apart along the section perimeter to ensure load eccentricity. Concrete strains were also monitored with two strain gauges delicately attached along the centerline at column mid-height.

Column axial deformation was measured with four linear variable differential transformers (LVDTs) installed on the four sides of the columns as depicted in Figure 4-6.

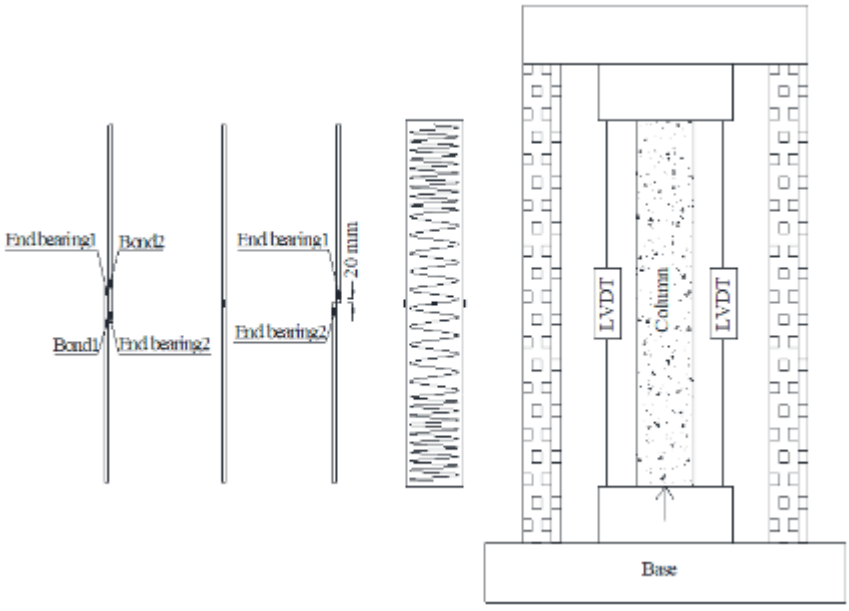

Figure 4-6. Position of reinforcement, concrete strain gauges, and LVDTs.

4.5. EXPERIMENTAL RESULTS AND OBSERVATIONS

The experimental data obtained during loading consisted of strains in constitutive materials, loading capacity, and longitudinal displacement. Table 4-4 provides a comparison of the mean stress values for all of the columns at the ultimate point. These stresses were

determined based on the stress–strain behavior of the reinforcement. The concrete strain values were recorded up to the spalling of the concrete cover. Table 4-4 presents the mean values of maximum strains measured by the strain gauges in each column. It is worth noting that the maximum strain in the concrete was reached simultaneously with concrete-cover spalling.

Table 4-4. Summary of results for all test specimens.

Specimen Designation	P (kN)	Failure mode*	Concrete strain at spalling (με)	f_{sc} (MPa)	f_e (MPa)	f_b (MPa)	Spiral stress at sliding (MPa)	Dis. at slippage (mm)
UR	3122	C	2603	-	-	-	-	4.4
S5-L4-80	3045	S	2503	226	119	107	NA	3.2
S5-L8-80	3364	S	2586	322	128	194	109	4.6
S5-LC-80	3521	B	2254	532	-	-	94	5.3
G5-L0-80	2871	S	2048	62	62	-	NA	4.0
G5-L4-80	3213	CS	2816	126	79	47	62	5.3
G5-L8-80	3255	CS	2662	134	82	52	23	4.6
G5-L24-80	3276	CS	2506	140	78	62	1	5
G5-L36-80	3290	B,R	2278	129	53	76	35	5.6
G5-LC-80	3290	B,C	2506	145	-	-	76	5.2

*C is concrete crushing; S is bar slippage and cover spalling at an upper load; B is bar buckling; CS is cover spalling and bar slippage simultaneously and R is rupture of spirals.
Note: f_{sc} is the splice strength; f_e is the stress developed by end bearing; f_b is the stress developed by bond; and NA is not available.

4.5.1. Modes of failure

The failure of the column without any reinforcement was characterized by the formation of an inclined failure plane throughout the specimen's height. Continued applied axial load caused relative movement of the two column parts along this plane. This was attributed to the absence of longitudinal reinforcement that could act as dowels to resist concrete sliding along the failure plane. The failure of the specimens with spliced bars occurred primarily due to concrete-cover spalling and bar sliding. In specimens with short splices, the spliced bars slid with cracks appearing on the column surface; loading continued up to concrete-cover spalling. This behavior was observed in the specimens reinforced with steel or zero-spliced GFRP bars (S5-L4-80, S5-L8-80, and G5-L0-80). The specimens with longer splice

lengths, however, sustained higher loads. The load–displacement curves for these specimens exhibited ascending branch nonlinear behavior at 70% to 80% of peak load (Figure 4-7) with the appearance of hairline cracks. The load-carrying capacity increased up to cover spalling. Bar sliding and cover splitting took place simultaneously in G5-L4-80, G5-L8-80, and G5-L24-80 at peak load. Figure 4-8 and Figure 4-9 show the typical failure modes and overview of the collapsed specimens, respectively. During the loading of G5-L12-80, cracking and cover spalling occurred far away from the splice region, as shown in Figure 4-9. Since cover spalling occurred out of the splice region, this failure was not related to spliced-bar weakness, and the results for the specimen cannot reflect the actual strength of a spliced bar. Thus, the results for this column were excluded from the analysis because of premature failure. Deep longitudinal cracks, as shown in Figure 4-9, imply buckling of the longitudinal reinforcement as a failure mode for the specimens constructed with continuous bars and G5-L36-80. The plateau area in the descending branch for these specimens can be seen in Figure 4-7. Due to the lack of confinement, the second peak load was not distinctive. Crushing of the concrete core and bar buckling occurred in S5-LC-80, G5-L36-80, and G5-LC-80.

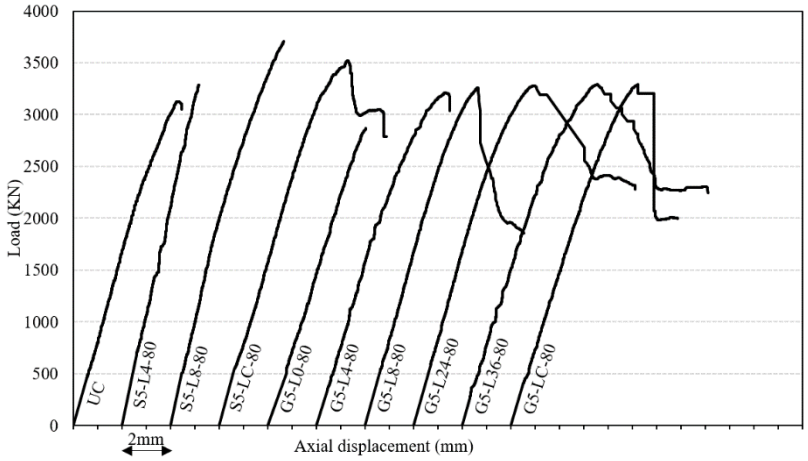

Figure 4-7. Load vs. axial deformation curves for the test specimens.

a) b) c) d)

Figure 4-8. Typical failure mode: (a) concrete-cover spalling, (b) concrete crushing, (c) rupture of GFRP stirrups, and (d) GFRP-bar buckling.

Figure 4-9. Overview of the column specimens after failure.

4.5.2. Concrete Component in Loading Capacity

Specimen UR was cast without any reinforcement. The compression strength of the concrete in this specimen was almost 89% of the compressive strength of the cylinder specimens. The obtained ratio is close to the factor of 0.85 commonly used to predict the loading capacity of a RC column.

4.5.3. Sliding of Reinforcement

For the specimens with splices, a decrease in the strain value of a spliced bar with increasing total load was assumed to indicate bar slippage (Chun et al. 2010b). The load corresponding

to this threshold was considered as the ultimate load. This behavior was clearly observed in S5-L4-80, S5-L8-80, and G5-L0-80. The sliding of GFRP bars with longer splice lengths occurred at peak load. A sharp drop in strain in longitudinal bars was observed after concrete-cover spalling. The concrete remaining around the bars couldn't keep them in place and transfer the stress between them. The descending branch of the load–displacement curves (Figure 4-7) also showed sharp drops without significant post-peak responses, except for G5-L36-80. Thus, the spliced GFRP bars slid after cover splitting. The corresponding load was considered as the ultimate load capacity of the spliced bars.

4.5.4. Components of Splice Strength

The strength developed by each component was distinguished with strain gauges at the beginning and end of the spliced bars. To illustrate, Figure 4-10 shows the load distribution versus measured strain in G5-L8-80 and G5-L24-80 in terms of end-bearing and bond contributions separately. End bearing typically increased linearly up to the ultimate load, as shown in Figure 4-10. At low levels of loading, the end-bearing portion was much higher than the strain developed by bond. Therefore, the end-bearing contribution was more pronounced in the loading capacity of columns at lower load levels. The contribution of bond strain, however, became more significant as the applied load increased. As shown in Figure 4-10, the bond contribution at an initial level of loading was insignificant, as indicated for G5-L8-80 and G5-L24-80. It increased rapidly, however, approaching the ultimate load. Figure 4-10 also provides the strain distribution of the continuous bars in G5-LC-80. As observed, the strain increased nonlinearly up to bar buckling.

The maximum strain measured by strain gauges before bar slippage was multiplied by the reinforcement elastic modulus and considered as end-bearing and bond strength, as presented in Figure 4-10. End-bearing strength ranged from 53 to 82 MPa, irrespective of splice length. The bond strength, however, increased from 46 to 72 MPa proportionally to the increase in splice length.

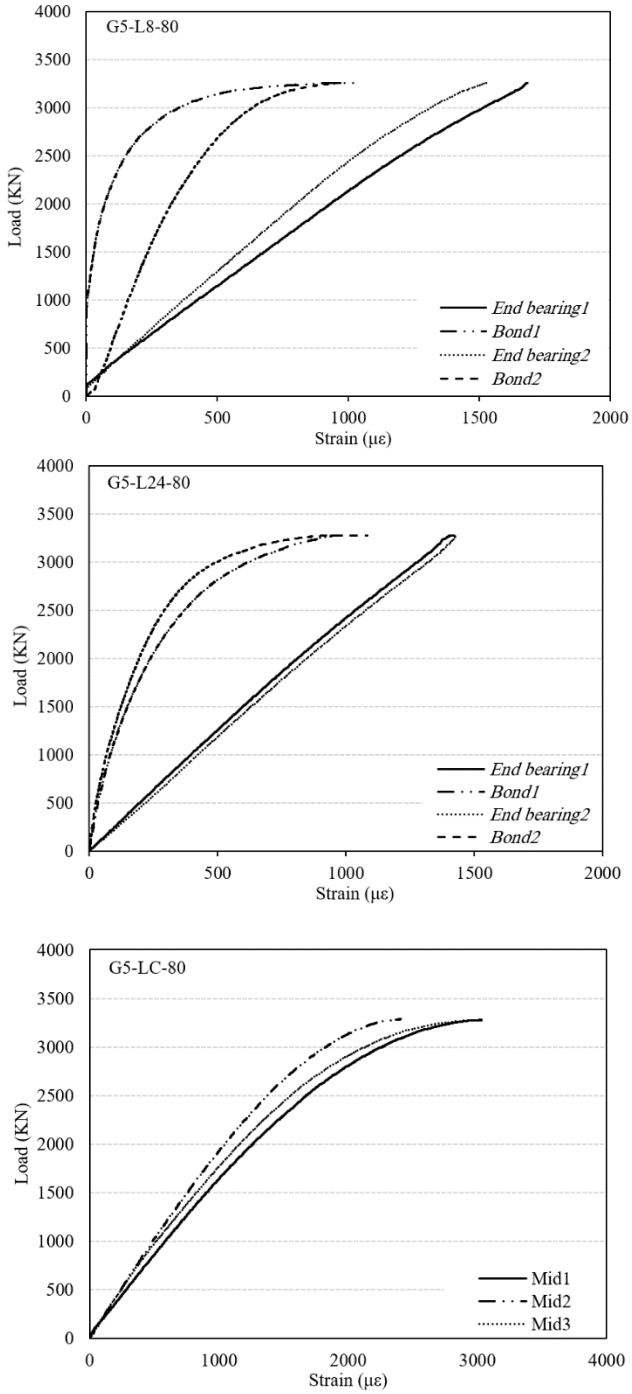

Figure 4-10. Load vs. end bearing, bond, and mid-strain for G5-L8-80, G5-L24-80, and G5-LC-80 (1, 2, and 3 denote the location of strain gauges).

4.5.5. Splice Length and Strength

In general, increasing the splice length induced a rise in the load-carrying capacity of the columns. Figure 4-10 provides the splice strength and its components for each specimen.

The strength of the spliced steel bars with a splice length of 4 times the longitudinal-bar diameter was 226 MPa. Doubling this splice length (S5-L8-80) increased the strength to 322 MPa. A comparison of S5-L8-80 and S5-L4-80 indicates that splice strength would not be linearly proportional to the splice length. A similar trend was observed with the GFRP-reinforced columns.

Due to the zero splice length in G5-L0-80, its reinforcement strength was limited to the end-bearing component (equal to 62 MPa). Increasing the splice length from zero (G5-L0-80) to 64 mm (G5-L4-80) yielded a splice strength of 126 MPa. The increased splice length in G5-L8-80, G5-L24-80, and G5-L36-80 improved the splice strength to 134 MPa, 140 MPa, and 129 MPa, respectively.

4.6. **DISCUSSION**

4.6.1. End-Bearing Contribution

The splice strength in G5-L0-80 was attributed solely to end bearing, since there was no bond contribution given the zero splice length. The end-bearing strength in this column was about 62 MPa which is much higher than the cylinder compressive strength of concrete. The higher end-bearing value compared to the concrete-cylinder compressive strength was also confirmed by Pfister and Mattock (1963) for compression lap-spliced steel bars. This difference can be explained by considering the confinement effect of spiral stirrups and concrete cover, are provided to the concrete at the end part of a spliced bar. The triaxial strength of concrete has been determined to be much higher than its uniaxial strength.

In reality, both bond and end-bearing action would occur simultaneously in a compression lap splice. Therefore, an accurate estimation of splice strength requires that the combined effects of end-bearing and bond stresses be considered.

The stress values developed by end bearing in the specimens were normalized by the square root of concrete compressive strength and presented in Figure 4-11. The end-bearing contribution is irrelevant to splicing length and remained nearly constant for all of the specimens. The average value and the coefficient of variation of the normalized end bearing

for all the GFRP-reinforced specimens were calculated, respectively, as 10.2 and 0.17 (Figure 4-11). In other words, the mean strength developed by end-bearing performance was determined to be $10.2\sqrt{f_c'}$, which would be equal to 72 MPa, given the compressive strength of concrete of 49.3 MPa.

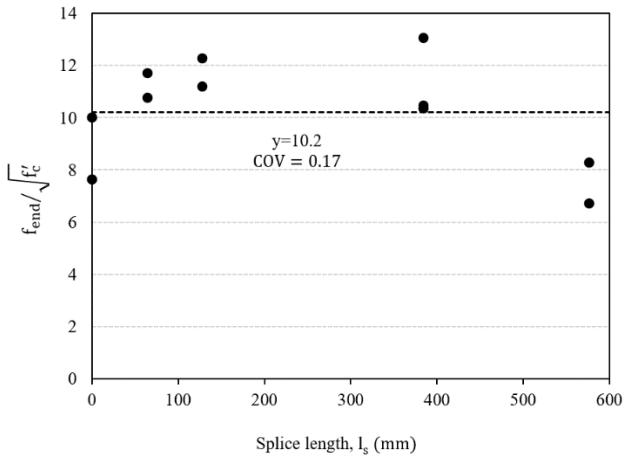

Figure 4-11. End-bearing contribution to the splice strength in the GFRP specimens.

4.6.2. Bond Contribution

Compression force adversely influences the bond contribution due to the lower tensile capacity of concrete under a combined tension and compression stress state (Beskos 1974; Kupfer and Gerstle 1969; Richart et al. 1928). As both compression and tension splices produce circumferential tensile stresses, the tensile capacity of concrete can considerably influence bond strength. Thus, the bond strength in a compression splice is lower than in a tension splice.

ACI Committee 408 (2003) and Canbay and Frosch (2005) scrutinized the parameters affecting the bond strength of steel reinforcement under tension. Based on their recommendation, the bond strength is proportional to the fourth root of the compressive strength of the concrete for compressive strengths under 55 MPa. Darwin et al. (1996) and Zuo and Darwin (1998, 2000) concluded that the bond strength increases proportionally to the ¾ and ¼ power of the concrete strength for confined and unconfined reinforcement, respectively. Harajli (2004) stated that the fourth root of compressive strength underestimates the effect of concrete on the bond strength of spliced steel bars under tension,

particularly for short splices. Furche and Eligehausen (1992) posited a provision correlated with the square root of the compressive strength of concrete to predict the ultimate load of studs under tension, accompanied by blowout failure mode. In addition, guidelines such as ACI 440.1R(2015), CAN/CSA S6-14 (2014) and CAN/CSA S806-12 (2012) considered the effect of concrete strength on bond strength by using its square root. Based on the abovementioned studies and for simplification purposes, the bond stress of bars was normalized with the square root of compressive strength. It is worth mentioning that, in the current study, the compressive strength of concrete was not a test parameter and remained constant.

Concrete crushing is a probable failure mode for columns under compression forces. Within the range of concrete crushing strain, the developed stress in a GFRP bar cannot be as high as that in a steel bar because GFRP bars have a lower elastic modulus than steel reinforcement. As the end-bearing component plays a predominant role in compression splices, the contribution of bond stress in the strength developed by spliced GFRP bars is lower than for steel reinforcement. As a result, it is expected that the required length for GFRP compression splices will be short. This conclusion is consistent with the outcomes of this study.

The results of the experimental tests confirmed that doubling the splice length would not double the strength. This finding was also confirmed in past studies on spliced FRP bars in tension. Canbay and Frosch (2005) and Chun et al. (2010b) stated that bond strength in tension is approximately proportional to the square root of the splice length to the bar-diameter ratio. Thus, it would be expected that the bond strength of GFRP bars spliced under compression could also be considered as a power of the splice length.

The bond stress was calculated by deducting the end-bearing strain from the total strain developed in the spliced bars (see Figure 4-12). According to the regression analysis of the experimental data, the bond strength of a spliced GFRP bar under compression can be expressed by

$$f_{bond} = \left(2.63\sqrt[4.8]{l_s}\right)\sqrt{f_c'} \quad (4\text{-}1)$$

The coefficient of determination (R^2) for Eq. (4-1) was determined to be 0.83, implying good correlation between the predicted and experimental results. As shown in Figure 4-12, the bond strength would generally improve by increasing the splice length. This increment is more evident at shorter splice lengths. The stress developed in G5-L24-80 reached approximately the same load level as the specimen with continuous GFRP bars (difference of less than 8%). In addition, the stress value in the spliced GFRP bar in the specimen with $8d_b$ was about 134 MPa, which is 92% of the target stress developed in the GFRP bar in G5-LC-80. Thus, for the conditions considered in construction of the column specimens in this study, a length of $8d_b$ can be reliably considered as the required splice length for No. 5 GFRP bars in compression. Regarding Figure 4-12, the values predicted by Eq. (4-1) for short splice lengths is in good agreement with the experimental results.

The bond contribution can also be given by a simpler relation such as

$$f_{bond} = \left(0.51\sqrt{l_s}\right)\sqrt{f_c'} \tag{4-2}$$

where R^2 is 0.75. The lower the coefficient of determination, the lower the correlation between the experimental and predicted results. The latter equation is, however, simpler and more practical, yet accurate enough for design purposes. For bars with short splices, Eq. (4-2) underestimates the bond strength, whereas it slightly overestimates the strength of bars with long splices, as observed in Figure 4-12. It should be noted, however, that the difference in the load-carrying capacity of the specimens with longer splice lengths was determined to be negligible. Therefore, the discrepancy in the results for the longer splices would be insignificant. In addition, the required splice length of GFRP bars is not expected to be on that part of the curve. The root mean square deviation (RMSD) value for Eqns. (4-1) and (4-2) is 1.77 and 2.26, respectively. Given the range of variation among the experimental data, both RMSD values can be considered acceptable. In conclusion, Eq. (4-2) can be used to predict bond strength, since it is more simple and conservative in the practical range of splice lengths required for GFRP bars in compression.

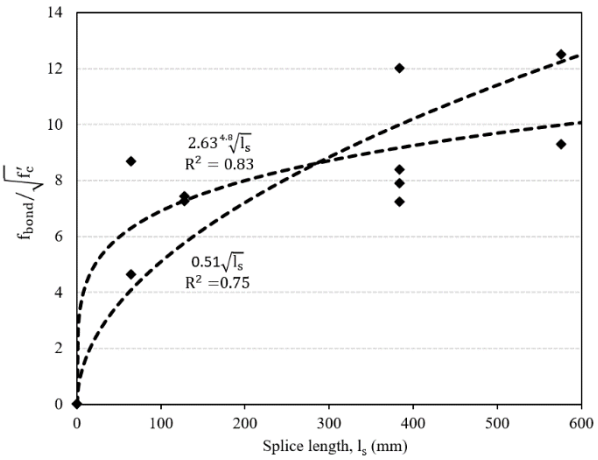

Figure 4-12. Bond contribution to the splice strength of the GFRP bars.

4.6.3. Influence of Reinforcement Type

Figure 4-13 presents the axial-compression capacity of the tested columns with lap-spliced and continuous GFRP and steel reinforcing bars. The peak loads of G5-LC-80 (the column with continuous GFRP bars), G5-L4-80, and G5-L8-80 were, respectively, 3,290, 3,213, and 3,255 kN. These results indicate no appreciable difference in terms of peak capacity between the concrete columns reinforced with continuous and spliced bars with a splice length of eight times the bar diameter. The peak strength of S5-LC-80 (the column reinforced with continuous steel bars), S5-L4-80, and S5-L8-80 were 3,045, 3,364, and 3,521 kN, respectively. The difference in the ultimate loading capacity of the steel- and GFRP-reinforced columns was within a tolerance of 5% to 8%, which is in line with the findings in past studies (Afifi et al. 2014b; Tobbi et al. 2012). Despite the GFRP reinforcement being stronger than steel reinforcement, it can hardly reach its ultimate capacity as the failure strain of a column is far less than the ultimate strain of GFRP bars. In addition, the elastic modulus of steel is greater than that of GFRP reinforcing bars. Consequently, the steel-reinforced columns can withstand an ultimate load 5% to 8% greater than the GFRP-reinforced ones with the same reinforcement ratio.

4.6.4. Comparison between Predicted and Experimental Results

According to ACI 318M (2014), the nominal compressive capacity of a column reinforced with continuous steel reinforcement is expressed as

$$P_0 = \alpha f_c'(A_g - A_{st}) + f_y A_{st} \quad (4\text{-}3)$$

where A_g is the gross cross-sectional area of the column, A_{st} is the cross-sectional area of the longitudinal reinforcement, f_y is the yield strength of the steel reinforcement, and α is a coefficient that accounts for the difference in concrete compressive strength in a large column and small cylinder specimen. Tobbi et al. (2014) stated that the ultimate loading capacity of a column reinforced with continuous FRP bars can be estimated by

$$P_0 = \alpha f_c'(A_g - A_f) + \varepsilon_0 E_f A_f \quad (4\text{-}4)$$

where ε_0 is the compressive strength of the concrete at ultimate load. Moreover, E_f and A_f are the elastic modulus and cross-sectional area of longitudinal GFRP bars. In Eqns. (4-3) and (4-4) the greatest compressive stresses that can be developed in a steel or GFRP reinforcing bar—are, albeit approximately, estimated by the terms f_y and $\varepsilon_0 E_f$, respectively. In columns reinforced with splices, these stresses can be substituted for those measured in spliced bars. Thus, $\varepsilon_0 E_f$ for spliced bars is equal to f_{sc}, as reported in Table 4-4. This stress includes end-bearing and bond stress. The constant coefficient of α is normally taken as 0.85, although, based on the results of specimen UR, it was determined to be 0.89.

Table 4-5 provides a comparison of the experimental loading capacity of the columns with the predicted values, assuming α = 0.85 and α = 0.89. While both coefficients can predict the ultimate capacity with reliable accuracy, taking α to be equal to 0.89 could result in fewer discrepancies. A negative value indicates that the proposed equation is on the conservative side. Specimens S5-L4-80 and G5-L0-80 collapsed due to reinforcement slippage while the stress in the concrete was low. The positive difference for these specimens can be attributed to the low stresses developed in the concrete.

Table 4-5. Prediction of load carrying capacity of the specimens

Specimen	P_{exp} (kN)	Bar strain (με)	α = 0.89		α = 0.85	
			P_{pre} (kN)	Difference (%)	P_{pre} (kN	Difference (%)
S5-L4-80	3045	1130	3267	7	3133	3
S5-L8-80	3321	1609	3382	2	3248	-2
S5-LC-80	3521	2659	3601	2	3464	-2
G5-L0-80	2871	1209	3070	7	2936	2

G5-L4-80	3213	2457	3147	-2	3012	-6
G5-L8-80	3255	2618	3157	-3	3022	-7
G5-L24-80	3276	2734	3164	-3	3029	-8
G5-L36-80	3290	2524	3151	-4	3017	-8
G5-LC-80	3290	2832	3222	-2	3085	-6

4.6.5. Contribution of End Bearing vs. Bond

The contribution of end bearing and bond components in the strength of the spliced bars is demonstrated in Figure 4-13 for all the specimens, separately. More than half of the strength of the spliced bars in the columns reinforced with GFRP bars was provided by end bearing except G5-L36-80. Extremely long splices, as in G5-L36-80, could reduce the contribution of end-bearing strength in comparison to bond strength. Considering the splice length, it can be concluded that doubling the splice length could slightly influence the bond contribution. This is mainly attributed to the non-uniform distribution of bond stress along the splice length. The bond stress is believed to be higher close to the free end of spliced bars (Cairns and Arthur 1979; Chun 2017; Pay et al. 2014). Consequently, increasing the splice length could slightly increase the bond strength. On the other hand, steel has a higher bond stress than GFRP bars due to different surface treatments and elastic moduli (Benmokrane et al. 1996). As shown in Figure 4-13, doubling the splice length from $4d_b$ to $8d_b$ could increase the bond strength by 13% and 2% for steel and GFRP bars, respectively. Thus, the bond stress in spliced steel bars is more sensitive to length than in GFRP splices. Therefore, doubling the splice length in specimens reinforced with spliced steel bars could notably enhance the bond contribution, thereby reducing the end-bearing contribution.

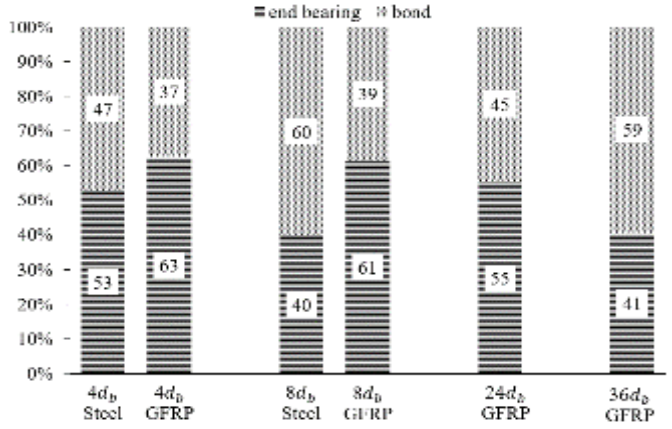

Figure 4-13. Contribution of end bearing and bond to the splice strength of specimens.

4.7. **CONCLUSIONS**

This study is part of an ongoing research program at the University of Sherbrooke investigating the structural performance of GFRP-reinforced concrete columns under axial loads. A total of 11 large-scale RC columns were prepared and tested to study the required lap-splice length for GFRP bars under compression. The influence of compression splice length and type of reinforcement on the strength of the spliced bars was assessed. The following concluding remarks are based on the analysis of the experimental results.

- Specimens constructed with spliced GFRP bars failed by cover spalling, followed by bar sliding at the splice region. Buckling of GFRP bars occurred in the specimens reinforced with continuous bars and a spliced length of $36d_b$. Buckling of spliced bars led to GFRP spiral rupture.
- The spliced GFRP- and steel-reinforced concrete columns exhibited similar linear load–displacement behavior in the ascending part.
- The spliced GFRP bars failed to sustain the axial load at a load level corresponding to the appearance of the surface cracking in the specimens with shorter splices or simultaneously with cover spalling in the specimens with longer splices but less than $36d_b$.
- The test observations revealed that the splice strength of the GFRP bars would not be linearly proportional to the splice length. A similar trend was also observed with the steel-reinforced concrete columns. The bond strength is proportional to a power of splice length.
- As the strength of the compression splice consists of end-bearing and bond components, the contribution of each part was scrutinized in detail in this study using measured strains. The test results indicate that the end-bearing strength of the spliced GFRP bars increased linearly up to peak load and contributed significantly to the splice strength, much more so than does the bond strength. Upon crack initiation, the bond-strength component became more active in contributing to the splice strength.

- The test results indicate that the required compression splice length for GFRP bars is less than that required for steel. This can be attributed to the difference in the modulus of elasticity and corresponding strain developed in the bars under compression.
- Finally, it was found that a length of $8d_b$ can be reliably considered as the required splice length for No. 5 GFRP bars in compression. Based on the regression analysis of the test results, simple design equations were proposed to predict the bond and end-bearing strength of GFRP spliced bars. There are, however, other parameters that need to be addressed related to the compression splice, such as confinement, bar diameter, concrete cover, concrete strength, and bar surface treatment. More experimental evidence and research are needed to accurately derive a design equation to predict the required splice length for GFRP bars under compression.

CHAPTER 5 COMPRESSION SPLICES OF GFRP BARS IN UNCONFINED AND CONFINED CONCRETE COLUMNS

Foreword

Authors and affiliation:

- Amirhomayoon Tabatabaei, PhD candidate, Department of Civil Engineering, University of Sherbrooke, Quebec, Canada.
- Abolfazl Eslami, Postdoctoral Fellow, Department of Civil Engineering, University of Sherbrooke, Quebec, Canada.
- Hamdy M. Mohamed, Postdoctoral Fellow, Department of Civil Engineering, University of Sherbrooke, Quebec, Canada
- Brahim Benmokrane, Professor of Civil Engineering and Tier-1 Canada Research Chair in Advanced Composite Materials for Civil Structures and NSERC Chair in FRP Reinforcement for Concrete Structures, Department of Civil Engineering, University of Sherbrooke, Quebec, Canada.

Journal: Journal of Composites for Construction.

Status: Accepted, Aug-2018.

5.1. ABSTRACT

While the use of glass-fiber-reinforced-polymer (GFRP) bars as compression reinforcement in reinforced-concrete (RC) columns has been deeply investigated, no research studies have focused on spliced GFRP bars under compression. This study consists of an experimental program aimed at developing a fundamental understanding of the effect of confinement on

spliced GFRP bars under compression. The test matrix comprised 14 circular concrete columns tested under concentric compression loading. When lap splicing reinforcing bars, confinement plays a consequential role in increasing concrete compressive strength and limiting crack development. On the other hand, splice strength is highly dependent on splice length. Thus, this study considered confinement and compression-bar splice length as the test variables to evaluate the splice strength under compression. Nine specimens were confined with two different volumetric ratios of GFRP spirals, while the rest were reinforced longitudinally without transverse reinforcement. The columns were compared in terms of load displacement, failure modes, splice strength, and stress–strain behavior. A significant improvement in the post-peak behavior of the columns was observed with increasing the level of confinement. The post-peak portion of the load–displacement curves of the confined specimens dropped sharply, while the well-confined specimens achieved a second peak load. Considering that the splice strength consists of end bearing and bond, the contribution of each component is described in detail. By conducting regression analysis of the experimental data, an analytical model linearly proportional to splice length was developed to predict the strength of spliced GFRP bars under compression with various amounts of transverse reinforcement. The model was found to estimate splice strength with satisfactory accuracy.

Key words: Compression; lap splice; GFRP bars; end bearing; bond; column; analytical model; design codes

5.2. INTRODUCTION

Fiber-reinforced-polymer (FRP) bars are well-known as a promising substitute for conventional steel in reinforced-concrete (RC) members subjected to harsh environments. Despite this widespread acceptance, knowledge of the behavior of FRP bars under compression remains vague. Valuable studies (Afifi et al. 2014a; Hadhood et al. 2016; Lotfy 2010; Luca et al. 2010; Tobbi et al. 2012) have experimentally and theoretically investigated the performance of FRP bars as compression reinforcement in concrete members under concentric and eccentric loads. The test results indicated that concrete columns internally reinforced with glass-FRP (GFRP) bars can achieve a strength comparable to that of their

steel-reinforced counterparts. North American codes recommendations ((ACI 440.1R 2015; CAN/CSA S806-12 2012); however, ignore the contribution of FRP bars under compression due to the paucity of available research. Thus, no design provisions have yet been provided for the requisite splice length of FRP bars in compression. A comprehensive literature review indicated no study has been conducted on the behavior of spliced FRP bars in compression. Most studies on spliced GFRP bars have focused on investigating the requisite splice length under tension. To develop the concept of compression lap splicing, a summary of past studies and design provisions for compression lap-spliced steel bars in RC columns is presented in the following.

5.3. RESEARCH ON THE COMPRESSION SPLICING OF STEEL BARS

Compression action is very different from tension. The strength of a spliced bar under compression consists of both end-bearing and bond components, whereas the former would not contribute in tension splices (Pfister and Mattock 1963). The influence of transverse reinforcement on the contribution of each component has not yet been extensively investigated. Stirrups can prevent the opening of cracks and ensure a more ductile failure mode (Park and Paulay 1974). Design guidelines for steel reinforcement generally neglect the effect of end bearing and transverse reinforcement underestimating the splice strength. Based on the experimental results of 51 full-scale concrete columns reinforced with steel bars, Cairns and Arthur (1979) concluded that developing a design approach based solely on the bond strength would be unrealistic. Transverse reinforcement, located at the splice end, would also improve the splice strength. A numerical study performed by (Cairns 1985) showed that transverse reinforcement plays a prominent role in the strength of spliced bars under compression and its effect would be three times greater than that of tension. This increment was limited; however, to a certain level of reinforcement volume; beyond which, the strength reached a plateau. Chun et al. (2010a) tested 42 unconfined columns reinforced with steel bars and asserted that the strength of the spliced bars was proportional to the square root of the concrete compressive strength and the ratio of splice length to bar diameter. Using

the regression analysis of their data, a relation was then derived to calculate the strength of compression splices in unconfined columns defined by

$$f_{sc,p} = \left(11.1 \times \sqrt{{l_s}/{d_b}} + 16.4\right)\sqrt{f_c'} \quad (5\text{-}1)$$

where l_s is the splice length in mm; d_b is the bar diameter in mm, and f_c' is the cylinder compressive strength of the concrete in N/mm^2.

In Eq. (5-1), the constant value indicates the end-bearing effect since the strain remained constant at the end of the bars irrespective of other splice properties. In order to include the effect of confinement, Chun et al. (2010b) conducted another experimental evaluation using 48 RC column specimens. They observed that the failure modes of all specimens were accompanied by sudden cover splitting. The cover splitting in the specimens reinforced with transverse reinforcement along the splice length was; however, less severe than those reinforced only at their splice end. Chun et al. (2010b) stated that the transverse bars prevented crack propagation into the splice region, thereby improving both splice performance and strength. Using their experimental findings, Eq. (5-1) was modified to include the effect of confinement in spliced steel bars in compression and was given by

$$f_{sc,p} = \left[\left(11.1 + 1.5\frac{K_{tr}}{d_b}\right)\sqrt{\frac{l_s}{d_b}} + 16.4 + 1.8\delta\right]\sqrt{f_c'} \quad (5\text{-}2)$$

$$K_{tr} = \frac{40A_{tr}}{sn} \quad (5\text{-}3)$$

In the above equations, A_{tr} is the area of transverse reinforcement perpendicular to the splitting plane in mm^2; s is the spacing of transverse reinforcement in mm; n is the number of bars; and δ equals one if stirrups are provided at the splice ends otherwise zero.

5.4. OBJECTIVES OF THE RESEARCH STUDY

Although the performance of concrete columns reinforced with GFRP bars has been assessed in recent years (ACI 440.1R 2015), the lap splicing of GFRP bars in compression has not been addressed yet. The outcomes of this study will be useful, particularly in field applications where lap splicing of FRP bars is unavoidable. The experimental results will help in establishing design equations to determine the strength of spliced-GFRP bars in

compression. The effect of confinement provided by the transverse reinforcement was also investigated with respect to the contributions of both end-bearing and bond components in a compression splice. The results could also clarify the overall behavior of columns constructed with spliced GFRP bars. A number of research objectives were designated as follows.

- To assess the compression strength of full-scale circular concrete columns reinforced with spliced GFRP bars.
- To investigate the effect of compression splice length of GFRP bars and confinement on the ultimate capacity, strain in the GFRP bars, and failure mechanisms.
- To assess the strength and compression capacity of spliced GFRP bars considering their bond and end-bearing strength components.
- To develop design equations to predict the required splice length of GFRP bars in compression to avoid sliding and premature failure.

5.5. EXPERIMENTAL PROGRAM

5.5.1. Specimen Design and Fabrication

A total of 14 RC circular columns were tested under a monotonically increasing concentric compression load. The columns were 1,600 mm in height and 300 mm in diameter. A clear concrete cover of 25 mm was provided over the transverse reinforcement in all specimens. The columns were designed according to CAN/CSA S806-12 (2012). Six No. 5 (15.9 mm diameter) sand-coated GFRP bars were used in all of the specimens as longitudinal bars providing a longitudinal-reinforcement ratio (ρ_s) of 1.6%. In addition, No. 3 (9.5 mm diameter) sand-coated GFRP spirals were used as transverse reinforcement. To provide different levels of confinement, the spiral spacing was 40 mm and 80 mm in the middle half of the columns. Figure 5-1 provides the column details.

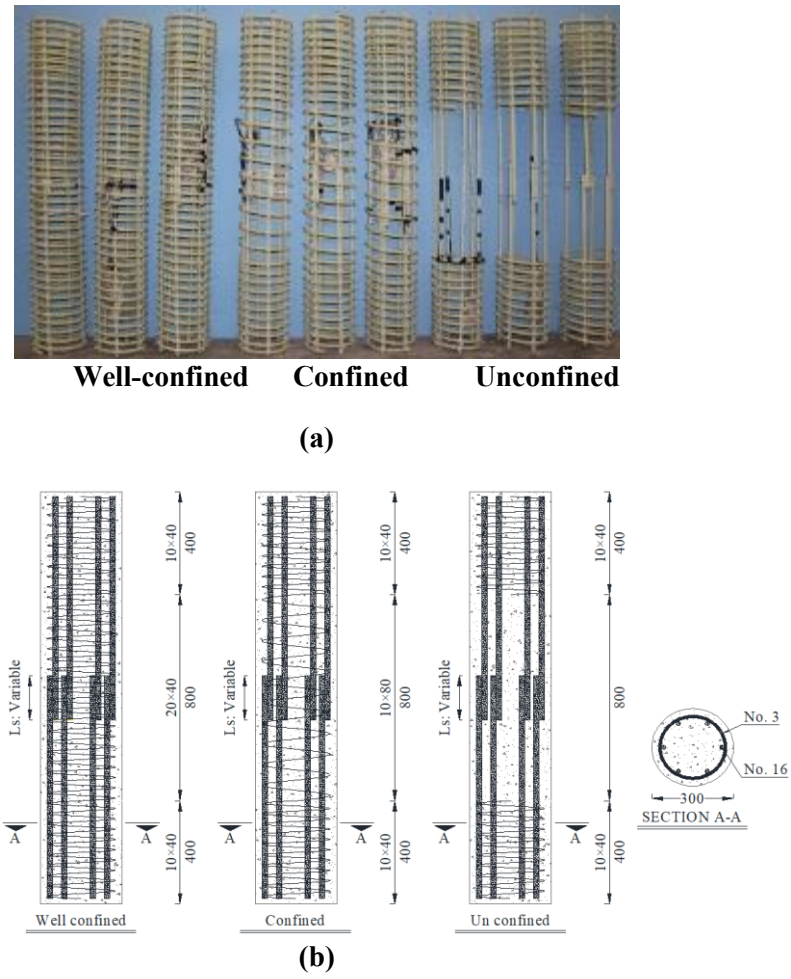

Figure 5-1. Details of columns: (a) Overview of GFRP cages; (b) dimensions and reinforcement details.

The specimens were divided into three groups to evaluate the confinement effect on splice length. The first group consisted of unconfined columns; the second group consisted of the confined columns; and the third group comprised of the well-confined columns. The 40 mm spacing for the well-confined specimens were defined according to a research conducted by Afifi et al. (2014a). The center-to-center spacing of spirals in the splice region of the confined columns was twice of that of the well-confined (i.e. 80 mm). Each group was composed of five specimens. Four were constructed with lap-spliced GFRP bars of different lengths while one was reinforced with continuous longitudinal GFRP bars and was used as a control specimen. Figure 5-2 (b) shows GFRP bars held together with plastic ties in the splice region. Since sections with lap splices are generally believed to be weaker, ACI 318M 2014, Cairns 2014 and Metelli et al. 2017 encouraged staggering spliced bars to improve the

ductility, confinement, and safety of lap splices. Nonetheless, in this study, all the longitudinal bars were lapped in a section to study the most critical situation. In addition, the ratios of the splice length to bar diameter in the spliced specimens were taken as 0, 4, 8, and 12 to assess the evolution of splice strength with different splice length. It is worth noting that zero splice length presents the net end-bearing contribution without any bond interference. Furthermore, the longest splice length for steel bars considered in past studies (Cairns and Arthur 1979; Chun et al. 2010b) was around 20 times the bar diameter. Since the contribution of GFRP bars to the axial capacity of RC columns is less than that of steel, the longest splice length in this study was taken as 12 times the bar diameter (Afifi et al. 2014a). The splice length to bar diameter ratios of 4 and 8 can provide a basis for evaluating the evolution of splice strength. Table 5-1 provides details of the test specimens. The column identification pattern initiated with the reinforcement type (G) followed by the bar diameter. The number after L indicates the splice length as a factor of the bar diameter while the letter C refers to the specimens reinforced with continuous bars. The last number stands for the spiral spacing, except in the case of the unconfined columns, whose identification ends with UC. So, 80 and 40 refer to confined and well-confined columns, respectively.

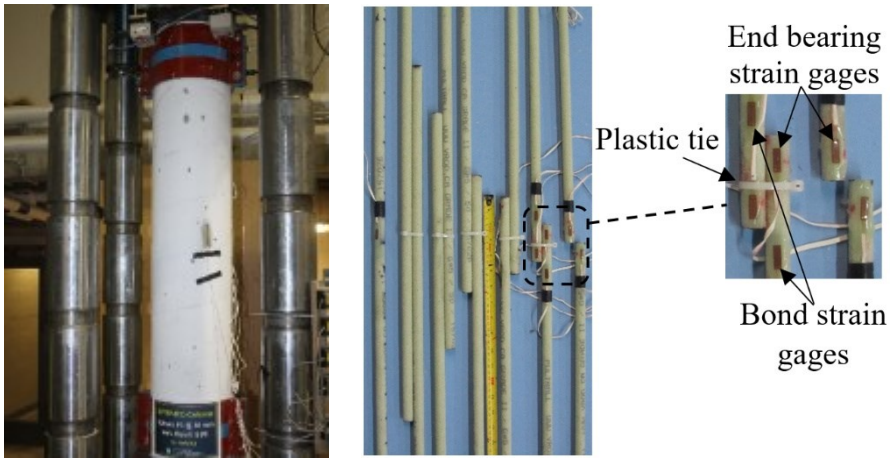

Figure 5-2. (a) Test setup and (b) instrumented GFRP bars at splices.

The specimens were ideally supposed to fail at the splice zone located at mid-height. To ensure failure occurred at this desired location, the spiral spacing was reduced to 40 mm along a length of 400 mm from the both ends of the specimens (Figure 5-1). A spacing under

40 mm would result in a separation between the cover and concrete core. Two pairs of thick steel collars were also fastened to the ends of all specimens during testing to avoid any premature failure. All of the columns were cast on the same day with a normal-weight, ready-mix concrete provided by a local company. The concrete compressive strength, determined by the average test results of five cylindrical samples (100×200 mm), was about 40.5 MPa and 49.3 MPa after 28 days and on the testing date, respectively.

Table 5-1. Details of the test specimens.

Test Series	Specimen Designation	Longitudinal Reinforcement	Splice Length, l_s (mm)		Spiral Pitch (mm)
Unconfined	G5-L4-UC	6 #5	4db	64	-
	G5-L8-UC	6 #5	8db	128	-
	G5-L12-UC	6 #5	12db	192	-
	G5-LC-UC	6 #5	CONTINUOUS		-
Confined	G5-L0-80	6 #5	0	0	80
	G5-L4-80	6 #5	4db	64	80
	G5-L8-80	6 #5	8db	128	80
	G5-L12-80	6 #5	12db	192	80
	G-5-LC-80	6 #5	CONTINUOUS		80
Well-confined	G5-L0-40	6 #5	0	0	40
	G5-L4-40	6 #5	4db	64	40
	G5-L8-40	6 #5	8db	128	40
	G5-L12-40	6 #5	12db	192	40
	G-5-LC-40	6 #5	CONTINUOUS		40

5.5.2. GFRP Bars and Spirals

The longitudinal GFRP bars and spirals used in this study, were made of continuous glass fibers impregnated with a thermosetting vinyl-ester resin, additives, and fillers. The surface of bars was sand-coated to enhance the bond between bars and surrounding concrete (Pultrall, 2015). No. 5 GFRP bars were used as the longitudinal reinforcement while spirals

were made of No. 3 GFRP bars. The tensile properties of GFRP-bar were determined as per ASTM D7205 (2011) test method and are summarized in Table 5-2.

Table 5-2. Mechanical properties of the GFRP reinforcement.

Bar Number	Diameter (mm)	Immersion Area (mm2)	Nominal Area† (mm2)	Modulus of Elasticity (GPa)	Tensile Strength (MPa)	Tensile Strain (%)
#3	9.5	81.5	71	54.1	1206*	2.2
#5	15.9	221.9	198	51.2	1374	2.7

† The strength and modulus were calculated based on this area

* Based on the results of straight bars.

5.5.3. Test Setup and Loading Procedures

In order to minimize the eccentricity of loading during the test and to facilitate the uniform distribution of load, both ends of the columns were covered with a thin layer of a high-strength grout. The columns were subjected to monotonic axial compression, as indicated in Figure 5-2 (a). The load was incrementally applied to the specimen at a rate of 0.5 kN/s. Testing was continued after attaining the first drop in the loading capacity either up to a 35% decrease in the maximum applied load or reaching the second peak in the post-peak region.

The specimens were instrumented to continuously record the experimental data including the applied load, displacement, and internal strains using a computerized data-acquisition system. Four linear variable deformation transducers (LVDTs) were installed around the columns to monitor column axial deformations. Two strain gauges were mounted on the surface of the columns to record concrete strains up to the onset of cover spalling. To separately measure the contribution of the end-bearing and bond components, four strain gauges were also attached to a pair of spliced GFRP bars. Two of the strain gauges were attached to the beginning of lap splicing and the rest to the ends of the bars, indicating the end-bearing component as illustrated in Figure 5-2 (b). The difference between the strain gauges located at the start and end of a splice is considered as the bond contribution. One strain gauge was mounted on the spiral reinforcement in each specimen at the mid-height to measure strain in the transverse reinforcement. Figure 5-2 provides additional details about the instrumentation.

5.6. TEST RESULTS AND OBSERVATIONS

5.6.1. General Behavior and Failure Mode

The mechanical behavior of the specimens was significantly affected by the splice length and level of confinement. Figure 5-3 shows an overview of the collapsed columns and their failure modes. The surface of the specimens was visually free of cracks up to 65% to 80% of their ultimate load. Thereafter, some hairline cracks appeared at the column mid-height. These cracks widened and propagated as loading increased up to the peak load; the greater the splice length, the higher the loading capacity. Table 5-3 presents the highest loading value measured during testing for each specimen. Upon reaching the peak load, the unconfined specimens failed in a brittle and explosive manner. The main reason for this precipitate behavior is the lateral expansion tendency of concrete subjected to axial compression stress. Nothing would have prevented this lateral expansion in the unconfined specimens. The confined specimens experienced a more ductile failure, attributed to the moderate level of confinement. The cracks on the surface of the columns progressively induced cover splitting and all covers spalled upon reaching the peak loads. This could increase the stress in the concrete and GFRP bars leading to the column failure. A swift drop in the loading capacity of the confined columns occurred after attaining their peak loads. The post-peak behavior of these columns was short and insignificant. The load–displacement behavior of the well-confined specimens; however, withstood increasing load after their first drop and achieved a second peak load. Nonetheless, the magnitude of the second peak load was lower than the first peak. In other words, the concrete core strength was enhanced by condensed spiral reinforcement after cover spalling. The confining pressure provided by the spirals was effectively activated when the cover spalled off and the concrete core was able to experience higher strain when spirals ruptured at the intersection with longitudinal bars. Table 5-3 presents the column failure modes and all the experimental data from the strain gauges.

Figure 5-3. Failure modes of the tested columns.

Table 5-3. Summary of the test results.

Confinement	ID	Fail. Mode	Load (kN)		Concrete Strain at Peak (με)	Max. Bar Strain (με)		Spiral Strain at Peak (με)	Dis. at Peak (mm)
			Bar Sliding	Peak		End	Bond		
Unconfined	G5-L4-UC	[1]C	3130	3130	2216	1074	410	-	4.53
	G5-L8-UC	C	3172	3172	2357	1373	950	-	4.43
	G5-L12-UC	C	3235	3235	2737	1361	1359	-	4.02
	G5-LC-UC	C	-	3207	2553	2281		-	4.93
Confined	G5-L0-80	[2]S+C	2871	3081	2564	1046	-	NA	4.03
	G5-L4-80	C+S	3213	3213	2892	1476	639	1153	5.34
	G5-L8-80	C+S	3255	3255	3509	1537	996	423	4.6
	G5-L12-80	[4]NA	NA	NA	NA	NA	NA	NA	NA
	G5-LC-80	C	-	3290	3060	3033		1401	5.2
Well-confined	G5-L0-40	S+C	3130	3172	2210	1236	-	778	4.56
	G5-L4-40	C+S	3270	3270	2470	1552	744	805	5.56
	G5-L8-40	C+S+[3]R	3368	3368	2493	1297	1280	1036	5.51
	G5-L12-40	C+S+R	3368	3368	2407	1093	1700	908	5.65
	G5-LC-40	C+[5]B	-	3368	2342	2732		343	5.0

[1] Concrete crushing
[2] Bar sliding
[3] Spiral rupture
[4] Not achieved
[5] Buckling

5.6.2. Bar Sliding

A close observation of strain measurement indicated a decrease in the strain values in the bars after the first peak load was reached. Consequently, this load and its corresponding strain were considered as the ultimate strength of a GFRP splice which was reported as bar sliding load in Table 5-3. If the bars had not slipped, strain in bars should have continue to rise. Specimens G5-L0-80 and G5-L0-40, however, evidenced a decrease in bar strain values before achieving the first peak load (Figure 5-7). This drop in bar strain while the specimen was still carrying load can be considered as an indicator of bar sliding. Increments in the load-carrying capacity, even after slippage, are due to either stress redistribution among other bars or an increase in the contribution of the concrete core. Therefore, for these two specimens, the strain at which the load has been dropped, was considered as the ultimate strain of the splice. Unfortunately, during the loading of G5-L12-80 premature failure occurred outside the splice region. Thus, its results were not included in the data analysis.

Load–Displacement Behavior

The variation of the load values is plotted against the axial displacement for all specimens in Figure 5-4. Displacement values are the average measurements of the four LVDTs.

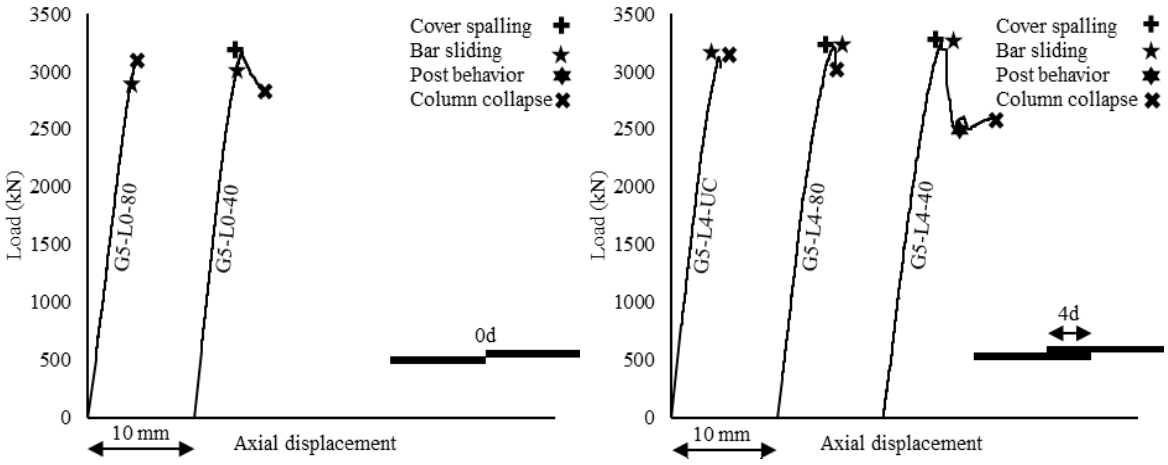

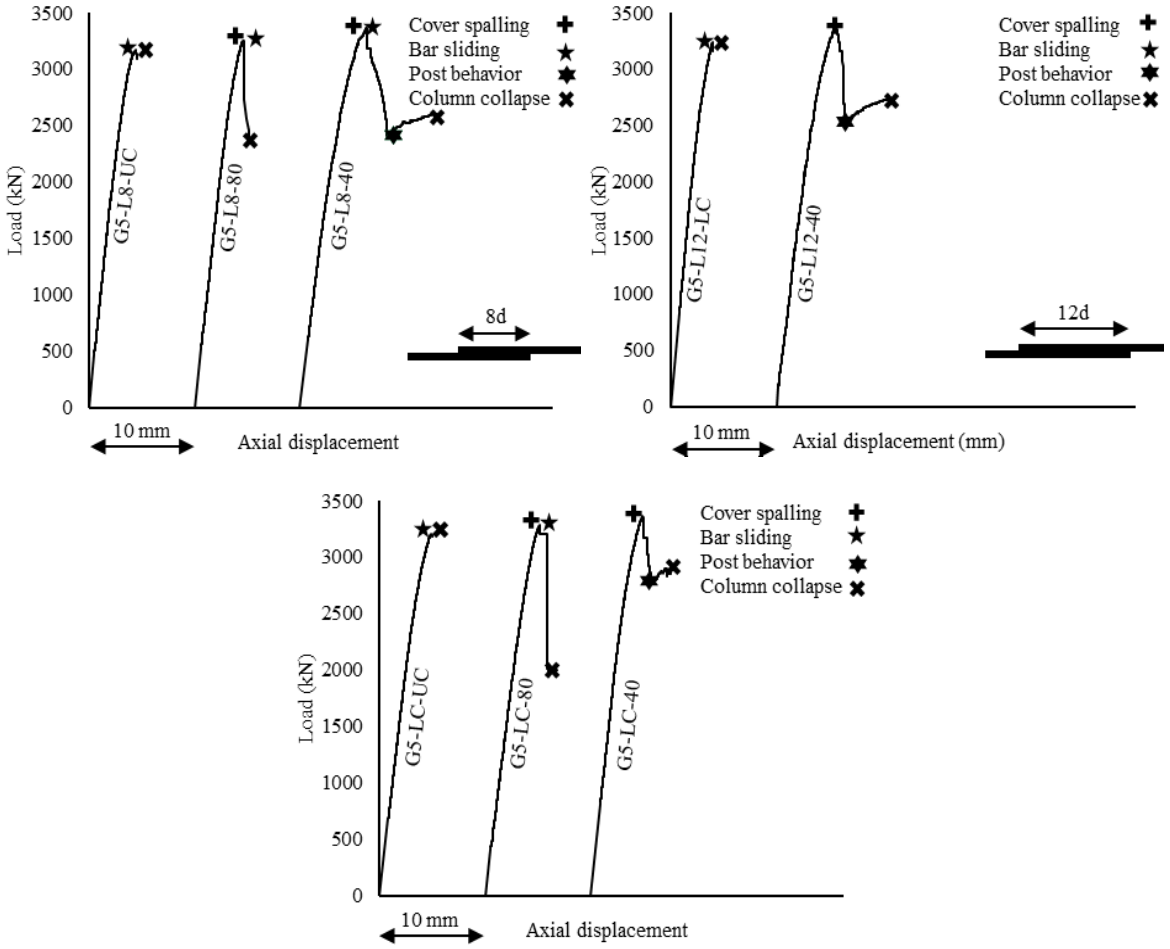

Figure 5-4. Effect of confinement on the load–displacement curves for the test specimens with different splice lengths.

All the columns initially presented a similar linear behavior up to about 60% of their peak load. This load coincided with the appearance of cracks on the concrete surface. Crack propagation in the columns resulted in a gradual reduction in the axial stiffness and slope of the curves. The nonlinear behavior of the columns was noted as cracks spread over the splice region. The amount of confinement impacted the peak load and corresponding displacement. Although confinement slightly improved the peak load, the post-peak behavior significantly depended on the level of confinement. The unconfined specimens presented an explosive and brittle performance at their peak load without indicating any post-peak behavior. The confined specimens underwent a sharp strength deterioration beyond their peak load, even though increasing the splice length could extend the descending branch to some extent. For reasons of safety, the loading procedure was stopped after a sharp reduction in the load–displacement curve to prevent an explosive failure mode. The specimens reinforced with

spirals with 40 mm intervals exhibited significant post-peak behavior, except for G5-L0-40, which failed at its first peak load upon bar slippage.

Table 5-4 provides the measured peak loads and the enhancement provided by the confinement. The peak loads were around 3,130, 3,213, and 3,270 kN for G5-L4-UC, G5-L4-80 and G5-L4-40, respectively (specimens with 64 mm splice length). Their counterparts with 128 mm splice length withstood 3,172, 3,255, and 3,368 kN. The achieved ultimate loads for specimens reinforced with continuous GFRP bars were 3,207, 3,290, and 3,368 kN for G5-LC-UC, G5-LC-80, and G5-L4-40, respectively. The moderate level of confinement provided 3% improvement in the ultimate load, whereas higher confinement increased the ultimate load from 4% to 6%, depending on the splice length. The most significant improvement was observed in G5-L8-40 with a 128 mm splice length.

Table 5-4. Confinement effect on the loading capacity.

Splice Length	Ultimate Load (kN)			Strength Difference (%)	
	Unconfined	Confined	Well-Confined	Confined	Well-Confined
4L	3130	3213	3270	3	5
8L	3172	3255	3368	3	6
12L	3235	-	3368	-	4
LC	3207	3290	3368	3	5

The well-confined specimens underwent strength decays of 24%, 29%, 25%, and 17% (G5-L4-40, G5-L8-40, G5-L12-40, and G5-LC-40, respectively). At this point, activation of the passive confinement pressure provided by the spirals enabled the columns to withstand the increased load. The second peak load was 2,591, 2,605, 2,731, and 2,912 kN for G5-L4-40, G5-L8-40, G5-L12-40, and G5-LC-40, respectively.

5.6.4. Spiral Strain

Figure 5-5 provides the distribution of strain values in the spiral reinforcement for all the specimens measured at their mid-height. The measured strains developed in the spirals in the initial steps of loading were almost the same for all the specimens. After reaching the peak load, the spirals were activated and their strain progressively increased while the

concrete cover spalled off. The behavior of confined and well-confined columns was different. While the former collapsed shortly after cover spalling, the concrete core in the latter kept carrying load after the first peak load. An adequate level of confinement provided by the GFRP spirals in the well-confined specimens resulted in a second peak load. As a result, failure of G5-L8-40 and G5-L12-40 was accompanied with their spiral rupture.

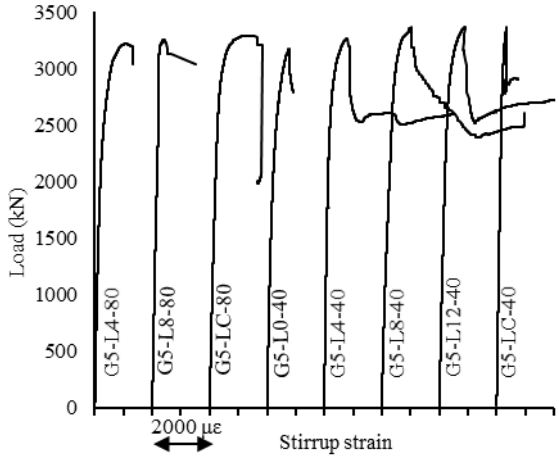

Figure 5-5. Load versus spiral strain at mid-height.

5.6.5. Concrete Strain

The concrete-strain response of the columns was monitored at their mid-height up to the cover spalling as illustrated in Figure 5-6. The obtained load–strain curves were similar and parallel, except in terms of the ultimate point. The concrete-strain behavior was initially linear up to the cover spalling. Then, it gradually became nonlinear up to the onset of damage to the strain gauges. The recorded strain values varied from 2,200 to 3,000 με, except for G5-L8-80 whose ultimate concrete strain at cover spalling was about 3,500 με. This higher strain value can be attributed to the nonhomogeneous nature of concrete.

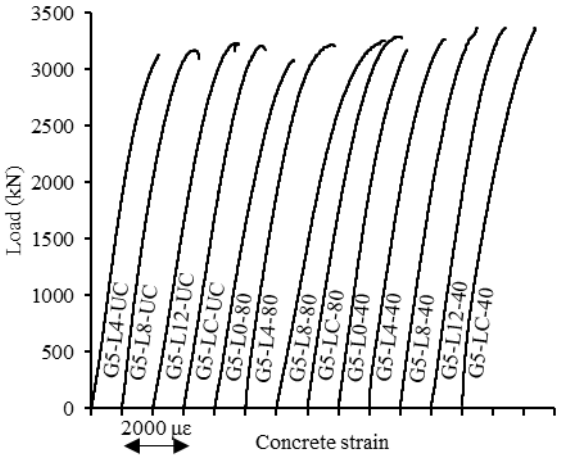

Figure 5-6. Load versus surface concrete strain at mid-height.

5.6.6. Splice Strength

Figure 5-7 and Figure 5-8 show the distribution of load versus the end-bearing and bond strains in each splice length, respectively. The end-bearing strains increased almost linearly up to the peak load. Concerning the bond contribution, the bond strain was insignificant at the early stages of loading. Then, it exponentially raised up to the ultimate point. The only major difference among the curves was in their ultimate strain. Despite some discrepancies, it can be generally concluded that both the end-bearing and bond contributions improved with increasing levels of confinement and splice length as shown in Table 5-3. Comparing the bond strain in different specimens reveals that confinement can have a positive effect on the bond strain: the greater the confinement provided by the spirals, the greater the bond contribution would be. Compared to the unconfined columns, the bond strains in G5-L4-80 and G5-L4-40 were approximately 56% and 82% higher, respectively. The improvement was about 5% for G5-L8-80 and 35% for G5-L8-40. The bond strain of G5-L12-40 was determined to be around 25% higher than that of its unconfined counterpart.

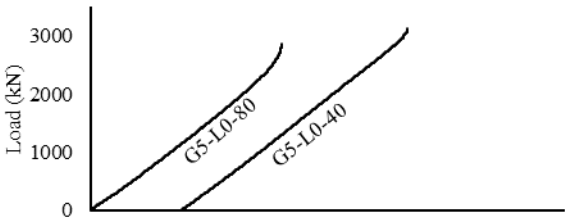

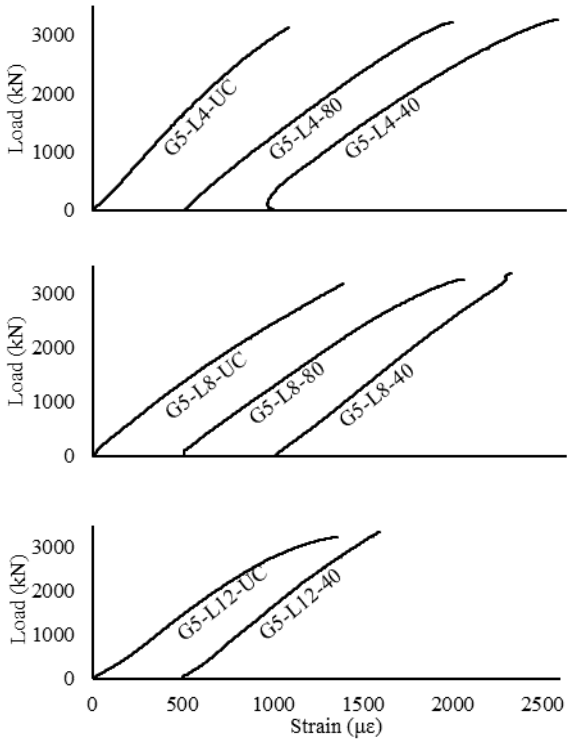

Figure 5-7. Load versus longitudinal-bar strain for each splice length (end contribution).

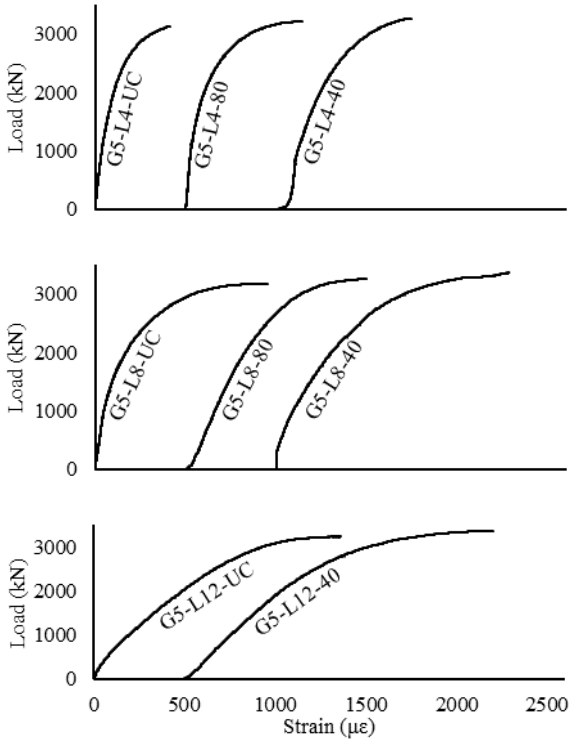

Figure 5-8. Load versus longitudinal-bar strain for each splice length (bond contribution).

5.7. DISCUSSION

5.7.1. Influence of Confinement

The experimental results indicated that the GFRP spirals with 40 mm spacing could more efficiently enhance the strength of concrete core than those of 80 mm spacing; the conclusion that has also been reported by other researchers (Afifi et al. 2014a). Moreover, reducing the spacing has altered the failure mechanism. The failure mode of the unconfined specimens was brittle and catastrophic, with a massive volume of concrete cover and core spalling off. Providing a moderate level of confinement (spirals with 80 mm spacing) resulted in a gradual and gentle cover spalling. A sharp reduction in the load-carrying capacity; however, led to the column collapse after reaching the peak load. The decreased bar strain after the peak load indicates that the longitudinal reinforcement slipped after cover spalling. Therefore, the confinement provided by the spirals with 80 mm interval could not prevent GFRP-bar slippage at the peak stage. The failure mode of well-confined specimens (spirals with 40 mm spacing) was more ductile, considering the post-peak behavior of the load–displacement curves. In other word, the descending branch of the load–displacement curves were smoother than that of the confined specimens. Introducing a high level of confinement by sufficient spiral spacing could strongly confine the concrete core and spliced-bars until the spirals ruptured during the test. Therefore, a closer spacing of transverse reinforcement can lead to a less brittle compression failure of the columns. Reduced spiral spacing also can increase the peak load of the well-confined specimens compared to the confined ones. The unconfined columns withstood less load than their confined counterparts. On average, the ultimate loading capacity of the confined and well-confined columns were 3% and 5% higher than that of the unconfined columns, respectively. This improvement is significant considering the total contribution of GFRP longitudinal bars in ultimate strength of columns under axial compression which fluctuated from 5 to10% (Luca et al. 2010; Tobbi et al. 2012).

The well-confined columns experienced the greatest axial displacement at their peak load. This might be related to the higher level of confinement, which could enhance the concrete core, allowing greater deformation without buckling or bar slippage. The axial-displacement

values were recorded at around 5.51, 4.60, and 4.43 mm for the well-confined, confined, and unconfined specimens with a splice length of $8d_b$, respectively. Their counterparts with a splice length of $4d_b$ indicated axial displacements of 5.56, 5.34, and 4.53 mm, respectively.

The developed strain in the spirals was low before cracking. However, it gradually rose as the cracks widened on the column surface. After reaching the peak load, the increase in the spiral strain was insignificant for the confined specimens, but considerable for the well-confined specimens accommodating a post-peak behavior. The measured spiral strains at failure were 1,340 and 1,500 με for G5-L4-80 and G5-L8-80, respectively. For the well-confined series, the maximum strains were 4,600 με for G5-L4-40 and about 5,000 με for G5-L8-40. The corresponding value for G5-L12-40 was 4,500 με. During the experiment, the spirals ruptured in G5-L8-40 and G5-L12-40.

5.7.2. Influence of Splice Length

Figure 5-9 depicts the impact of splice length on the load-carrying capacity of the specimens. Before reaching the peak load, the splice length had only a trivial effect on the load–displacement behavior. Considering the load–strain curves of the longitudinal bars in G5-L0-80 and G5-L0-40, bar sliding occurred before attaining the peak load. The relevant values were reported in Table 5-3 as bar sliding load: the greater the splice length, the greater the sliding load. Figure 5-10 provides the load increments in specimens with different splice lengths compared to the specimens with zero splice length at the various levels of confinement. The sliding load of G5-L4-80 and G5-L8-80 increased respectively by approximately 12% and 14%. The corresponding values for G5-L4-40 and G5-L8-40 were 5% and 8%, respectively. The increases for G5-L8-UC and G5-L12-UC were 1% and 3%, respectively, compared to G5-L4-UC. The splice length had a noticeable effect on the post-peak behavior. The specimens without confinement failed explosively after achieving their peak load upon crushing their concrete core. The specimens with a spiral spacing of 80 mm presented a sharp decay in their loading capacity upon reaching the peak load. Their descending branch, however, became smoother as the splice length increased. Aside from G5-L0-40, the well-confined columns have indicated a strain hardening behavior in their

post-peak region. The specimens with a longer splice length had a higher second peak load: 2,591, 2,605, and 2,731 kN for G5-L4-40, G5-L8-40, and G5-L12-40, respectively.

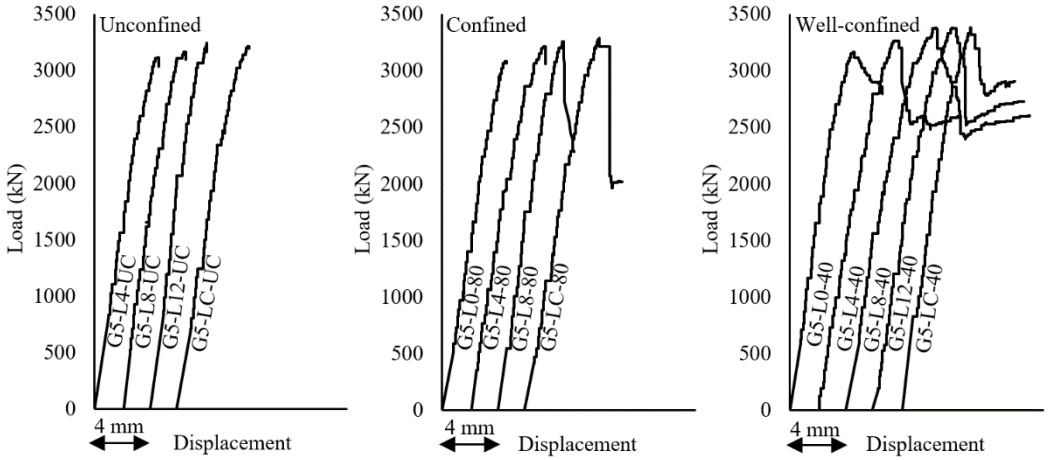

Figure 5-9. Effect of the splice length on load–axial displacement behavior of the columns with different amounts of confinement.

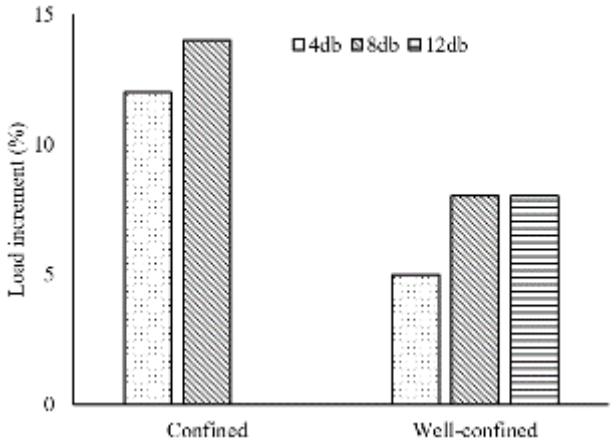

Figure 5-10. Increase in peak load for the columns with different splice lengths compared to the specimens with zero splice length.

5.8. STRENGTH MODEL FOR COMPRESSION SPLICES

This study aimed at determining the strength of spliced GFRP bars under compression considering the effect of confinement provided by transverse reinforcement. Pursuing this objective, concrete columns reinforced with lap splices at three different levels of confinement were considered in the experimental campaign. The results were used in developing an equation to estimate the achieved strength in such splices. In the following, the strength of the unconfined spliced GFRP bars is initially assessed using an equation

derived from the regression analysis of the experimental outcomes. The equation was then modified to include the effect of confinement, subsequent to assessing its influence on each component of compression splices separately.

5.8.1. Unconfined GFRP Splices

End-bearing strains are those recorded by gauges at the end of bars during the test. The maximum strain before slippage multiplied by the elastic modulus of GFRP bars equals the end-bearing strength. Figure 5-11 provides the stress normalized by the square root of the concrete compressive strength. The end-bearing contribution is a constant value, irrelevant of the splice length, as reported in other studies (Cairns 1985; Chun et al. 2010b; Pfister and Mattock 1963). As illustrated in Figure 5-11, the average value of the normalized end-bearing strength is around 9.2 for the unconfined specimens with a coefficient of variation (COV) of 10%. Therefore, the contribution of end bearing to splice strength can be determined as $9.2\sqrt{f_c'}$ MPa. Given that the concrete compressive strength was 49.3 MPa in this study, the end-bearing strength would be equal to 64 MPa. This was greater than the compressive strength of the concrete cylinder. This difference can be due to the triaxial confinement provided by the adjacent concrete at the end of spliced bars. Therefore, its capacity is higher than the uniaxial compressive strength obtained from conventional cylinder testing (Kupfer and Gerstle 1969).

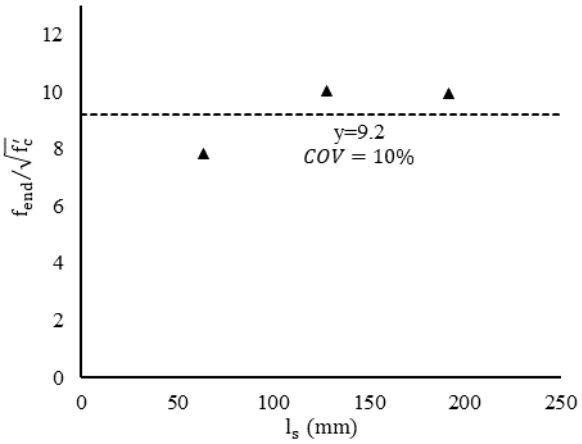

Figure 5-11. End-bearing contribution to splice strength for the unconfined GFRP bars.

The bond strain was obtained by subtraction of the strain values recorded by the strain gauges at the beginning and end of the spliced bars. Similarly, these strains were then multiplied by the elastic modulus of the GFRP bar to determine the bond stress. Nonlinear regression analysis was conducted on the relation between the normalized bond stress and splice length for the specimens with different amounts of confinement, as illustrated in Figure 5-12. The best coefficient of determination (R^2) was obtained when the bond strength was assumed proportional to a power of the splice length. This assumption satisfies the nature of bond strength, since it equals zero when the splice length is zero. Figure 5-12 shows that the bond strength would be proportional to the power of 1.104, 0.640, and 0.755 of the splice length for the unconfined, confined, and well-confined specimens, respectively. The mean value for this power is 0.833. For the sake of simplicity, the bond strength was considered linearly proportional to the splice length (hereafter, the power equals one). Figure 5-13 provides the results of the regression analysis for the unconfined specimens based on this assumption. An equation providing the bond strength for the unconfined specimens with an adopted intercept of zero is defined as

$$f_{bond} = (0.052 l_s)\sqrt{f_c'} \quad (5\text{-}4)$$

The coefficient of determination (R^2) for Eq. (5-4) is 0.992, implying a good correlation between the predicted and experimental results. Splice strength is the accumulation of the end-bearing and bond strength. Therefore, the splice strength of the unconfined spliced GFRP bars is given by

$$f_{splice} = (0.052 l_s + 9.2)\sqrt{f_c'} \quad (5\text{-}5)$$

The first and the second terms in Eq. (5-5) represent the bond and end-bearing contributions, respectively.

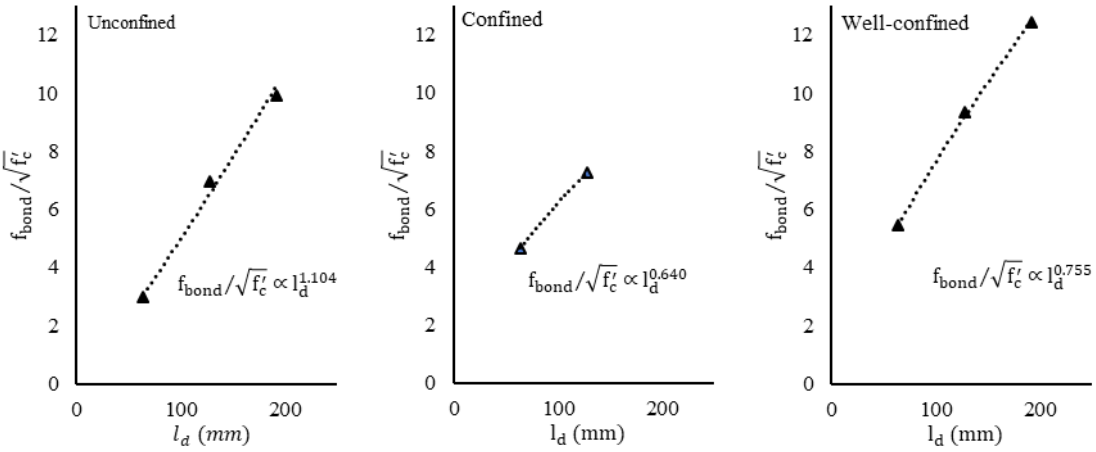

Figure 5-12. Ratios of bond strength to splice strength.

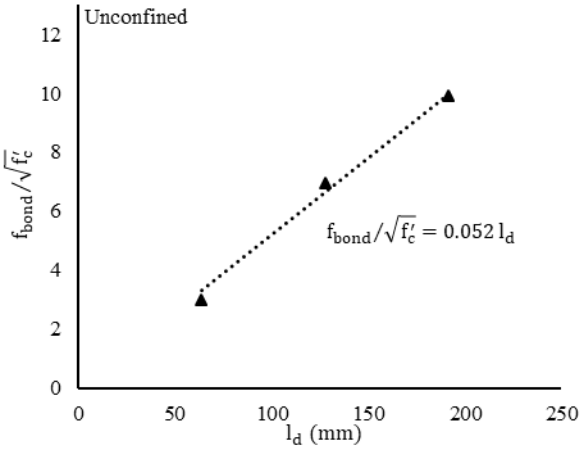

Figure 5-13. Normalized bond strength according to concrete strength versus the splice length of the unconfined specimens.

5.8.2. Confined GFRP Splices

Cairns and Arthur (1979 and Chun et al. (2010b, 2012) concluded that transverse reinforcement can only affect end-bearing strength if some stirrups are provided at the splice ends. Technically, transverse reinforcement would principally cover splice ends, if provided as spirals. Therefore, the analysis assessing the effect of confinement on end-bearing strength should involve all the confined and well-confined specimens.

Figure 5-14 shows the values of normalized end-bearing strength for the confined specimens. As seen, the average value of the normalized end-bearing strength for the confined specimens was about $9.6\sqrt{f_c'}$ MPa with a COV of 14%. Comparing the confined

and unconfined specimens, it was found that confinement could increase the end-bearing contribution by $0.4\sqrt{f_c'}$ MPa.

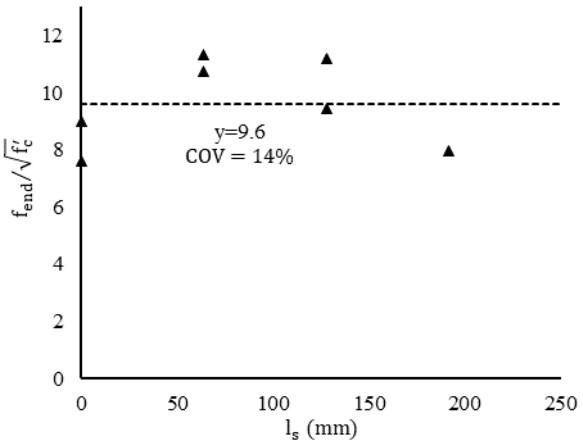

Figure 5-14. End-bearing contribution to splice strength for the confined GFRP bars.

Transverse reinforcement can also improve the bond performance by limiting crack progression. The normalized bond stresses of the spliced bars in the test specimens are presented in Figure 5-15. The horizontal axis represents the confinement variable, k_{tr}, as introduced in ACI 318M (2014) and is given by

$$k_{tr} = \frac{40A_{tr}}{sn} \tag{5-6}$$

The specimens with the same splice length were considered together and a regression analysis was conducted for each splice length. Figure 5-15 shows the trend lines of each splice length. The linear relation between bond strength and transverse reinforcement is similar to the findings of past studies (Cairns 1985; Chun et al. 2010c). The intercepts of the trend lines are close to the bond strength of the unconfined specimens, as reported in Table 5-3. Therefore, it can be deduced that the bond strength of the confined spliced bars was equal to the bond strength of the unconfined specimens plus the confinement effect. The trend lines are almost parallel with slopes of 0.191, 0.185, and 0.187 for the specimens with splice lengths of 12, 8, and 4 times the bar diameter, respectively. The mean value of the slopes is 0.188. Therefore, the bond-strength enhancement provided by the transverse reinforcement can be stated as $0.188k_{tr}$. This strength was added to the bond strength of the unconfined spliced GFRP bars.

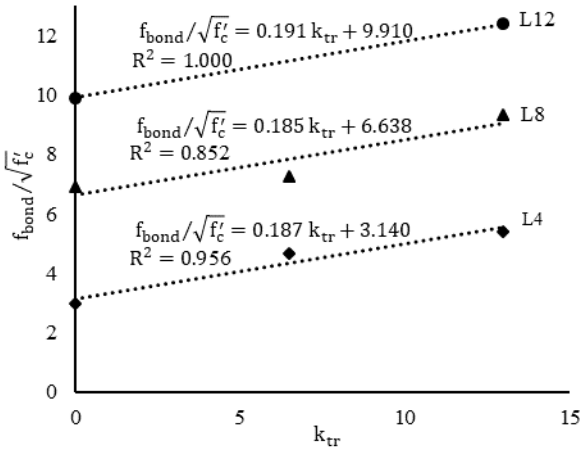

Figure 5-15. Effect of transverse reinforcement on bond strength.

All in all, the strength of a spliced GFRP bar can be defined as

$$f_{splice} = (0.052l_s + 0.188k_{tr} + 9.2 + 0.4\delta)\sqrt{f'_c} \quad (5\text{-}7)$$

where the parameter δ is taken as 1.0 if transverse reinforcement is provided at the end of splices; otherwise, it equals zero. Eq. (5-7) comprises all variables affecting splice strength. The first term represents the bond-strength component with no confinement, while the effect of confinement on it is introduced in the second part. The third term refers to the end-bearing component with no confinement and the fourth term modifies the end bearing.

The splice strength of the specimens predicted by Eq. (5-7) was compared to the experimentally obtained values in Table 5-5 and Figure 5-16. Despite some discrepancies, a good correlation can be observed between the analytical and experimental values. It should be noted that all the estimated values are on conservative side, except for specimens with zero splice length. Use of splices with zero splice length, however, are not practical in real field application. In this case, butt joints are more appropriate than lap splicing (ACI 318M 2014; Pfister and Mattock 1963).

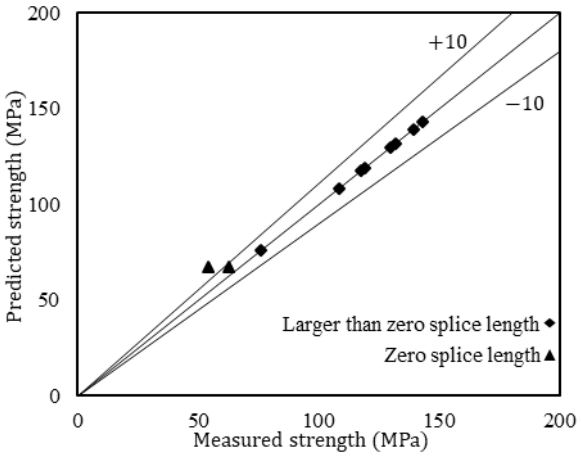

Figure 5-16. Comparison of predicted and measured splice strengths.

Table 5-5. Comparison of experimental and predicted strength.

ID	$f_{sc,e}$ (MPa)	$f_{e,e}$ (MPa)	$f_{b,e}$ (MPa)	$f_{sc,p}$ (MPa)	$f_{e,p}$ (MPa)	$f_{b,p}$ (MPa)	$(f_{sc,e}-f_{sc,p})/f_{sc,e}$ %
G5-L4-UC	76	55	21	88	65	23	-16
G5-L8-UC	119	70	49	112	65	47	6
G5-L12-UC	139	70	70	135	65	70	3
G5-L0-80	54	54	-	68	68	0	-26
G5-L4-80	108	76	33	100	68	32	7
G5-L8-80	130	79	51	123	68	55	5
G5-L12-80	NA	NA	NA	147	68	79	-
G5-L0-40	63	63	-	68	68	0	-8
G5-L4-40	118	79	38	102	68	34	15
G5-L8-40	132	66	66	132	68	64	0
G5-L12-40	143	56	87	155	68	87	-8

$f_{sc,e}$, $f_{e,e}$ and $f_{b,e}$ are the splice strength, end bearing, and bond recorded with strain gauges, respectively; $f_{sc,p}$, $f_{e,p}$ and $f_{b,p}$ are splice strength, end bearing and bond predicted with Eq. (5-7), respectively; NA means not available.

5.9. CONCLUSIONS

This study dealt with the lap splicing of GFRP bars under compression involving three levels of confinement. Specifically, it investigated the structural performance of 14 concrete columns reinforced with spliced GFRP bars under monotonically increasing axial compression. This research is in progress to derive a design equation for the splice length of GFRP bars under compression that takes various parameters into consideration. The test

parameters included the splice length and transverse-reinforcement ratio. Based on the limited experimental tests conducted herein, the following conclusions can be made:

- Transverse reinforcement can affect the deformability and strength of concrete columns reinforced with spliced GFRP bars. Reducing the spiral spacing can increase the loading and displacement capacities.
- The transverse-reinforcement ratio changed the failure mode of specimens from a brittle to a more ductile behavior. The unconfined columns explosively failed subsequent to concrete core crushing. In the specimens with a spiral spacing of 80 mm, the concrete cover spalled off at the peak load and the loading capacity decreased suddenly. The well-confined specimens with the 40 mm spiral spacing evidenced a much smoother descending branch after attaining their peak load.
- Failure of the well-confined specimens was more ductile than that of the unconfined specimens. At the post-peak stage, the former achieved a second peak load, followed by spiral rupture. The second peak load was smaller than the first, since the longitudinal reinforcement had already slipped, and the column strength attributed solely to the confined concrete core.
- The splice length affected not only the peak load but also the post-peak behavior: the longer the spice length would be, the higher the peak load is. The decrease in the column loading capacity was slower and softer for the specimens with larger splice lengths.
- An equation was proposed for the strength spliced bars under compression. The proposed equation provides a relatively simple approach for predicting the strength of spliced bars under compression. The estimated values are in good agreement with the experimental results.
- The end-bearing component of the splice strength is a constant value related to the compressive strength of concrete. In addition, confinement can favorably affect the end-bearing contribution. However, in this study, the end-bearing component remained constant regardless of the splice length and transverse-reinforcement ratio.

- The bar stress developed by the bond component in the unconfined columns can be estimated, albeit approximately, as a function of the splice length. Accordingly, a simple linear relation was derived for the design purposes.
- The bond contribution was improved with increasing the transverse reinforcement proportionally to the transverse-reinforcement index. The bond stress for the confined columns was formulated as the sum of the bond stress in the unconfined columns and augmentative effect of the transverse reinforcement.
- The experimental evidence from this study provides some experimental backbone for the lap splicing of GFRP bars in confined and unconfined concrete under compression. More experimental evidence and tests are needed, however, to validate and strengthen the findings of this study and more accurately define the FRP lap splice length under compression considering new parameters.

CHAPTER 6 AN EXPERIMENTAL AND ANALYTICAL INVESTIGATION OF THE REQUISITE SPLICE LENGTH OF GFRP BARS UNDER COMPRESSION

6.1. **INTRODUCTION**

Glass Fiber Reinforced Polymer (GFRP) reinforcement is a practical alternative for steel wherever durability is an issue of concern. Despite the fact that FRP bars has gained a major attraction as tension reinforcement, its applicability in compression elements has remained an open field of investigation yet. The current versions of major North American design codes (ACI 440.1R 2015; CAN/CSA S806-12 2012) advice to neglect the contribution of GFRP bars under compression. In order to calculate the strength of a GFRP reinforced concrete (RC) column, Zadeh and Nanni (2013) proposed replacement of GFRP bars in sections under compression with an equivalent concrete area. Afifi et al. (2014a) stated that behavior of columns reinforced with GFRP bars is practically the same as those reinforced with steel bars in terms of ultimate load capacity. Based on their results, GFRP and steel bars contribute, respectively, 5% to 10% and 8% to 12% to the ultimate loading capacity of an RC columns. Distribution and reinforcement ratio of GFRP bars can also affect the ductility index of columns (Luca et al. 2010). Hadhood et al. (2017a) conducted an investigation involving ten GFRP RC columns under concentric and eccentric loading. According to their results, increasing the longitudinal reinforcement ratio up to 3.2% could significantly enhance the ultimate strength and post peak behavior of columns. They also concluded that assumptions stipulated in ACI 440.1R (2015) or CAN/CSA S806-12 (2012) would be unconservative in predicting the axial force and bending moment capacities. Besides, taking into account the contribution of GFRP bars under compression can lead to a more reasonable estimation.

Although many studies examined the performance and strength of GFRP bars under compression in detail, no information about compression lap splicing can be found in the literature. Nonetheless, reinforcement splicing in field application is inevitable due to the reasons such as the limitation in length of bars, multistage construction, or changes in the bar size. On the other hand, apply provisions of ACI 318M (2014) to determine the requisite splice length for GFRP bars under compression are not prudent because of the intrinsic differences between steel and GFRP bars. Therefore, outcomes of this study can provide a reliable design equation for splice length with the aim of more adaptation of GFRP bars as reinforcement in columns.

6.2. **RESEARCH SIGNIFICANCE**

The main objective of this research was to determine the requisite splice length of GFRP bars under compression. To develop an accurate design expression, splice strength was considered as a function of splice length, bar diameter, confinement. The expression was derived based on the analysis of experimental data obtained from the current study and previous literature. It also considered the contribution of both the end bearing and bond components in strength of compression lap splices. The outstanding significance of the research was to enrich and fill the existing gap in ACI 440.1R (2015) about GFRP bar as compression reinforcement.

6.3. **REVIEW OF THE CURRENT DESIGN EXPRESSION**

The current versions of major design guidelines related to FRP bars have not recommended using FRP bars as a compression reinforcement. Consequently, the design formula related to steel bars are briefly presented in the following to get an insight into a possible expression to predict a compression lap splice length of GFRP bars and to elaborate on the different aspects affecting the requisite splice length.

6.3.1. ACI 318-14

According to ACI 318M (2014), the required splice length of steel bars in compression can be determined by

$$0.071 f_y d_b \qquad if f_y \leq 420\ MPa \tag{6-1}$$

$$(0.13 f_y - 24)\, d_b \qquad if f_y > 420\ MPa \tag{6-2}$$

where f_y is the yield strength of steel bars in MPa and d_b is the bar diameter in mm. To introduce the effect of transverse reinforcement on splice length, some reduction factors have also been proposed. For stirrups, a reduction coefficient of 0.83 can be applied on the splice length if the area of transverse reinforcements throughout the splice region is at least equal to 0.0015 hs in each direction where h is the perpendicular leg of stirrup to that direction and s is the center to center spacing of stirrups. The splice length is also permitted to be reduced by 25% for columns with spiral reinforcement if the clear space between each spiral step is greater than the maximum of 25 mm and $4/3 d_a$ and less than 75mm, where d_a is the aggregate diameter. However, the deducted length shall be taken at least 300 mm.

6.3.2. CAN/CSA A23.12

CSA A23.3-14 (2014) states the minimum lap length for bars shall not be less than 300 mm and may be calculated by

$$0.073 f_y d_b \qquad if f_y \leq 400\ MPa \tag{6-3}$$

$$(0.133 f_y - 24)\, d_b \qquad if f_y > 400\ MPa \tag{6-4}$$

6.3.3. CAN/CSA S6-14

Although the effect of confinement was considered to be the same as those mentioned in ACI 318M (2014), Eq. (6-5) is proposed by CAN/CSA S6-14 (2014) to calculate the length of spliced steel bars.

$$(0.133 f_y - 24) d_b \tag{6-5}$$

6.3.4. JSCE NO.15

No explicit expression can be found in Japan Society of Civil Engineers (2007) explaining compression splice length in columns. However, it takes into account the development length of a steel bar in compression as 80% of that in tension. The splice length in a column shall be 1.7 times the development length if more than half of the longitudinal reinforcement is spliced otherwise 1.3 times development length. It also advised to provide sufficient transverse reinforcement around the spliced bars to prevent any brittle failure mode. Splice length shall be more than 20 times bar diameter and 1.5 times spiral spacing while the spacing of spiral shall be less than 100 mm. The development length, l_d, is given by

$$l_d = \frac{\left(\frac{f_y}{1.25\sqrt{f_c'}} - 13.3\right) d_b}{0.318 + 0.795\left(\frac{c}{d_b} + \frac{15A_t}{sd_b}\right)} \tag{6-6}$$

where f_c' is the concrete compressive strength; c is the concrete cover and A_t is the area of transverse reinforcement perpendicular to splitting surface. Further, factor α has been introduced to consider all the parameters affecting development length such as bar type, bar diameter, strength of concrete and transverse reinforcement. So that, Eq. (6-6) can be simplified as

$$l_d = \alpha \frac{f_y d_b}{4 f_{bod}} \tag{6-7}$$

where f_{bod} is the design bond strength of concrete and equals $0.28{f_c'}^{2/3}$; k_c is $\frac{c}{d_b} + \frac{15A_t}{sd_b}$ and α is determined in Table 6-1.

Table 6-1. Factor α based on k_c.

1.0	$k_c \leq 1.0$
0.9	$1.0 < k_c \leq 1.5$
0.8	$1.5 < k_c \leq 2.0$
0.7	$2.0 < k_c \leq 2.5$
0.6	$2.5 < k_c$

6.4. BACKGROUND

6.4.1. Force Transfer Mechanism

To transfer compression axial force from one bar to another through lap splicing, a specific lap length shall be provided. This length is believed to be less than the requisite one for spliced bars under tension which is primarily due to the force transfer mechanism by bond mechanism in tension splices (Chun et al. 2010c). In compression splices, however, another component acting at the free end of bars (referred to as end bearing) would also contribute to the force transmission as illustrated in Table 6-1 (Chun 2017; Park and Paulay 1974). Thus, the strength of spliced bars under compression can be expressed by

$$f_{sc} = f_b + f_e \tag{6-8}$$

where f_{sc} is the splice stress, f_b is the bond stress in a bar and f_e is the end bearing stress at the free end of a bar. Pfister and Mattock (1963) showed a considerable amount of force transfer through end bearing component in spliced bars under compression. It is worth noticing that the entire strength of the bond and end bearing stresses cannot be developed while their simultaneous action is present. This might be ensued from two reasons: 1) Both stresses reach their peak value at different strain levels so that they are not at the peak at the onset of splice failure, and 2) They both produce bursting force leading to cover spalling. Available resistance (provided by the confinement reinforcement and concrete tensile strength) counteracting the bursting forces remains constant regardless of simultaneous stresses. Then, the stresses developed would be less than their ultimate strength before failure when they are both present at the end of spliced bars (Cairns and Arthur 1979; Chun 2017). As a result, it would lead to an unconservative estimation of the splice strength and length if bond stress of spliced bars under compression is considered the same as that under tension. It seems that the bond and end bearing stresses for compression spliced bars needs to be investigated precisely.

According to Elinea et al. (1999), the parameters affecting the strength of a spliced bar comprises bar diameter, surface treatment, concrete strength and confinement level. In the following, these parameters would be described in detail.

6.4.2. Confinement

It is believed that transverse reinforcement can significantly reduce the overlap splice length of deformed bars (Elinea et al. 1999). Its effect can be explained regarding general theory of surface friction of solids bodies as explained by Hales et al. (2017) and Saatcioglu and Razvi (1992). Figure 6-1 shows a free body diagram of a spliced bar confined by spiral. Based on the equilibrium of forces, the radial force acting on a longitudinal bar, f_r, is given by

$$f_r = \frac{2A_s f_s}{d_s} \tag{6-9}$$

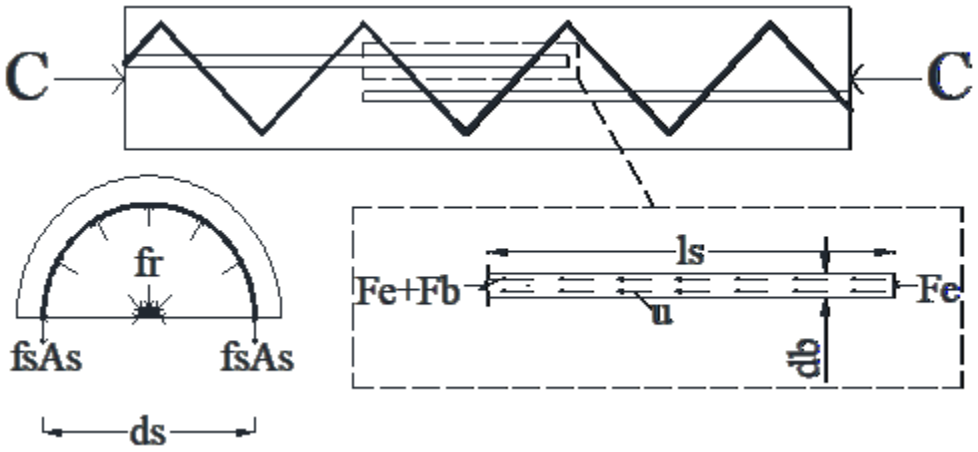

Figure 6-1. Free body diagram of a spliced bar.

where A_s, f_s, and d_s are, respectively, the area, developed stress, and diameter of the transverse reinforcement. According to the friction theory, the transferred force over a sliding area between two bodies is proportional to the coefficient of friction (μ) and the normal force acting between them. It was already mentioned that transmission of force between a coupled spliced bar is based on the bond (shear) stress through surrounding concrete. Then, the following equations can be derived from the implementation of this theory on a spliced bar embedded in concrete.

$$f_r \pi d_b l_b \mu = f_b A_b\,, \tag{6-10}$$

$$l_b = \frac{1}{2\pi\mu}\left(\frac{f_b}{f_s}\right)\left(\frac{A_b}{A_s}\right)\left(\frac{d_s}{d_b}\right) \tag{6-11}$$

where A_b is the area of longitudinal reinforcement. The value of μ depends on surface deformation of the bar and properties of concrete (ACI 318M 2014). Eq. (6-11) shows that the splice length can be impacted by the strength of spiral as well as the spiral diameter (d_s).

According to Elinea et al. (1999), the lateral confinement can enhance the compressive strength of concrete. This improvement would increase the bond and end bearing contribution and consequently reduce the splice length.

Orangon et al. (1977) developed an expression including transverse reinforcement effect to predict the strength of a spliced steel bar under tension, f_{sts}, defined as

$$f_{sc} = \left[\left(0.4 + 1.08\frac{c}{d_b}\right)\frac{l_s}{d_b} + 17.6 + 0.1\frac{A_{tr}f_{yt}l_s}{sd_b^2}\right]\sqrt{f_c'} \quad (6\text{-}12)$$

where f_{yt} is the yield strength of transverse reinforcement. Cairns (1985) analyzed the experimental data conducted on spliced steel bars under compression. To predict splice strength of steel bars under compression, f_{scs}, he obtained an approximately similar equation to Eq. (6-12) which is given by

$$f_{sc} = \left[1.4\frac{l_s}{d_b} + 29.4 + 0.32\frac{A_{tr}f_{yt}l_s}{sd_b^2}\right]\sqrt{f_c'} \quad (6\text{-}13)$$

The third parameter in Eq. (6-12) and (6-13) presents the effect of transverse reinforcement. Considering their coefficient, transverse reinforcement contributes three times more to the splice strength under compression than tension.

Cairns and Arthur (1979), Darwin et al. (1996a) and Zuo and Darwin (2000) declared the effect of confinement on the strength of spliced bars as a function of the roughness and relative rib area of bars. Considering the low relative rib area of GFRP bars, their bond would be also less than that of steel bars (Benmokrane et al. 1996; Tighiouart et al. 1998). Therefore, the effect of confinement on the splice strength of GFRP bars is supposed to be less than that of steel.

6.4.3. Bar Diameter and Splice Length

According to Cairns and Arthur (1979) and Chun (2017), the distribution of bond stress is variable along the splice length. For simplification, however, it is considered to be constant over the splice length for lap splices under tension. This assumption can be fairly accurate particularly for short splice length (Canbay and Frosch 2005). In addition, the relation between the bond stress and splice length is not linear. Increasing the splice length would result in decreasing its effectiveness (Ferguson and Breen 1965). On the other hand, the splice length is a relative value. While a given splice length could be inadequate for a large size bar, it might be adequate for a bar with smaller diameter. So, Darwin et al. (1996b) and Orangon et al. (1977) developed equations to predict bond stress of steel bars under tension proportional to the ratio of d_b/l_s. Wambeke and Shield (2006) also investigated the strength of spliced GFRP bars under tension and expressed average bond stress as a function of d_b/l_s by

$$u = 0.083\left(4 + 0.3\frac{c}{d_b} + 100\frac{d_b}{l_b}\right)\sqrt{f_c'} \quad (6\text{-}14)$$

where u_{stg} is the average bond stress of spliced GFRP bars under tension.

Chun et al. (2010b) derived an equation based on the square root of d_b/l_s to present the contribution of bond stress for spliced steel bars under compression.

6.4.4. Concrete Strength

Based on the literature survey, Canbay and Frosch (2005) indicated that the effect of concrete on the strength of steel spliced bars under tension can be most accurately presented by the fourth root of the compressive strength of concrete. However, Zuo and Darwin (2000) showed this effect is related to the confinement so that $\sqrt[4]{f_c'}$ more appropriately reflects the effect of concrete strength on bond strength for the unconfined spliced bars while $\sqrt{f_c'}$ appear to be more reliable for the confined ones. For normal strength concrete ranging from 31 to 52 MPa, the square root of concrete strength gives a precise representation of the concrete

effect on the bond strength (Darwin et al. 1996b). Elinea et al. (1999) and Orangon et al. (1977) used $\sqrt{f_c'}$ to derive their expression for tension spliced steel bars. On the other hand, the absence of tension cracks in concrete for splices under compression would improve the bond and shear stress between concrete and bar (ACI 408 2003). So Cairns (1985) and Chun et al. (2010a, 2012) normalized the strength of steel spliced bars under compression with the square root of concrete strength. They also referred to the shorter length of splices under compression than tension. It is notable that according to Cairns and Arthur (1979), the effect of concrete strength is more pronounced in short splices. Therefore, normalizing the strength of lap splices under compression with the square root of concrete compressive strength would be rational.

In this study, the compressive strength of concrete remained constant for all the specimens. Nonetheless, the strengths of different schemes of spliced bars were normalized by the square root of concrete strength for ease of comparison.

6.5. EXPERIMENTAL PROGRAM

The test program was composed of 29 circular columns, three of which were reinforced with steel and the remainder with GFRP bars. The reinforcements were sand coated GFRP bars and conventional deformed steel bars ranging in size from No. 5 (15.9 mm) to No. 8 (25.4 mm). The mechanical properties of reinforcing materials are provided in Table 6-2 and Table 6-3. The compressive strength of concrete measured from cylinders of $100 \times 200\ mm$ was around 49.3 MPa on the beginning day of testing. The specimens were 1600 mm in height and 300 mm in diameter. To minimize the load eccentricity, careful attention was made during building of columns to have a symmetric cross section. Reinforcement detailing of the columns met the requirement of ACI 318M (2014), CAN/CSA S806-12 (2012) and CSA A23.3-14 (2014) except for the lack of transverse reinforcement in the unconfined specimens. Figure 6-2 provides a schematic illustration of the splice configurations. Also, the details of the test specimens are given in Table 6-4. Splice length ranged from 0 to 36 times bar diameter. The specimens can be divided into four groups. The first group was pertaining to the effect of bar type. The main parameter of the second group was the splice

length. The third group focused on the amount of transverse reinforcement along the splice length in order to evaluate the effect of confinement. The purpose of the fourth group was to evaluate the behavior of spliced bars of different bar diameter. The nomenclature used for the designation of the test specimens is initiated with a letter to indicate the bar type (S for Steel, and G for GFRP). Also, the first number indicates the diameter of longitudinal bars (5 for No. 5 GFRP or M15 steel, 6 for No. 6 GFRP, and 8 for No. 8 GFRP bars). In addition, the number and the letter "C" following the letter "L" indicate the splice length in terms of the bar diameter and specimens with continuous bars, respectively. The last number is the spacing of spiral reinforcement (80 mm or 40 mm) while "UC" stands for the unconfined specimens. To evaluate the splice strength, two parts of a spliced bar in each column were instrumented with the electrical resistance strain gages. To measure the end bearing contribution, the end gages were mounted at a distance of 20 mm from the end of bars to allow full development of stresses. In addition, two additional gages were attached at the beginning of the splice to determine the entire strength of spliced bars. Also, the axial displacement of the columns was measured using a set of linear variable deferential transducers (LVDTs) during the test. The experimentation was carried out using a monotonically increasing concentric load applied with a constant rate of 0.5 kN/s. During the test, all the data including strain, axial displacement, and compressive load were recorded using a computerized data acquisition system.

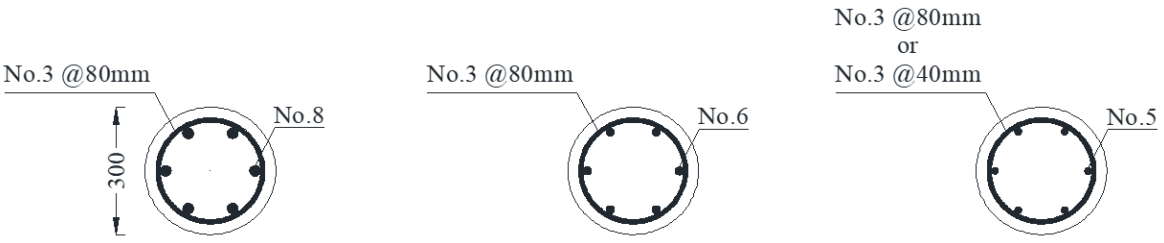

a)

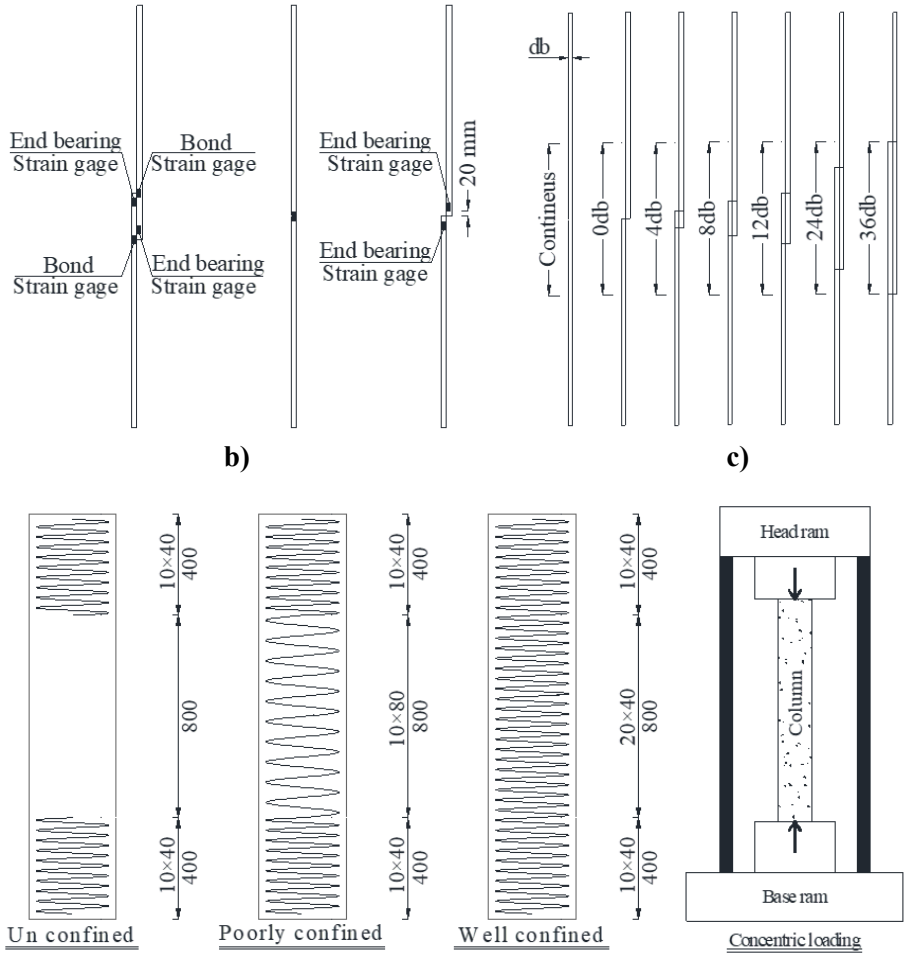

Figure 6-2. Geometry and details of the specimens: a) reinforcement; b) strain gages locations; c) applied splice lengths d) confinement patterns; e) test setup.

Table 6-2. Mechanical properties of steel reinforcement.

Bar number	Diameter (mm)	Area (mm^2)	Modulus of elasticity (GPa)	Yield strength (MPa)	Ultimate tensile strength (MPa)	Tensile strain (%)
M10	9.5	71	200	450	660	0.2
M15	16	200	200	460	660	0.2

Table 6-3. Mechanical properties of the GFRP reinforcement.

Bar Number	Diameter (mm)	Immersion Area (mm2)	Nominal Area† (mm2)	Modulus of Elasticity (GPa)	Tensile Strength (MPa)	Tensile Strain (%)
#3	9.5	81.5	71	54.1	1206*	2.2
#5	15.9	209	198	51.2	1374	2.7
#6	19.1	299	286	52.4	1258	2.4
#8	25.4	543.4	507	51.2	1269	2.5

† The strength and modulus were calculated based on this area

* Based on the results of straight bars.

Table 6-4. Summary of test results.

Group	Specimen ID	Fai. mode	k_{tr}	Splice length (d_b)	Splice length (mm)	Strain (με)		Stress (MPa)			
						End bearing	Bond in bar	End bearing	Bond in bar	Ave. bond	Splice strength (f_{sce})
I	S5-L4-80	C[1]+S[2]	35.5	4	64	428	652	85.60	130.40	8.15	216
						766	413	153.20	82.60	5.16	235.8
	S5-L8-80	C+S	35.5	8	128	641	968	128.20	193.60	6.05	321.8
	S5-LC-80	C+B[4]	35.5	-	-	1986		397.2		-	-
						2337		467.4		-	-
						3654		730.8		-	-
II	G5-L0-80	S+C	35.5	0	0	1371	0	70.20	0	0	70.2
						1046	0	53.56	0	0	53.6
	G5-L4-80	C+S	35.5	4	65.2	1606	639	82.23	32.72	2.04	114.9
						1476	1193	75.57	61.08	3.82	136.7
	G5-L8-80	C+S	35.5	8	130.4	1683	1020	86.17	52.22	1.63	138.4
						1537	996	78.69	51.00	1.59	129.7
	G5-L24-80	C+S +R[5]	35.5	24	391.2	1434	1789	73.42	91.60	0.95	165.0
						1647	1150	84.33	58.88	0.61	143.2
						1420	1421	72.70	72.76	0.76	145.5
						993	1082	50.84	55.40	0.58	106.2
	G5-L36-80	C+S+ R+B	35.5	36	586.8	920	1715	47.10	87.81	0.61	134.9
						1136	1276	58.16	65.33	0.45	123.5
	G5-LC-80	C+B	35.5	-	-	3033		155.3		-	-
						2406		123.2		-	-
						3029		155.1		-	-
III	G5-L0-40	S+C	71	0	0	1105	0	56.58	0	0	56.6
						1236	0	63.28	0	0	63.3
	G5-L4-40	C+S	71	4	65.2	1552	744	79.46	38.09	2.38	117.6
						1397	947	71.53	48.49	3.03	120.0
	G5-L8-40	C+S	71	8	130.4	1297	1280	66.41	65.54	2.05	131.9
						1053	2037	53.91	104.29	3.26	158.2
	G5-L12-40	C+S	71	12	195.6	1093	1700	55.96	87.04	1.81	143.0
						1573	636	80.54	32.56	0.68	113.1
	G5-LC-40	C+B	71	-	-	2732		139.9		-	-
						2592		132.7		-	-
						2648		135.6		-	-
	G5-L4-UC	C+S	0	4	65.2	1074	1041	54.99	53.30	3.33	108.3
						1707	410	87.40	20.99	1.31	108.4
	G5-L8-UC	C+S	0	8	130.4	1466	950	75.06	48.64	1.52	123.7
						1373	1147	70.30	58.73	1.84	129.0
	G5-L12-UC	C+S	0	12	195.6	1361	1359	69.68	69.58	1.45	139.3
						939	1683	48.08	86.17	1.80	134.3
	G5-LC-UC	C	0	-	-	2281		116.8		-	-
						2121		108.6		-	-
IV	G6-L0-80	S+C	35.5	0	0	980	0	51.35	0	0	51.4
						1287	0	67.44	0	0	67.4
	G6-L4-80	S+C	35.5	4	78	1660	NA	86.98	NA	NA	87.0
						1519	732	79.60	38.36	2.40	118
	G6-L8-80	S+C	35.5	8	156	1560	644	81.74	33.75	1.05	115.5
						1572	633	82.37	33.17	1.04	115.6
	G6-L12-80	S+C	35.5	12	234	1227	1584	64.29	83.00	1.73	147.3
						1754	579	91.91	30.34	0.63	122.3
	G6-LC-80	C+B +R	35.5	-	-	2811		147.3		-	-
						1978		103.7		-	-
						2789		146.1		-	-
	G8-L0-80	C+S	35.5	0	0	1616	0	82.74	0	0	82.7
						1907	0	97.64	0	0	97.6
	G8-L4-80	C+S	35.5	4	105.2	1516	1410	77.62	72.19	4.51	149.8
						1884	373	96.46	19.10	1.19	115.6
	G8-L8-80	C+S +R	35.5	8	210.4	1306	961	66.87	49.20	1.54	116.1
						1478	479	75.67	24.52	0.77	100.2
	G8-L12-80	C+S	35.5	12	315.6	1335	1139	68.35	58.32	1.21	126.7
						1378	1012	70.55	51.81	1.08	122.4
	G8-LC-80	C+B	35.5	-	-	3870		198.1		-	-
						2550		130.6		-	-

C is concrete core crushing; S is bar sliding; NA is not achieved; B is bar buckling; R is spiral rupture.

6.6. **TEST RESULTS**

Table 6-4 summarises the failure modes observed during testing of the columns. Also, Figure 6-3 shows examples of the specimens after testing. Most of the specimens failed by splitting of concrete cover at the splice region followed by bar sliding. For the columns with zero splice length and those reinforced with No. 6 GFRP bars, bar sliding occurred before concrete splitting. Thus, it can be broadly concluded that all the specimens failed in a brittle and sudden manner except the well confined columns and those reinforced with continuous bars. The more confinement provided by the transverse reinforcement, the more ductile performance observed in the post peak behavior. The specimens with continuous bar failed upon bar buckling after the peak load.

Figure 6-3. Failure modes of the specimens.

The strain values measured at the onset of sliding in the spliced bars are given in Table 6-4. The corresponding stresses were then calculated regarding the modulus of elasticity of each bar type. As illustrated in Figure 6-2, the end bearing strains were determined from the strain gages installed at the free end of spliced bars. To obtain the bond strain in bars, the measured end bearing strains were deducted from the strains measured by strain gages at the end of spliced bars. The bar stresses and average bond stress (u) developed on the surface of one of the spliced bars were drawn in Figure 6-1 (Macgregor, James G. Wight 2012). The average bond stress acting on the perimeter of a bar, u, can be determined as

$$u = {}^{df_b}/_{4l} \quad (6\text{-}15)$$

The values of average bond stresses calculated for all specimens tested in this study are given in Table 6-4. Hereafter, these average bond stresses are used to calculate the required splice length.

6.7. **SPLICE STRENGTH**

The required splice length for M15 steel bar is 573 mm based on the recommendation of ACI 318M (2014) (Eq. (6-2)). However, the splice length provided for the spliced bars in specimens S5-L4-80 and S5-L8-80 is 11% and 22% of the required length, respectively. The total stress measured in the spliced bars (the sum of end bearing and bond stress contributions) for S5-L4-80 and S5-L8-80 is 43% and 61% of the ultimate stress of continuous reinforcement monitored in column S5-LC-80, respectively. On the other hand, their counterparts in group II (G5-L4-80 and G5-L8-80) could gain 92% and 97% of the ultimate stress developed in longitudinal bars of column G5-LC-80, respectively. Considering the steel and GFRP reinforced specimens with the same splice length, the ratio of stress developed in the spliced bars to that of the continuous bars was much closer to one for the specimens reinforced with GFRP bars. For instance, 22% of the calculated splice length was provided for the bars in specimen G5-L8-80 regarding Eq. 1. Nonetheless, the spliced bars could withstand almost the same stress as the continuous bars in G5-LC-80. It means that equations offered by ACI 318M (2014) can not be applicable for GFRP bars and a new approach is needed to predict the splice length of GFRP bars under compression.

The method implimented in this study, is based on the free body diagram illustrated in Figure 6-1. The force developed in a spliced bar (splice strength) is comprised of the end bearing force and average bond stress acting on the surface of a bar along the splice length. Transverse reinforcement would desirably improve the contribution of both components. Comparison of the results of specimens in groups II and III would outline the effect of confinement on the end bearing and bond stresses. Then, the unconfined strength of spliced bars in all specimens can be achieved by subtracting the increment provided by the transverse reinforcement. Subsequently, the unconfined strength was used to determine the

components of the strength of spliced bars on the basis of the splice length and bar dimeter. Finally, the equation to predict the strength of a spliced GFRP bar under compression can be achieved by combining the components of a splice strength with additional contribution provided by the confinement. If the equation is solved for the length as a variable, the required splice length can be obtained through the replacement of a strength supposed to be developed in a compression spliced bar.

6.7.1. End Bearing

Cairns and Arthur (1979) and Chun et al. (2012) clarified transverse reinforcements would improve the end bearing if they are placed at the free ends of splices. Regardless of the spiral spacing, the free ends of spliced bars are technically confined in the columns transversally reinforced with spirals. Hence, the confined specimens in group II and III were treated together to evaluate the effect of confinement on the end bearing strength. Figure 6-4 shows the end bearing stresses normalized by the square root of the concrete strength versus the splice length for No.5 GFRP bars. Irrespective of the splice length, the end bearing contribution remained constant for the specimens with a reasonable COV (coefficient of variation). The difference between the amount of end bearing stresses in the confined and unconfined specimens appears to be marginal. Nevertheless, the contribution of confinement was subtracted from the end bearing stress measured in the specimens reinforced with Nos. 6 and 8 bars to provide precise values of the unconfined end bearing stress. The outcomes are shown in Figure 6-5 where the best fit lines are horizontal which outlined the negligible effect of splice length on the end bearing stress. Regardless of the splice length, the unconfined end bearing strengths were measured to be about $9.63\sqrt{f_c'}$, $10.66\sqrt{f_c'}$ and $11.19\sqrt{f_c'}$ for Nos. 5, 6 and 8 GFRP bars, respectively. The normalized mean value of the unconfined end bearing stress for three different sizes of bar diameters ranging from 16 mm to 25 mm is plotted in Figure 6-6. A trendline with the highest coefficient of determination (R2) is presented in Figure 6-6. Generally, the closer the R^2 is to 1.0, the better an equation characterize parameters. The trendline shows that the end bearing strength is linearly proportional to the bar diameter. Hence, the unconfined end bearing stress, f_{unce}, can be predicted as

$$f_e = (0.14d + 7.6)\sqrt{f_c'} \quad (6\text{-}16)$$

Considering the additional strength provided by the confinement, the end bearing contribution, f_e, can be evaluated by

$$f_e = (0.14d + 7.6 + 0.06\delta)\sqrt{f_c'} \quad (6\text{-}17)$$

in which, δ is the factor representing the effect of confinement and is taken as one where free ends of the spliced bars are confined, otherwise zero.

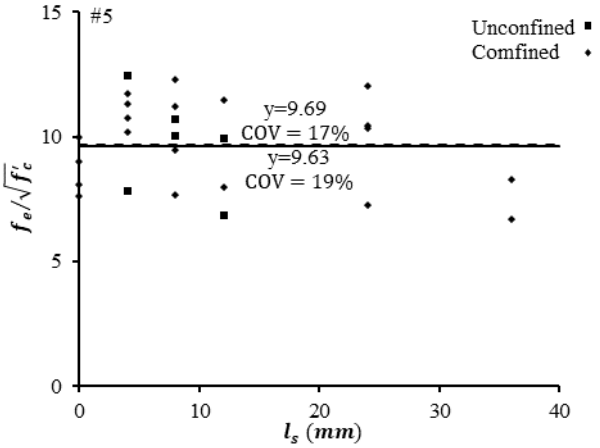

Figure 6-4. Effect of confinement on end bearing stress.

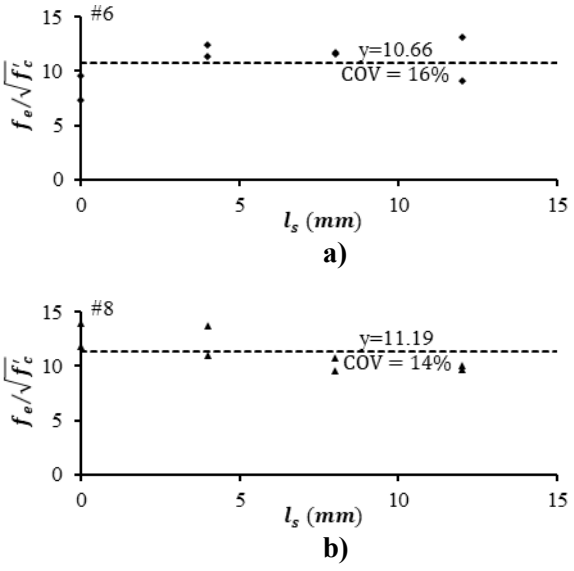

Figure 6-5. Normalized end bearing stress for specimens reinforced with: a) bar #6, b) bar #8.

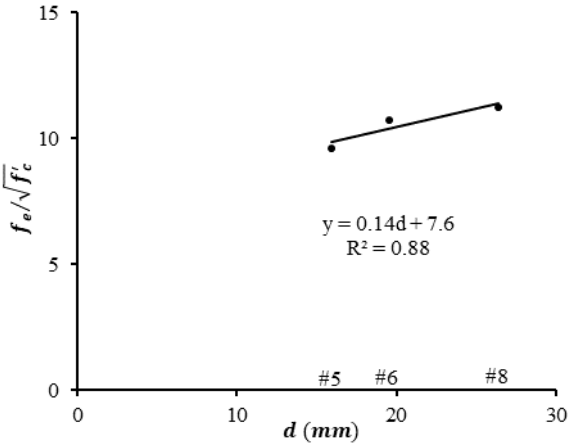

Figure 6-6. Effect of bar diameter on normalized end bearing.

6.7.2. Bond

The total bond stress developed in a spliced bar together with the calculated average bond stress are summarized in Table 6-4. The bond stress developed in a bar was taken as the difference between stress values measured by two strain gauges mounted at the ends of an individual bar along the splice. The average bond stress then can be calculated by substituting the bond stress in Eq. (6-15). In order to evaluate the effect of transverse reinforcement, the average bond stresses of the specimens in group II and III categorized according to their splice length are presented in Figure 6-7. The average bond values normalized by the square root of concrete strength are shown along vertical axis while the transverse reinforcement index on the horizontal axis is generalized as

$$k_{tr} = \frac{40A_{tr}}{sn} \tag{6-18}$$

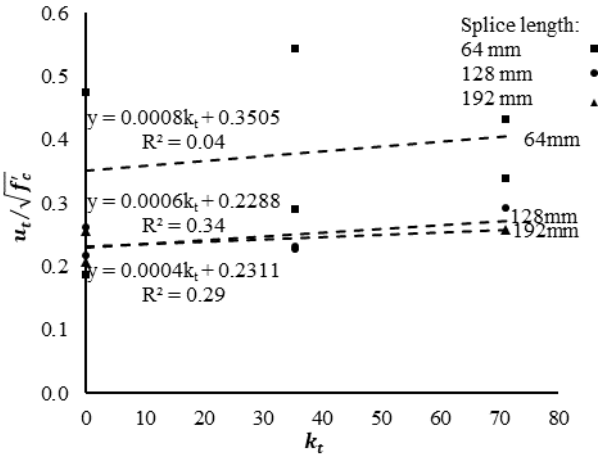

Figure 6-7. Effect of transverse reinforcement on average bond stress.

In the above equation, n is the number of bars being spliced along the plan of splitting. In the case of lap splices confined with spiral reinforcement, n is taken as one (Cairns 1985). Rupture of spiral was just observed for some specimens after peak load and ultimate strength of spiral has no effect on the strength of spliced bars at the peak. Then, the transverse reinforcement index should not take into account the ultimate strength of transverse reinforcement. Figure 6-7 shows that increasing the transverse reinforcement index could improve the average bond stress. The parallel best trend lines (the highest R^2) for each splice length can indicate the similar effect of transverse reinforcement regardless of the splice length. Consequently, the contribution of transverse reinforcement to the average bond stress, u_t, can be defined as

$$u_{tr} = 0.0006k_{tr}\sqrt{f_c'} \quad (6\text{-}19)$$

Wambeke and Shield (2006) ignored the effect of transverse reinforcement on the average bond stress treating their unconfined and confined tests similarly. In this study, however, the contribution of transverse reinforcement was subtracted from the average bond values of the confined specimens. The results normalized with the square root of concrete strength is plotted in Figure 6-8 versus the ratio of the splice length to the bar diameter ($^{l_s}/_{d_b}$). To obtain a high coefficient of determination (R^2), the best curves fitted with experimental data for each bar diameter were then determined. The curves showed a similar behavior. In addition, it could be observed that increasing the splice length led to decreasing the average

bond stress. To investigate the general effect of l_s/d_b, all specimens were analyzed together and the best fit curve producing the highest R^2 (equal to 0.64) for all the bar diameters is illustrated with a continuous line in Figure 6-8. This curve can be expressed as

$$u_{uncb}/\sqrt{f_c'} = 0.88\left(l_s/d_b\right)^{-0.68} \tag{6-20}$$

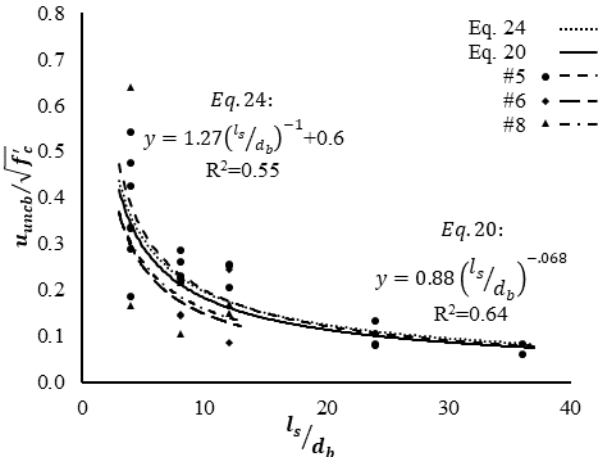

Figure 6-8. Normalized average bond stress vs splice length (Effect of confinement was eliminated).

where u_{uncb} is average bond stress for unconfined GFRP bars under compression. Combining Eqs. (6-20) with (6-19), the average bond stress of a confined spliced GFRP bar, u_b, can be determined by

$$u_b = \left[0.88\left(l_s/d_b\right)^{-0.68} + 0.0006k_{tr}\right]\sqrt{f_c'} \tag{6-21}$$

The obtained equation (Eq. (6-21)) for the compression splices was evaluated against the available equation for the average bond stress of spliced GFRP bars under tension (Eq. (6-14)) in Figure 6-9. The mean values of the ratios of the average experimental to the calculated bond stress obtained from Eqs. (6-14) and (6-21) were around 0.16 and 0.97, respectively. The proposed equation predicted the average bond stress with a reasonable accuracy. However, the predictions of Eq. (6-14) are unconservative which leads to an unconservative estimations of required splice length. That is a comprehensive and reliable equation statistically derived base on the data of 75 beams gathered from the literature review in which the influence of confinement, bar location, cover, bar surface and diameter

were evaluated. Considering the studies conducted on the reinforced beams with GFRP bars (Aly et al. 2006; Ehsani et al. 1996; Pay et al. 2014; Tighiouart et al. 1999), the strain measured in the spliced bars under tension is several times greater than the strain of bars under compression. It is because, the maximum strain in a GFRP bars under compression is controlled by the ultimate compression strain of concrete which is much less than the ultimate tensile strain of GFRP bars. Thus, expression developed for estimating the bond stress of spliced GFRP bars under tension should inherently provide greater values than those derived for spliced GFRP bars under compression.

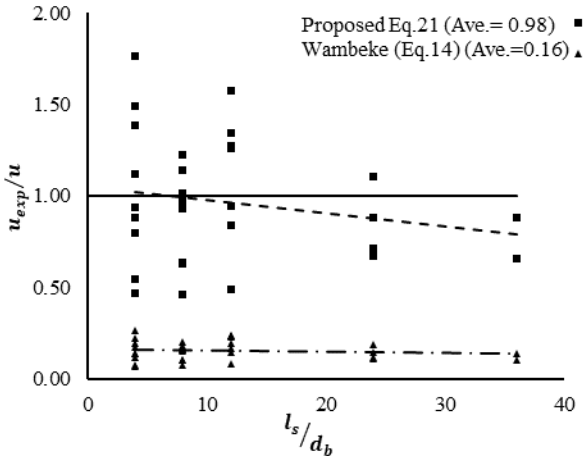

Figure 6-9. Comparison of average bond stress calculated by Eq. (6-21) and Eq. (6-14).

Combining Eqs (6-8), (6-15), (6-17) and (6-21), the total strength of a spliced bars under compression can be given by

$$f_{scp} = \left[3.52\left(l_s/d_b\right)^{0.32} + 0.0024k_{tr}\left(l_s/d_b\right) + 0.14d + 7.6 + 0.06\delta\right]\sqrt{f_c'} \quad (6\text{-}22)$$

Comparing Eq. (6-22) with the experimental results of Table 6-4. Summary of test results. revealed a good agreement between them. The mean value for the ratio of experimental to predicted splice strength (f_{exp}/f_{sc}) for the columns was calculated to be approximately 0.98 with a standard deviation of 0.14.

6.8. **DESIGN DEVELOPMENT LENGTH**

For design purposes, prediction of the splice length is more desirable than the splice strength. Eq. (6-22) can serve as a basis for developing a design expression. Based on the results of 39 RC columns collected from the literature (Afifi et al. 2014b; Hadhood et al. 2017a; b; c, Tobbi et al. 2012, 2014) and the columns reinforced with continues GFRP bars herein, it could be inferred that the ultimate strain that can be developed in GFRP bars depends on the ultimate strain of concrete under compression. This conclusion is due to the fact that a section under compression fails at the onset of concrete crushing regardless of the ultimate strength of GFRP bars. Considering a maximum concrete strain of 0.003 proposed by ACI 440.1R (2015), and the modulus of elasticity of GFRP bar, Eq. (6-22) can be numerically solved for a splice length to achieve the maximum compression strength. Although each term in Eq. (6-22) has a physical meaning regarding the effective parameters in splice strength under compression, it is impossible to precisely solve that equation for the splice length.

For practical purposes, the average bond stress is considered to be linearly proportional to the ratio of d_b/l_s. This assumption is aligned with the bond strength of spliced GFRP bars under tension (Wambeke and Shield 2006). The best curve estimating the experimental results with regard to this assumption is shown in Figure 6-8. Modification of Eqs. (6-20) to (6-22) would lead to

$$f_{scp} = 0.003E_{GFRP} \tag{6-23}$$

$$u_{uncb}/\sqrt{f_c'} = 1.27\left(l_s/d_b\right)^{-1} + 0.06 \tag{6-24}$$

$$u_b = \left[1.27\left(d_s/l_b\right) + 0.06 + 0.0006k_{tr}\right]\sqrt{f_c'} \tag{6-25}$$

$$f_{scp} = \left[5.08 + 0.24\left(l_s/d_b\right) + 0.0024k_{tr}\left(l_s/d_b\right) + 0.14d + 7.6 + 0.06\delta\right]\sqrt{f_c'} \tag{6-26}$$

Comparison of the average bond stress calculated by Eq. (6-21) and Eq. (6-25) in Figure 6-10 shows an acceptable accuracy for both equations. Eq. (6-26) can be analytically solved to determine the splice length as

$$l_s = d_b \frac{0.003E_{GFRP}/\sqrt{f_c'} - 12.68 - 0.14d_b - 0.06\delta}{0.24 + 0.0024k_{tr}} \quad (6\text{-}27)$$

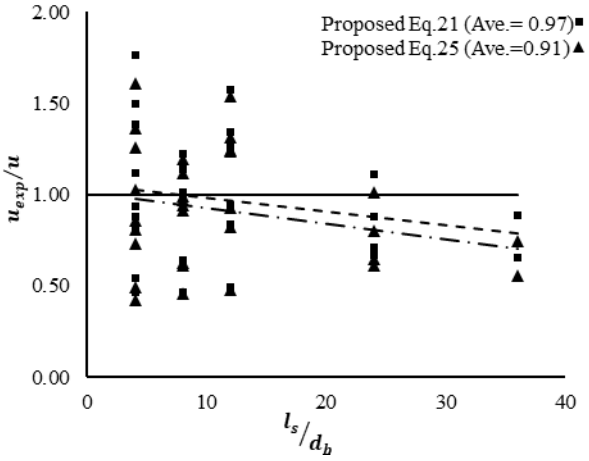

Figure 6-10. Comparison of average bond stress calculated by Eq. (6-21) and Eq. (6-24).

This expression represents the requisite splice length to reach the maximum stress which can be developed in GFRP reinforcing bars under compression. Although using transverse reinforcement can impede the explosive failure, neglecting the effect of confinement may lead to a conservative and simpler equation as

$$l_s = d_b \frac{3E_{GFRP}/\sqrt{f_c'} - 12680 - 140d}{240 + 2.4k_{tr}} \quad (6\text{-}28)$$

6.9. CONCLUSION

This study reports on the results of an experimental and analytical equation on lap splicing of GFRP bars under compression. Through the regression analysis of the results of experimental tests conducted herein and available in the literature, a design expression was derived to predict the requisite splice length of GFRP bars under compression. The equation accounts for the major effective parameters such as size of spliced bars, elastic modulus of

bars, compressive strength of concrete, and amount of confinement. Based on the analysis of the experimental results, the following remarks can be drawn:

- Splice length of GFRP bars under compression was determined to be much less than that of steel bars.
- The end bearing and bond stresses as components of splice strength can be characterized as a function of splice length, bar diameter and confinement.
- Increasing the lateral confinement by transverse reinforcement could result in improving the end bearing and bond stress and consequently reducing the splice length. The area and spacing of transverse reinforcement could affect the splice length. However, the ultimate strength of transverse reinforcement has not played a considerable role in the splice strength.
- The end bearing stress at the free end of a spliced bar and the average bond stress developed on the perimeter of a bar were determined to be proportional to the bar diameter. The bond stress, however, has been reduced by increasing the bar diameter.
- The average bond stress is expressed by the ratio of d_b/l_s to the power of 0.68. It could be reasonably well estimated by the linear ratio of the bar diameter and splice length as well. The mean value of the test over predicted bond strength was obtained around 0.9 with a standard deviation of approximately 0.32.
- In developing the simplified design equation for prediction of the required splice length, the marginal effect of transverse reinforcement on the end bearing component was conservatively eliminated. However, confining the splice length is beneficial to achieve a more ductile behavior.

Although, the design expression proposed in this study to estimate the required spliced length correlates well with the test results, the accuracy of the equation should be more investigated through further experimental investigations. Such programs should aim at evaluating the parameters which are not included herein, such as surface condition of spliced bars, compressive strength of concrete, elastic modulus of GFRP bars, and concrete cover.

CHAPTER 7 GENERAL CONCLUSIONS AND RECOMMENDATIONS

7.1. SUMMARY

The current study has investigated the behavior of concrete columns reinforced with lap spliced GFRP bars. 30 large-scale concrete columns reinforced with steel and GFRP bars were tested under concentric loading and a non-linear analysis was developed to compare the results. The test variables were chosen to examine effect of type, splice length, bar diameter and confinement. Strength of the columns, strains of materials and deformation were investigated. The basic objective of this study was to precisely evaluate strength components of spliced bars comprising end bearing and bond stress. A model was presented to calculate the length of over lap spliced GFRP bars including the parameters affecting the strength of spliced bars. The proposed model was evaluated against the tested columns.

7.2. CONCLUSIONS

Based on the analysis of the experimental results, the following conclusions can be drawn:

7.2.1. Reinforcement type

- The spliced GFRP- and steel-reinforced concrete columns exhibited similar linear load–displacement behavior in the ascending part.
- The test results indicate that the required compression splice length for GFRP bars is less than that required for steel. This can be attributed to the difference in the modulus of elasticity and corresponding strain developed in the bars under compression.
- Specimens constructed with spliced GFRP bars failed by cover spalling, followed by bar sliding at the splice region. Buckling of GFRP bars occurred in the specimens reinforced with continuous bars and a spliced length of $36d_b$. Buckling of spliced bars led to GFRP spiral rupture.

- The splice strength of GFRP bars would not be linearly proportional to the splice length. A similar trend was also observed with the steel-reinforced concrete columns.

7.2.2. Confinement

- Transverse reinforcement can affect the deformability and strength of concrete columns reinforced with spliced GFRP bars. Reducing the spiral spacing can increase the loading and displacement capacities.
- The transverse-reinforcement ratio changed the failure mode from a brittle to a more ductile behavior. The unconfined columns explosively failed subsequent to concrete core crushing. In the specimens with a spiral spacing of 80 mm, the concrete cover spalled off at the peak load and the loading capacity decreased suddenly. The well-confined specimens with the 40 mm spiral spacing evidenced a much smoother descending branch after attaining their peak load.
- Failure of the well-confined specimens was more ductile than that of the unconfined specimens. At the post-peak stage, the former achieved a second peak load, followed by spiral rupture. The second peak load was smaller than the first, since the longitudinal reinforcement had already slipped, and the column strength attributed solely to the confined concrete core.
- The area and spacing of transverse reinforcement affected the splice length. However, the yield strength of transverse reinforcement could not play a considerable role in splice strength.
- Increasing the lateral confinement by transverse reinforcement could result in reducing the splice length.

7.2.3. Splice length

- The required splice length of GFRP bars under compression was determined to be much less than that of steel bars.
- The splice length affected not only the peak load but also the post-peak behavior: the longer the spice length would be, the higher the peak load is. The decrease in the

column loading capacity was slower and softer for the specimens with larger splice lengths.

7.2.4. End bearing strength

- The strength of the compression splice consists of end-bearing and bond components. The end-bearing strength of the spliced GFRP bars increased linearly up to peak load and contributed significantly to the splice strength, much more so than does the bond strength. Upon crack initiation, the bond-strength component became more active in contributing to the splice strength.
- The end-bearing component of the splice strength is a constant value related to the compressive strength of concrete. In addition, confinement can favorably affect the end-bearing contribution.
- The end bearing stress at the free end of a spliced bar was determined to be proportional to the bar diameter.

7.2.5. Bond strength

- The bar stress developed by the bond component in the unconfined columns can be estimated, albeit approximately, as a function of the splice length.
- The bond strength is expressed by the ratio of d_s/l_b to the power of 0.68. It can be reasonably well estimated by the linear ratio of the bar diameter and splice length as well.
- The bond contribution was improved with increasing the transverse reinforcement proportionally to the transverse-reinforcement index. The bond stress for the confined columns was formulated as the sum of the bond stress in the unconfined columns and augmentative effect of the transverse reinforcement.
- The average bond stress developed on the perimeter of a bar was determined to be proportional to the bar diameter. The bond stress, however, has been reduced by increasing the bar diameter.

7.3. RECOMMENDATIONS FOR FUTURE WORK

This study is expected to provide a step toward using GFRP reinforcement in columns. The findings of the current study state the applicability of using spliced GFRP bars as reinforcement in columns and provide a simplified design equation. However, it also serves to identify areas of needed research. Some of these areas recommended for future research are given below.

- The most important next step is to verify the effect of elasticity modules of reinforcement. Toward that, different bar type (Basalt and Carbon) can be examined.
- Investigate the surface condition of reinforcement on the behavior of columns reinforced with spliced bars.
- Studying the effect of staggered spliced GFRP bars on the performance of reinforced concrete columns.
- It is recommended to investigate the behavior of bundled GFRP reinforced concrete columns using over lap splicing.
- It is recommended to investigate the behavior of GFRP reinforced concrete columns using different concrete properties.
- Additional experimental work on different cross section geometry is required to study the effect of different cross section shape and reinforcement ratios.

French version of this section is presented below:

7.4. RÉSUMÉ

La présente étude a examiné le comportement de poteaux en béton armé de barres de PRFV ayant des jonctions par recouvrement. Trente (30) poteaux pleine grandeur en béton armé d'acier et de PRFV ont été testés sous charges concentriques et une analyse non linéaire a été effectuée pour comparer les résultats. Les paramètres d'études ont été choisis de façon à étudier l'effet du type de barre, de la longueur de recouvrement, du diamètre des barres et du confinement. La résistance des poteaux ainsi que les déformations des matériaux ont été évaluées. L'objectif premier de cette étude était d'évaluer avec précision la résistance de

toutes les composantes qui contribuent à la résistance des barres ayant des jonctions par recouvrement telles que les contraintes d'appui bout à bout et d'adhérence. Un modèle intégrant les paramètres affectant la résistance des barres ayant des jonctions par recouvrement a été présenté pour calculer la longueur de recouvrement des barres de PRFV. Le modèle proposé a été évalué au moyen des poteaux testés.

7.5. CONCLUSIONS

Sur la base de l'analyse des résultats expérimentaux, les conclusions suivantes peuvent être tirées :

7.5.1. Type d'armature

- Les poteaux en béton armé de PRFV et d'acier ayant des jonctions par recouvrement ont présenté un comportement linéaire similaire de la partie ascendante de la courbe charge - déplacement pendant la phase de chargement.
- Les résultats des essais indiquent que la longueur de recouvrement requise pour les barres de PRFV en compression est inférieure à celle requise pour l'acier. Ceci peut être attribué à la différence du module d'élasticité et à la déformation correspondante développée dans les barres en compression.
- Les poteaux fabriqués avec des barres de PRFV ayant des jonctions par recouvrement ont subi une rupture par éclatement de l'enrobage du béton, suivi d'un glissement des barres au niveau de la zone de recouvrement. Le flambement des barres en PRFV s'est produit dans les poteaux comportant des barres d'armature continues et dans les poteaux fabriqués avec des barres d'armature ayant des jonctions de longueur de recouvrement égale à $36d_b$. Le flambement des barres ayant des jonctions par recouvrement a entraîné la rupture des spirales en PRFV.
- La résistance des jonctions par recouvrement des barres de PRFV ne serait pas linéairement proportionnelle à la longueur de recouvrement. La même tendance a également été observée avec les poteaux en béton armé d'acier.

7.5.2. Confinement

- Les armatures transversales peuvent affecter la déformabilité et la résistance des poteaux en béton armé de PRFV ayant des jonctions par recouvrement. La réduction de l'espacement des spirales peut augmenter les capacités de chargement et de déplacement des poteaux.
- Le taux d'armature transversal a modifié le mode de rupture, le faisant passer d'une rupture fragile à une rupture plus ductile. Les poteaux non confinés ont subi une rupture caractérisée par une explosion du béton à la suite de l'écrasement du noyau du béton. Les poteaux ayant un espacement de spirales de 80 mm ont subi un éclatement de l'enrobage à l'atteinte de la charge maximale et une diminution soudaine de la capacité du poteau. Les poteaux ayant un confinement adéquat, avec un espacement des spirales de 40 mm ont présenté une partie descendante de la courbe de chargement moins abrupte, après l'atteinte de leur charge maximale.
- La rupture des poteaux adéquatement confinés était plus ductile que celle des poteaux non confinés. Une rupture des spirales a été observée après l'atteinte d'un second pic de chargement. La deuxième charge de pic était inférieure à la première, car les armatures longitudinales avaient déjà subi un glissement et la résistance de la colonne était attribuée uniquement au noyau de béton confiné.
- La surface et l'espacement des armatures transversales ont affecté la longueur de recouvrement des barres. Cependant, la limite d'élasticité des armatures transversales ne pouvait pas jouer un rôle considérable dans la résistance de la jonction par recouvrement.
- L'augmentation du confinement latéral à l'aide d'armatures transversales pourrait réduire la longueur de recouvrement requise des barres.

7.5.3. Longueur de recouvrement

- La longueur de recouvrement requise des barres de PRFV en compression est inférieure à celle des barres en acier.

- La longueur de recouvrement a affecté non seulement la charge au pic, mais également le comportement post-pic : plus la longueur de recouvrement est grande, plus la charge au pic est élevée. La diminution de la capacité portante du poteau était plus lente et moins abrupte pour les poteaux ayant des longueurs de recouvrement plus élevées.

7.5.4. Résistance d'appui bout à bout

- La résistance de la jonction en compression comprend celle de l'appui bout à bout et celle de l'adhérence. La résistance de l'appui bout à bout des barres en PRFV ayant une jonction par recouvrement a augmenté de façon linéaire jusqu'à l'atteinte de la charge de pointe et a contribué de manière significative à la résistance de la jonction par recouvrement, beaucoup plus que la force d'adhérence. Lors de l'initiation de la fissure, la composante de la résistance d'adhérence est devenue plus active dans sa contribution à la résistance de la jonction par recouvrement.
- La composante de la résistance de l'appui bout à bout de la jonction par recouvrement est une valeur constante liée à la résistance à la compression du béton. De plus, le confinement peut avoir une incidence favorable sur la contribution de la résistance de l'appui bout à bout.
- La contrainte de l'appui bout à bout exercée sur l'extrémité libre de barres ayant une jonction par recouvrement était proportionnelle au diamètre de la barre.

7.5.5. Résistance d'adhérence

- La contrainte dans la barre développée par la composante de l'adhérence dans les poteaux non confinés peut être estimée approximativement en fonction de la longueur de recouvrement.
- La résistance d'adhérence est exprimée par le rapport de d_s/l_b à la puissance de 0,68.

  Il peut être raisonnablement bien estimé par le rapport linéaire du diamètre de la barre et de la longueur de recouvrement.

- La contribution de l’adhérence a été améliorée avec l'augmentation des armatures transversales proportionnellement à l'indice des armatures transversales. La contrainte d’adhérence pour les poteaux confinés a été établie comme étant la somme de la contrainte d’adhérence dans les poteaux non confinés et de l'effet d'augmentation des armatures transversales.
- La contrainte d’adhérence moyenne développée sur le périmètre d’une barre était proportionnelle au diamètre de la barre. Cependant, la contrainte d’adhérence a été réduite en augmentant le diamètre de la barre.

7.6. **RECOMMANDATIONS POUR LES TRAVAUX FUTURS**

Cette étude devrait constituer un pas vers l'utilisation des armatures en PRFV dans les poteaux. Les conclusions de la présente étude indiquent qu'il est possible d'utiliser des barres de PRFV ayant une jonction par recouvrement comme armatures dans les poteaux et fournissent une équation de calcul simplifiée. Cependant, elles servent également à identifier les champs de recherche nécessaires. Certains de ces champs de recherche future sont listés ci-dessous.

- La prochaine étape la plus importante consiste à vérifier l'effet des modules d'élasticité des armatures. Pour l’atteinte de cet objectif, différents types de barres (basalte et carbone) peuvent être examinés.
- Étudiez l’effet du type de surface des barres d’armature sur le comportement des poteaux comportant des barres d’armature ayant des jonctions par recouvrement.
- Étudier l’effet du décalage des barres d’armature en PRFV ayant des jonctions par recouvrement sur les performances des poteaux en béton armé.
- Il est recommandé d'étudier le comportement de groupes de poteaux en béton armé de PRFV ayant des jonctions par recouvrement.
- Il est recommandé d'étudier le comportement des poteaux en béton armé de PRFV en utilisant différents types de béton.

- Des travaux expérimentaux supplémentaires sur différentes géométries de section sont nécessaires pour étudier l'effet de différentes formes et du taux d'armature.

CHAPTER 8 REFERENCES

ACI 318M. (2014). *Building code Requirements for Structural Concrete (ACI 318M-14) and Commentary (ACI318RM-14)*. American Concrete Institute, Farmington Hills, MI.

ACI 440.1R. (2015). *Guide for the Design and Construction of Structural Concrete Reinforced with FRP Bars (ACI 440.1R-15)*. American Concrete Institute, Farmington Hills, MI.

ACI 440.3R. (2012). *Guide Test Methods for Fiber-Reinforced Polymers (FRPs) for Reinforcing or Strengthening Concrete Structures (ACI 440.3R-12)*. American Concrete Institute, Farmington Hills, MI.

ACI Committee 318. (2008). *Building Code Requirements for Structural Concrete (ACI 318-08) and Commentary*. American Concrete Institute, Farmington Hills, MI.

ACI Committee 408. (2003). *Bond and Development of Straight Reinforcing Bars in Tension (ACI 408-03)*. American Concrete Institute, Farmington Hills, MI.

Afifi, M. Z., Mohamed, H. M., and Benmokrane, B. (2014a). "Axial Capacity of Circular Concrete Columns Reinforced with GFRP Bars and Spirals." *Journal Composite for Construction*, 18(1), 1–11.

Afifi, M. Z., Mohamed, H. M., and Benmokrane, B. (2014b). "Axial Capacity of Circular Concrete Columns Reinforced with GFRP Bars and Spirals." *Journal of Composites for Construction*, 18(1995), 1–11.

Afifi, M. Z., Mohamed, H. M., and Benmokrane, B. (2014c). "Strength and Axial Behavior of Circular Concrete Columns Reinforced with CFRP Bars and Spirals." *Journal Composite Construction*, 18(2), 1–10.

Afifi, M. Z., Mohamed, H. M., and Benmokrane, B. (2015). "Theoretical stress-strain model

for circular concrete columns confined by GFRP spirals and hoops." *Engineering Structures*, Elsevier Ltd, 102, 202–213.

Afifi, M. Z., Mohamed, H. M., Chaallal, O., and Benmokrane, B. (2014d). "Confinement Model for Concrete Columns Internally Confined with Carbon FRP Spirals and Hoops." *Journal of Structural Engineering*, 141(9), 04014219.

Ali, A. H., Mohamed, H. M., and Benmokrane, B. (2016). "Shear Behavior of Circular Concrete Members Reinforced with GFRP Bars and Spirals at Shear Span-to-Depth Ratios between 1.5 and 3.0." *J. Compos. Constr.*, 18(3), 1–10.

Ali, A. H., Mohamed, H. M., and Benmokrane, B. (2017). "Strength and Behavior of Circular FRP-Reinforced Concrete Sections without Web Reinforcement in Shear." *Journal of Structural Engineering*, 143(3), 04016196.

Aly, R., Benmokrane, B., and Ebead, U. (2006). "Tensile Lap Splicing of CFRP Reinforcing Bars in Concrete." *Journal of Composites for Construction*, 10(4), 287–294.

ASCE. (2013). "Infrastructure Grade Card for 2013." <http://www.infrastructurereportcard.org/> (Feb. 9, 2017).

ASTM. (2015a). *Standard Test Method for Compressive Properties of Rigid Plastics 1*. ASTM D695-15, West Conshohocken, PA.

ASTM. (2015b). *Standard Test Method for Slump of Hydraulic-Cement Concrete*. *Astm C143*, ASTM C143/C143M, West Conshohocken, PA.

ASTM. (2016). *Standard Practice for Making and Curing Concrete Test Specimens in the Laboratory*. *American Society for Testing and Materials*, ASTM C192/C192M, West Conshohocken, PA.

ASTM D7205. (2011). *Standard Test Method for Tensile Properties of Fiber Reinforced Polymer Matrix*. ASTM D7205M-06, West Conshohocken, PA.

Benmokrane, B., Tighiouart, B., and Chaallal, O. (1996). "Bond strength and Load

Distribution of Composites GFRP Reinforcing bars in Concrete." *ACI Materials Journal*, 93(3), 246–253.

Bentz, E. C., Massam, L., and Collins, M. P. (2010). "Shear Strength of Large Concrete Members with FRP Reinforcement." *Journal of Composites for Construction*, 14(6), 637–646.

Beskos, D. E. (1974). "Fracture of plain concrete under biaxial stresses." *Cement and Concrete Research*, 4(6), 979–985.

Boyle, H. C., and Karbhari, V. M. (1994). "Investigation of bond behavior between glass fiber composite reinforcements and concrete." *Polymer - Plastics Technology and Engineering*, Marcel Dekker Inc, 33(6), 733–753.

Cairns, J. (1985). "Strength of Compression Splices A Reevalution of Test Data." *ACI Journal*, 82, 510–516.

Cairns, J. (2014). "Staggered lap joints for tension reinforcement." *Structural Concrete*, 15(1), 45–54.

Cairns, J., and Arthur, P. D. (1979). "Strength of lapped splices in reinforced concrete columns." *Journal Proceedings*, 76, 277–296.

CAN/CSA S6-14. (2014). *Canadian Highway Bridge Design code*. Canadian Standards Association, Mississauga, Ontario, Canada.

CAN/CSA S806-12. (2012). *Design and construction of building structures with fiber reinforced polymers*. Canadian Standards Association, Mississauga, Ontario, Canada.

CAN/CSA S807-10. (2010). *Specification for fibre-reinforced polymers*. Canadian Standards Association, Mississauga, Ontario, Canada.

Canbay, E., and Frosch, R. J. (2005). "Bond strength of lap-spliced bars." *ACI Structural Journal*, 102(4), 605–614.

Chun, S. (2017). “Components of compression splice resistances in high-strength concrete.” *Magazine of Concrete Research*, 69(10), 502–511.

Chun, S. C., Lee, S. H., and Oh, B. (2010a). “Simplified Design Equation of Lap Splice Length in Compression.” *International Journal of Concrete Structures and Materials*, 4(1), 63–68.

Chun, S., Lee, S., and Oh, B. (2010b). “Compression Lap Splice in Unconfined Concrete of 40 and 60 MPa (5800 and 8700 psi) Compressive Strengths.” *ACI Structural Journal*, 107(2), 170–178.

Chun, S., Lee, S., and Oh, B. (2010c). “Compression Splices in Confined Concrete of 40 and 60 MPa (5800 and 8700 psi) Compressive Strengths.” *ACI Structural Journal*, 107(4), 1–10.

Chun, S., Lee, S., and Oh, B. (2012). “Compression Splices in High-Strength Concrete of 100 MPa (14,500 psi) and Less.” *ACI Structural Journal*, 108(6), 715–724.

CSA A23.3-14. (2014). *Design of concrete structures*. Canadian Standards Association, Mississauga, Ontario, Canada.

Darwin, D., Tholen, M. L., Idun, E. K., and Zuo, J. (1996a). “Bond Strength of High Relative Rib Area Reinforcing Bars.” *ACI Structural Journal*, 93(1), 95–107.

Darwin, D., Zuo, J., Tholen, M. L., and Idun, E. K. (1996b). “Development length criteria for conventional and high relative rib area reinforcing bars.” *ACI Structural Journal*, 93(3), 347–359.

Deitz, D. H., Harik, I. E., Asce, M., Gesund, H., and Asce, F. (2003). “Physical Properties of Glass Fiber Reinforced Polymer Rebars in Compression.” *Journal of Composites for Construction*, 7(4), 363–366.

Ehsani, M. R. (1993). *Glass-fiber reinforcing bars*. *Alternative materials for the reinforcement and prestressing of concrete*, (C. J.L., ed.), Blackie Academic &

Professional, London, UK.

Ehsani, M. R., Saadatmanesh, H., and Tao, S. (1996). “Design Recommendations for Bond of GFRP Rebars to Concrete.” *Journal of Structural Engineering*, 122(3), 247–254.

El-Gamal, S., El-Salakawy, E., and Benmokrane, B. (2005). “Brhaviour of restrained concrete bridge deck slabs reinforced with FRP reinforcing bars under concentrated loads, El-Gamal.pdf.” *ACI Structural Journal*, 727–735.

El-Sayed, A. K., El-Salakawy, E. F., and Benmokrane, B. (2012). “Shear strength of fibre-reinforced polymer reinforced concrete deep beams without web reinforcement.” *Canadian Journal of Civil Engineering*, 39(5), 546–555.

Elinea, A., Yehia, S., and Tadros, M. K. (1999). “Lap Splices in Confined Concrete.pdf.” *ACI Structural Journal*, 96(6), 937–946.

Farghaly, A., and Benmokrane, B. (2013). “Shear Behavior of Large Reinforced Concrete Beams without Web Reinforcement.” *Journal of Composites for Construction*, 17(6), 1–10.

Ferguson, P. M., and Breen, J. E. (1965). “Lapped Splices For High Strength Reinforcing Bars.” *Journal of the AMERICAN CONCRETE INSTITUTE*, 1063–1078.

Furche, J., and Eligehausen, R. (1992). “Lateral Blow-Out Failure of Headed Studs Near a Free Edge.” *Aci Special Publications*, 235–252.

Guadagnini, M., Pilakoutas, K., and Waldron, P. (2006). “Shear Resistance of FRP RC Beams: Experimental Study.” *Journal of Composites for Construction*, 10(6), 464–473.

Hadhood, A., Mohamed, H. M., and Benmokrane, B. (2016). “Experimental Study of Circular High-Strength Concrete Columns Reinforced with GFRP Bars and Spirals under Concentric and Eccentric Loading.” *Journal of Composites for Construction*, 3(2014), 04016078.

Hadhood, A., Mohamed, H. M., and Benmokrane, B. (2017a). “Strength of circular HSC

columns reinforced internally with carbon-fiber-reinforced polymer bars under axial and eccentric loads." *Construction and Building Materials*, Elsevier Ltd, 141, 366–378.

Hadhood, A., Mohamed, H. M., and Benmokrane, B. (2017b). "Axial Load–Moment Interaction Diagram of Circular Concrete Columns Reinforced with CFRP Bars and Spirals: Experimental and Theoretical Investigations." *Journal of Composites for Construction*, 21(2), 1–12.

Hadhood, A., Mohamed, H. M., and Benmokrane, B. (2017c). "Failure Envelope of Circular Concrete Columns Reinforced with Glass Fiber-Reinforced Polymer Bars and Spirals." *ACI Structural Journal*, 114(6), 1417–1428.

Hadhood, A., Mohamed, H. M., and Benmokrane, B. (2017d). "Experimental Study of Circular High-Strength Concrete Columns Reinforced with GFRP Bars and Spirals under Concentric and Eccentric Loading." *Journal of Composites for Construction*, 21(2).

Hadhood, A., Mohamed, H. M., and Benmokrane, B. (2018). "Assessing Stress-Block Parameters in Designing Circular High-Strength Concrete Members Reinforced with FRP Bars." *Journal of Structural Engineering (United States)*, 144(10).

Hadhood, A., Mohamed, H. M., Ghrib, F., and Benmokrane, B. (2017e). "Efficiency of glass-fiber reinforced-polymer (GFRP) discrete hoops and bars in concrete columns under combined axial and flexural loads." *Composites Part B: Engineering*, Elsevier Ltd, 114, 223–236.

Hadi, M. N. S., Hasan, H. A., and Sheikh, M. N. (2016). "Experimental Investigations on Circular Concrete Columns Reinforced with GFRP Bars and Helices under Different Loading Conditions." *Journal of Composites for Construction*, 20(4), 1–12.

Hales, T. A., Pantelides, C. P., Sankholkar, P., and Reaveley, L. D. (2017). "Analysis-oriented stress-strain model for concrete confined with fiber-reinforced polymer spirals." *ACI Structural Journal*, 114(5), 1263–1272.

Hamilton, H. R., Benmokrane, B., Dolan, C. W., and Sprinkel, M. M. (2009). "Polymer Materials to Enhance Performance of Concrete in Civil Infrastructure." *Polymer Reviews*, 49(1), 1–24.

Harajli, M. H. (2004). "Comparison of Bond Strength of Steel Bars in Normal- and High-Strength Concrete." *Journal of Materials in Civil Engineering*, 16(4), 365–374.

Hassan, M., Ahmed, E., and Benmokrane, B. (2014). "Punching Shear Strength of Flat Slabs Reinforced with Glass Fibre-Reinforced Polymer (GFRP) Bars." *Composite for Construction*, 19(1), 1–10.

Japan Society of Civil Engineers. (2007). *STANDARD SPECIFICATIONS FOR CONCRETE STRUCTURES "Design."*

Khan, Q. S., Sheikh, M. N., and Hadi, M. N. S. (2015). "Tension and compression testing of fibre reinforced polymer (FRP) bars." *The 12th Iternational Symposium on FIber Reinforced Polymers for Reinforced Concrete Structures (FRPRCS-12)*, Nanjing, China, 1–6.

Kobayashi, K., and Fujisaki, T. (1995). "Compressive behavior of FRP reinforcement in non-prestressed concrete members." *Non-metalic (FRP) Reinforcement for Concrete Structures*, L. Taerwe, ed., E & FN Spon, London, 267–274.

Kupfer, H. B., and Gerstle, K. H. (1969). "Behavior of Concrete Under Biaxial Stresses." *ACI Journal*, 66, 656–666.

Lotfy, E. M. (2010). "Behavior of reinforced concrete short columns with Fiber Reinforced polymers bars." *INTERNATIONAL JOURNAL OF CIVIL AND STRUCTURAL ENGINEERING*, 1(3), 545–557.

Luca, A. De, Matta, F., and Nanni, A. (2010). "Behavior of Full-Scale Glass Fiber-Reinforced Polymer Reinforced Concrete Columns under Axial Load." *ACI Structural Journal*, (107), 589–596.

M. Guérin B. Benmokrane, C. K. Shield, and A. Nanni, H. M. M. (n.d.). “Effect of Glass Fiber-Reinforced Polymer Reinforcement Ratio on Axial-Flexural Strength of Reinforced Concrete Columns.” *Structural Journal*, 115(4).

Macgregor, James G. Wight, J. K. (2009). *DESIGN, REIFORCE CONCRETE MECHANICS & Design*.

Mallick, P. K. (2007). *Fiber reinforced composites: materials, manufacturing and design*. Marcel Dekker, New York, USA.

Metelli, G., Marchina, E., and Plizzari, G. A. (2017). “Experimental study on staggered lapped bars in fiber reinforced concrete beams.” *Composite Structures*, Elsevier Ltd, 179, 655–664.

Mohamed, H. M., Afifi, M. Z., and Benmokrane, B. (2014). “Performance Evaluation of Concrete Columns Reinforced Longitudinally with FRP Bars and Confined with FRP Hoops and Spirals under Axial Load.” *Journal of Bridge Engineering*, 19(7), 04014020.

Mohamed, H. M., Ali, A. H., and Benmokrane, B. (2017). “Behavior of Circular Concrete Members Reinforced with Carbon-FRP Bars and Spirals under Shear.” *Journal of Composites for Construction*, 21(2), 04016090.

Mohamed, H. M., and Benmokrane, B. (2012). “Recent field applications of FRP composite reinforcing bars in civil engineering infrastructures.” *Proc., Int. Conf. ACUN6–Composites and Nanocomposites in Civil, Offshore and Mining Infrastructure*, 14–16.

Mohamed, H. M., and Benmokrane, B. (2014). “Design and Performance of Reinforced Concrete Water Chlorination Tank Totally Reinforced with GFRP Bars: Case Study.” *Journal of Composites for Construction*, 18(1), 05013001.

Mohammed, A., and Ali, H. (n.d.). “SHEAR STRENGTH AND BEHAVIOR OF CIRCULAR CONCRETE MEMBERS REINFORCED.”

Nkurunziza, G., Debaiky, A., Cousin, P., and Benmokrane, B. (2005). "Durability of GFRP bars: A critical review of the literature." *Progress in Structural Engineering and Materials*, 7(4), 194–209.

Orangon, C. O., Jirsa, J. O., and Breen, J. E. (1977). "A reevaluation of Test Data on Development Length and Splices." *ACI Journal*, 74, 114–122.

Park, R., and Paulay, T. (1974). *Reinforced Concrete Structures*. John Wiley & Sons Inc, New York.

Pay, C., Canbay, E., and Frosch, R. J. (2014). "Bond Strength of Spliced Fiber-Reinforced Polymer Reinforcement." *ACI Structural Journal*, (111), 257–266.

Pfister, J. P., and Mattock, A. H. (1963). "High Strength Bars as Concrete Reinforcement, Part 5:Lap splices in concentrically loaded columns." *Journal of the PCA Research and Development Laboratories*, 5(2), 27–40.

Quintana, C. B. (2008). "Behaviour of contact and noncontact lap compression splices." *IBRACON Structures and Materials Journal*, 1(3), 261–272.

Razaqpur, A. G., and Spadea, S. (2015). "Shear Strength of FRP Reinforced Concrete Members with Stirrups." *Journal of Composites for Construction*, 19(1).

Richart, F., Brandtzaeg, A., and Brown, R. L. (1928). "A Study of the Failure of Concrete under Combined Compressive Stresses." *University of Illinois Bulletin*, 26(12), 1–104.

Richart, F., and Brown, R. (1934). *An Investigation of Reinforced Concrete Columns*. *University of Illinois Bulletin*.

Saatcioglu, B. M., and Razvi, S. R. (1992). "Strength and ductility o f confined concrete." 118(26631), 1590–1607.

Singhvi, A., and Mirmiran, A. (2002). "Creep and Durability of Environmentally Conditioned FRP-RC Beams Using Fiber Optic Sensors." *Journal of Reinforced Plastics and Composites*, 21(4), 23.

Tabatabaei, A., Eslami, A., Mohamed, H. M., and Benmokrane, B. (2018). “Strength of compression lap-spliced GFRP bars in concrete columns with different splice lengths.” *Construction and Building Materials*, Elsevier Ltd, 182, 657–669.

Tavassoli, A., Liu, J., and Sheikh, S. (2015). “Glass Fiber-Reinforced Polymer-Reinforced Circular Columns under Simulated Seismic Loads.” *ACI Structural Journal*, 112(1), 103–114.

Tighiouart, B., Benmokrane, B., and Gao, D. (1998). “Investigation of Bond in Concrete Member with Fibre Reinforced Polymer (FRP) Bars.” *Construction and Building Materials*, 12(8), 453–462.

Tighiouart, B., Benmokrane, B., and Mukhopadhyaya, P. (1999). “Bond strength of glass FRP rebar splices in beams under static loading.” *Construction and Building Materials*, 13(7), 383–392.

Tobbi, H., Farghaly, A. S., and Benmokrane, B. (2012). “Concrete columns reinforced longitudinally and transversally with glass fiber-reinforced polymer bars.” *ACI Structural Journal*, 109(4), 551–558.

Tobbi, H., Farghaly, A. S., and Benmokrane, B. (2014a). “Behavior of Concentrically Loaded Fiber-Reinforced Polymer Reinforced Concrete Columns with Varying Reinforcement Types and Ratios.” *ACI Structural Journal*, 111(2), 375–386.

Tobbi, H., Farghaly, A. S., and Benmokrane, B. (2014b). “Strength model for concrete columns reinforced with fiber-reinforced polymer bars and ties.” *ACI Structural Journal*, 111(4), 789–798.

Tottori, S., and Wakui, H. (1993). “Shear capacity of RC and PC beams using FRP reinforcement.” *Aci Sp*, 138(27), 615–631.

Wambeke, B. W., and Shield, C. K. (2006). “Development lenght of glass fiber-reinforced polymer bars in concrete.” *ACI Structural Journal*, 103(1), 11–17.

Zadeh, H. J., and Nanni, A. (2013). “Design of RC Columns Using Glass FRP Reinforcement.” *Journal of Composites for Construction*, 17(3), 294–304.

Zadeh, H. J., and Nanni, A. (2017). “Flexural stiffness and second-order effects in fiber-reinforced polymer-reinforced concrete frames.” *ACI Structural Journal*, 114(2), 533–544.

Zaman, a., Gutub, S. a., and Wafa, M. a. (2013). “A review on FRP composites applications and durability concerns in the construction sector.” *Journal of Reinforced Plastics and Composites*, 32, 1966–1988.

Zhishen, W., Xin, W., and Gang, W. (2012). “Advancement of structural safety and sustainability with basalt fiber reinforced polymers.” *CICE2012, Rome*, 13, 15–29.

Zuo, J., and Darwin, D. (1998). “Bond Strength of High Relative Rib Area Reinforcing Bars.” *Report*, (January), 322.

Zuo, J., and Darwin, D. (2000). “Splice strength of conventional and high relative rib area bars in normal and high-strength concrete.” *ACI Structural Journal*, 97(4), 630–641.